Master's thesis

NTNU
Norwegian University of Science and Technology
Faculty of Natural Sciences
Department of Materials Science and Engineering

Håkon Nordengen

Optimisation of Zn-Mn co electrodeposition on aluminium utilising direct- and pulse current in alkaline and acidic electrolyte

Master's thesis in Chemical Engineering and Biotechnology
Supervisor: Andreas Erbe, Jan Halvor Nordlien
June 2019

NTNU
Kunnskap for en bedre verden

Håkon Nordengen

Optimisation of Zn-Mn co-electrodeposition on aluminium utilising direct- and pulse current in alkaline and acidic electrolyte

Master's thesis in Chemical Engineering and Biotechnology
Supervisor: Andreas Erbe, Jan Halvor Nordlien
June 2019

Norwegian University of Science and Technology
Faculty of Natural Sciences
Department of Materials Science and Engineering

NTNU
Kunnskap for en bedre verden

Abstract

Aluminium used in heat exchanger application is susceptible towards corrosion in aggressive environments. Protection of the aluminium surface is important for the metal to retain mechanical and chemical properties. Diffusion coating is considered a possibility for aluminium surface protection, where sacrificial metal is diffused into the metal surface and reducing the corrosion potential for the substrate. Zn has previously been utilised as sacrificial metal, but alloying elements in the diffusion coating are of interest due to their synergistic effect towards corrosion protection. Methods used for depositing coating on aluminium include thermal spray coatings. However problems with spray coating application, like overuse of feedstock, have lead to other possible methods being considered. One of these are electrodeposition. Deposition of coating with electrodeposition is easy to control with parameters like deposition time, temperature and current.

In this thesis, electrodeposition of Zn-Mn was attempted using aluminium as substrate and utilising two different electrolytes; alkaline pyrophosphate and acidic sulphate electrolyte. Usage of two different current application, direct and pulse current, were examined. Characterisation of deposits through morphology, chemical composition and chemical depth profile was achieved by using SEM/EDS, GDOES and Raman spectroscopy methods for examination. Current efficiency of the baths for both current application were also reviewed, and the optimal setup was concluded for at the end.

All samples in both electrolytes included oxygen in the final coating, with varying at. %. Most of the oxygen content was found, from EDS analysis, GDOES and Raman spectroscopy, to be from oxidation of metal deposited at the surface. Especially was this evident when Mn had deposited at surface, as the lowest content of oxygen found was that of the sample where Mn was mainly inside the coating. Inclusion of the less noble metal, Mn, in the coating was favoured for all samples when applying larger cathodic current densities. This result was effected from different hydrogen evolution intensity regarding deposition. Pulse current application favoured more compact and uniform deposit distribution for lower current densities, and less uniformity and more clustered morphology for larger current densities. Co-deposition of Zn-Mn was favoured using PC setup, and more specifically at the edges of the samples where the cathodic current density was largest. Current efficiency was overall larger for alkaline pyrophosphate than the acidic sulphate bath, and is the electrolyte displaying best properties.

Sammendrag

Aluminium som blir brukt i varmevekslere er utsatt for korrosjon i spesielt aggressive omgivelser. Beskyttelse av aluminiumoverflaten er viktig for å beholde mekaniske og kjemiske kvaliteter i prosessene den blir brukt til. Diffusjonsbelegg er tiltenkt en rolle for overflatebeskyttelse for aluminium. Belegget med offermetall vil diffundere inn i substratoverflaten og redusere korrosjonspotensialet for aluminium. Zn har tidligere tiltredd denne rollen som offermetall, men legeringer som offermetall i diffusjonsbelegg er av interesse grunnet synergetiske egenskaper innenfor korrosjonsbeskyttelse. Termisk spraybelegg har blir brukt før som metode for påsetting av belegg på aluminium, men denne teknikken har diverse utfordringer som overbruk av råstoff. Andre metoder er derfor av interesse, og en av disse er elektroplettering. Påsetting av belegg er enkelt å kontrollere ved å utnytte parameter som påsettingstid, temperatur og strøm.

I denne oppgaven ble elektroplettering Zn-Mn gjennomført ved bruk av aluminium som substrat og to elektrolytter; alkalinsk pyrofosfat- og surt sulfatelektrolytt. To forskjellige strømoppsett vil bli benyttet; direkte- og pulsstrøm. Karakterisering av belegget ble gjort igjennom studie av morfologi, kjemisk komposisjon og kjemisk dybdeprofil med analyseverktøy som SEM/EDS, GDOES og Raman spektroskopi. Strømeffektivitet for begge badene og strømoppsettene ble også analysert. Det optimalet badet for hver strømapplikasjon ble bestemt utifra resultatet.

Alle prøvene i begge elektrolyttene inneholdt oksygen i belegget, og med varierende atomisk prosent. Majoriteten av oksygenet i belegget ble bestemt, fra GDOES og Raman spektroskopi, til å ankomme fra oksidering av metall som var påsatt på toppen av belegget. Dette var spesielt tydelig når Mn var påsatt på toppen. Prøven med det laveste atomiske oksygeninnholdet var den der Mn var påsatt hovedsaklig inne i belegget. Inkludering av Mn i belegget var favorisert, for alle prøver, da det ble påsatt stor katodisk strømtetthet. Resultatet kom hovedsaklig fra mindre utvikling av hydrogengass under elektropletteringen. Bruk av pulsstrøm favoriserte gjevn og kompakt beleggdannelse for lave strømtettheter, og ugjevn og klumpete belegg for større strømtettheter. Påsettelse av Zn-Mn legering var favorisert ved bruk av pulsstrøm, og ved kantene på prøvene der strømtettheten var størst. Strømeffektiviteten var generelt høyere for den alkalinske elektrolytten enn for den sure elektrolytten for begge strømapplikasjoner, og er derfor den elektrolytten som viser størst potensialet for Zn-Mn elektroplettering.

Preface

This thesis is a continuation of the project ”Feasibility study of Zn-Mn electro co-deposition on aluminium” done by the author in the Fall 2018 in the course ”TMT4500 - Materials Technology, Specialization project”. The master thesis has been a collaboration between NTNU and Hydro Extruded Solutions, and my gratitude goes to Hydro for financing both the project and master thesis. All aluminium multi-port extruded tubes (MPE) utilized in both the project and master thesis have been produced by Hydro Extruded Solutions. All experimental work was done at Norwegian University of Science and Technology (NTNU).

I would like to thank my two supervisors, Andreas Erbe and Jan Halvor Nordlien, for help with analysing results, interpretation of data and guidance through Skype and physical meetings. I would also like to thank Magnus Følstad and Anita Storsve for aid with electrochemical equipment in the corrosion lab in Chemistry Block 2, and special thanks to Anita for aiding me in buying chemicals needed for the experiments. Help from Yingda Li and Sergey Khromov with SEM/EDS and GDOES analysis, and from Bartlomiej Gawel with Raman spectroscopy, have been greatly appreciated. Lastly I would like to thank John Erik Lein at Sintef for contributing with Zn anodes from the fall semester, and Kara Poon for help with mechanical work on the aluminium samples.

Contents

List of Tables

List of Figures

Abbreviations

i_{an}	=	Anodic current density
t_{off}	=	Anodic/off time
i_{avg}	=	Average current density
i_{cath}	=	Cathodic current density
t_{on}	=	Cathodic/on time
CE	=	Current efficiency
CV	=	Cyclic voltammetry/voltammogram
DC	=	Direct current
θ	=	Duty cycle
f	=	Frequency
GDOES	=	Glow-discharge optical emission spectroscopy
Mn	=	Manganese
PC	=	Pulse current
PRC	=	Pulse reverse current
Ag/AgCl (sat.)	=	Saturated silver-silver chloride reference electrode
SEM	=	Scanning electron microscopy
Zn	=	Zinc

Chapter 1

Introduction

1.1 Overview

1.1.1 Motivation

Aluminium and its useage in different fields has increased over the years due to its interesting properties: low density, good formability and thermal and electrical conductivity. Hydro Extruded solutions produces extruded aluminium products used in areas such as offshore, buildings and automotive industry. One of these products are the multi-port extruded tubes (MPE) which are typically in the 3xxx series (Al-Mn) aluminium alloy family. The metal is used in heat exchanger application and is susceptible to pitting corrosion in aggressive environment [1]. Protection against corrosion is therefore necessary for the aluminium to withstand the environment.

One possibility for protection of aluminium is with the use of thermal diffusion coating. A simple schematic for producing the sacrificial layer is shown in Figure 1.1. The method utilise sacrificial properties of the alloying element to form a corrosion resistant layer on top of the substrate [2]. A layer of alloy metal on the substrate surface is alloyed by increasing the temperature allowing the alloy metal to diffuse into the substrate [2]. Zinc (Zn) is widely used as sacrificial layer on steel, and has illustrated good corrosion protection when alloyed with aluminium giving the metal protection against pitting as it lowers the corrosion potential of aluminium into a passive zone [1, 3, 4]. Lately the research regarding inclusion of manganese (Mn) in Zn matrix has provided with excellent corrosion resistant when applied as sacrificial coating on steel [5, 6, 7, 8, 9, 10]. Mn inclusion in Zn matrix for thermal diffusion coating on aluminium is of interest, as the alloy coatings have showed synergistic effect towards inhibiting corrosion on the substrate [5, 7].

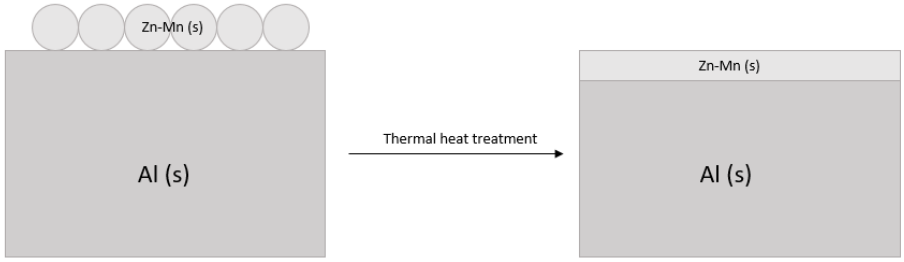

Figure 1.1: Schematic of proposed thermal diffusion coating process

Zn has mainly been applied as coating on aluminium with the use of thermal zinc spraying. The method takes advantage of Zn particles being heated with a thermal gun and sprayed on the substrate of choice [11]. Overusing of Zn feedstock and discontentment regarding the final properties of the applied coating are some problems this method exude, making other methods more interesting for examination. One of these is with the useage of electrodeposition [12, 13].

Electrodeposition is a simple method utilizing electrochemical properties of metals to reduce metal ions in an electrolytic bath to form a thin coating on the substrate by applying an external power source [12]. Deposition of coating is possible at room temperature, making electrodeposition a more energy efficient method compared to thermal spray coating. The deposition of coating is easily controlled with parameters such as temperature, current density, time, pH and coating material [13]. Zn-Mn co-deposition has been successfully achieved on steel as substrate with the use of electrodeposition in both alkaline and acidic environment [5, 6, 7, 8, 9, 10]. Mn content in the Zn matrix has been reported to be, depending on deposition parameters and additives, up to 30 wt% [7, 9]. However no research regarding using aluminium as a substrate for electrodeposition of Zn-Mn has been published.

1.1.2 Objective for the thesis

This thesis focus on electrodeposition of Zn-Mn on aluminium in both alkaline and acidic environment. The main objectives for the thesis are:

- Preparing Zn-Mn coatings on aluminium substrate by two electrodeposition methods, direct current (DC) and plating current (PC), in two different electrolytes
- Characterise deposited coating with techniques examining crystal structure, morphology, chemical composition and species and depth profile
- Evaluate efficiency of the process and explain inclusion of possible foreign chemicals or compounds
- Proposing what bath and current application that will include most Zn and Mn in the final coating

Chapter 2

Literature Review

2.1 Electrodeposition

Electrodeposition is an electrolytic plating process producing a thin metal coating on the surface of a substrate. The coating thickness can be varied, and range from 0.01 to 30 μm [13]. The coating can be used used for decorative purposes, giving the substrate a smooth and colorful surface, but is mostly used for corrosion protection of the surface [14]. The substrate to be plated has to be pre-treated and cleaned to establish an adhesive base for the coating to deposit on [15]. The process consists of a cathode, which is the item to be plated, and an anode which may consist of the metal to be plated or inert. In addition a reference electrode may be used for electrochemical analysis of the cathode reactions [14]. In addition to salt(s) of metal(s), which are to be plated on the substrate, several other chemicals may be added to the electrolytic bath for plating: buffers for pH control and additives for reducing proportion of free metal ions [13]. The metal reduction reaction on the surface follows the reduction reaction displayed in Equation 2.1. n is total number electrons necessary for reducing the cation.

$$\mathrm{M}^{n+}\,(\mathrm{aq}) + \mathrm{ne}^{-} \longrightarrow \mathrm{M}\,(\mathrm{s}) \tag{2.1}$$

2.2 Parameter influence

2.2.1 pH and reduction potential

The aforementioned reduction reaction of a metal is referred to, in standard conditions at 25°C and pH = 7, as the standard reduction potential [16]. The value gives a basis of what potential metal-ions of different species will reduce to to form solid metal. Some values for metals are given in Table 2.1.

Table 2.1: Standard reduction potentials [17]

Species	Potential vs. Ag/AgCl (sat.) [V]
H^+/H_2	- 0.19
Zn^{2+}/Zn	- 0.96
Mn^{2+}/Mn	- 1.38
Al^{3+}/Al	- 1.88

A complication arise with interaction between the aqueous environment and the metal-ions. Several other electrode reaction may occur, and leads to a dependence for metal-ions with pH [13]. Pourbaix diagrams were constructed for the purpose to envision the dominance of species in aqueous solutions given the electrode potential and the pH. These diagrams provides with an excellent starting point for choosing pH and electrode potentials for electroplating processes [18]. Pourbaix diagrams for aluminium, as well as the two plating metals of interest, are given in the Appendix.

By consulting the Pourbaix diagrams of Mn and Zn, the immediate area of interest presenting itself for deposition is the acidic environment at pH below 7. At this pH metal ions reduce to pure metal [18]. Acidic environment has been the primary electrolyte used for electroplating Zn and Zn-Mn coating [5, 6, 7, 8, 9, 10, 19, 20]. Recently alkaline environment has been suggested as a possibility for Zn-Mn deposition, where several additives are included to inhibit precipitation of hydroxides and deposited metal in similar fashion as the acidic bath [6, 21, 22, 23]. Following all baths discussed is the formation of hydrogen at low applied potentials for both acidic and alkaline baths, as foreshadowed by the Pourbaix diagram for water in Figure A4.

2.2.2 Additives

Apart from the essential source of coating material from included metal salts, additional chemicals may be added for improved properties for the deposited coating. Additives are used in a wide range of applications, but for electroplating one of the most important aspects is the interaction with hydrogen evolution and pH [15]. Additives like oxalic acid and boric acid are used for buffering the pH when hydrogen evolve at the cathode. Hydrogen evolution can lead to lower current efficiency as the bubbles created adheres to the substrate surface, leading less space for metal to be deposited on [15]. Hydrogen can be released from the surface by including wetting agents such as fatty acids. Additional salts may also be added to the electrolytic bath for increased conductivity [12].

2.3 Plating process

2.3.1 Direct current

A galvanostatic approach with direct current (DC) is the typical power source used for electrodeposition [12]. The method constantly polarise the electrode as the direction of the

current is constant throughout the process. The electric field arising from applying direct current allows the positive ions to move to the negatively polarized cathodes, and leads subsequently to deposition [15]. The thickness and mass of the coating is proportional to the applied current density and time, and can be used to express the current efficiency (CE) of the process with Faradays law [24]:

$$CE = \frac{m_{\text{deposition}}}{m_{\text{theo}}} \tag{2.2}$$

$$m_{\text{theo}} = \frac{i \cdot M \cdot A \cdot t}{n \cdot F} \tag{2.3}$$

$m_{\text{deposition}}$ is the mass gained from the deposition, i is the current density, A is the coating area, M is the molar mass of the metal deposited, t is the deposition time, n is the number of electrons transferred in the system (similar to n in Equation 2.1) and F is Faradays constant [12].

Thickness of the coating, d, can subsequently be calculated by knowing the current efficiency of the process and density of deposited metal, ρ, following the relation [12]:

$$d = \frac{i \cdot M \cdot CE \cdot t}{n \cdot F \cdot \rho} \tag{2.4}$$

2.3.2 Pulse plating

Another current application used, typically with deposition of alloys, is the use of pulse current (PC) [15]. The current is applied in short intervals with pulse amplitudes, making a square pulse or sinus shaped current trend. Periodically input of deposition current allows easier flow of ions to the substrate surface allowing for a more evenly distributed coating deposition [25]. Parameters to be varied are the on- and off time of deposition as well as peak cathodic current density i_{cath}. The ratio between on-time and the total time is referred to as duty cycle, θ, and is used to calculate the average current in PC process [26].

$$\theta = \frac{t_{\text{on}}}{t_{\text{on}} + t_{\text{off}}} \tag{2.5}$$

t_{on} and t_{off} are the cathodic/on and anodic/off time respectively. Typical values for θ are larger than 5 $\%$ [27]. Pulse reverse current (PRC) is another method for deposition, exploiting an anodic and cathodic pulse step to dissolve/oxidise and deposit metal on the surface respectively [26]. PRC setups have shown to reduce additive useage, reduce internal stress in the deposit, dissolve protrusions on the surface to make a uniform coating and create more compact and fine grained crystal structure [26]. The average current density, i_{avg}, obtained in all PC electrodeposition can be calculated using Equation 2.6 [25]. PC setup make use of 0 A during the anodic time, thus making the calculation for PC average current density, $\mathrm{i}_{\text{avg,PC}}$ rather simplistic.

$$i_{\text{avg}} = \frac{i_{\text{cath}} \cdot t_{\text{on}} - i_{\text{an}} \cdot t_{\text{off}}}{t_{\text{on}} + t_{\text{off}}} \tag{2.6}$$

$$i_{\mathrm{avg,\,PC}} = i_{\mathrm{cath}} \cdot \theta \tag{2.7}$$

i_{an} is the anodic current density. Deposited coating can be controlled in thickness down to atomic order by varying the width and amplitude of the pulse [25]. The hydrogen inclusion in the coating also decrease. Pulse deposition is more expensive than the DC method as a more expensive rectifier is needed for pulse plating to work [15].

The electrode potential can also be used for electrodeposition, and is used in potentiostatic application where the correlated current is applied for deposition. Potentials applied with this method are closely related to the standard reduction potentials, and can be estimated with the Pourbaix diagram or cyclic voltammetry. Disadvantages with potentiostatic application include fluctuation of current [12].

2.4 Kinetics

2.4.1 Cyclic voltammetry

Information of electrode kinetics and reaction mechanism can be examined with the use of voltammetry. The potential of an electrode in aqueous can be swept linearly with time by asserting a sweep rate, and the current behaviour exerted can be analysed. By reversing a linear-scan voltammetry a cyclic voltammetry curve arise, typically holding information of both cathodic and anodic behaviour (reverse reactions) [13]. For deposition purposes the cyclic voltammetry can provide information about potential ranges where deposition occur in the cathodic direction, pinpoint where hydrogen evolution occurs and if the deposit is multi-phased or single phased [13].

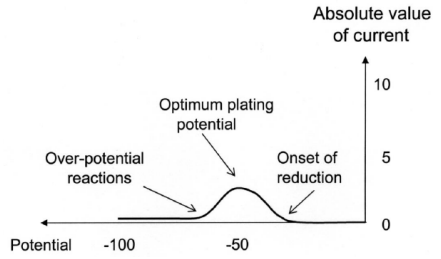

Figure 2.1: Voltammogram for single-metal deposition [28]

The peaks arising from the curve are extremes illustrating cathodic (negative) and anodic (positive) current peaks. The cathodic reaction is related to the reduction reaction (Equation 2.1), and the peak illustrate a potential range (with the accompanied current) at which the metal deposition can be achieved [28]. The optimum plating potential is at the peak, illustrated in Figure 2.1, while the area before and after are sub-optimal areas for metal deposition [28].

2.4.2 Overpotential

Migration of metal ions to the surface is favoured when the substrate is polarized. When the current is flowing a difference between the equilibrium- and operating potential may occur. This extra energy needed to force the reactions at the electrode to advance is called the overpotential [12, 13, 14]. Overpotential measures the extent of electrode polarization

and is a result of ohmic, kinetic and transport polarization. Kinetic overpotential is a factor of the speed of electrode reaction, transport overpotential arrives from supply of reactants or removal of products and ohmic overpotential originate from the ionic migration and its related slowness [13]. Typical overpotential reactions when dealing with electroplating includes hydrogen evolution [21, 23].

2.4.3 Incorporation of less noble metal

Co-deposition of two or more metals demands more attention to the properties of the metals in question. As discussed in Section 2.2.1 metals have different reduction potential, and these must be taken into account when plating. The less noble metal is the one with lowest reduction potential. When comparing Zn and Mn in Table 2.1 it can be stated that Mn is the less noble metal. The difference between the reduction potentials between two or more metals is known as a potential difference, and should be minimised for increased incorporation of Mn in the deposited coating [9, 23]. Several steps can be done to reduce the increase the incorporation of Mn. Increasing the current density or increasing the concentration of Mn in the electrolytic bath has reported increased Mn content in the final coating [9, 10, 23]. Additives, such as pyrophosphate, boric acid or citrate, can be used to decrease the aforementioned potential gap between the metals in question. However some drawbacks like precipitation of metal complex ions and low stability leads to lower current efficiency in these baths [22].

2.4.4 Determination of co-deposition potential

The aforementioned voltammogram discussed in Section 2.4.1 contains important information regarding the potential- and current range for deposition of metal. To determine the potential for co-deposition, an cathodic linear sweep voltammetry can be applied to the electrode [7, 21, 23]. The linear sweep should be from an anodic potential to a cathodic potential to clearly separate the trends from the voltammogram [28]. An anodic scan in the reverse direction can be applied to confirm what phases have been deposited [14]. An example of such voltammogram is illustrated in Figure 2.2.
The cathodic deposition (negatively scanned direction) shows a cathodic peak at around -1.45 V vs. SCE (sat.), and the following plateau to around -1.80 V vs. SCE (sat.) indicates the potential range of Zn and Zn complex deposition [21]. The decrease in potential leads to an increased cathodic current and increased hydrogen evolution. Potentials below -1.8V vs. SCE (sat.) also hides the deposition potential range for Mn as the bubble formation at the electrode surface becomes excessive [6, 21]. The reduction peaks, and their relation, determine if co-deposition is possible. If there are no separation of the two reduction peak, both of the metals can be separately reduced at lower potential than the deposition potential of the less noble metal (here Mn). If there is a clear separation of the reduction peaks, the metals can be co-deposited at the deposition potential of the less noble metal [28]. The anodic scan reveals several peaks between -1.40 and -1.00 V vs. SCE (sat.), confirming that several phases have been deposited during the cathodic scan. These include Zn phases at potentials above -1.80 V vs. SCE (sat.), and Zn-Mn phases at potentials below -1.80 V vs. SCE (sat.) [6, 21].

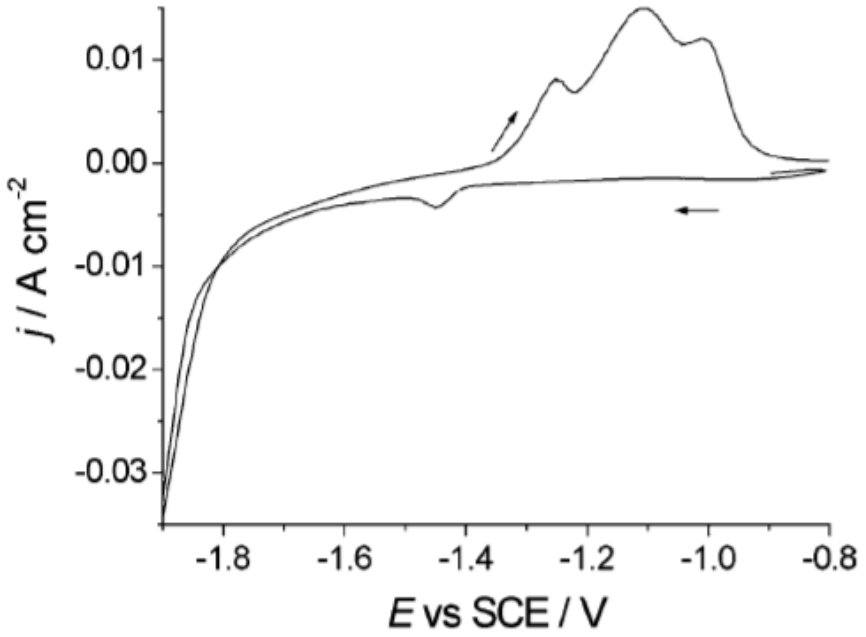

Figure 2.2: Cyclic voltammogram for a 35NCD16 steel electrode in alkaline Zn-Mn pyrophosphate based solution with sweep rate of 20 mV/s [21]

2.5 Aluminium

2.5.1 Surface properties

Aluminium provide several challenges regarding usage as substrate in plating processes. Aluminium oxide, Al_2O_3, is a chemically stable thin (2-3 nm thick) coating covering the metal surface. It forms when the metal is exposed to the atmosphere at room temperature [29, 30]. The oxide lack adhesive properties to metal coatings, and must be dealt with before subsequent deposition can occur [20, 29]. Aluminium possess a lower reduction potential than that of the two metals being plated (as shown in Table 2.1), making aluminium chemically reactive in most electrolytic baths as indicated by the Pourbaix diagram shown in the Appendix [18]. The electrochemical reactivity of aluminium in the electrolytic baths could aid the removal of the non-adhesive oxide layer, but several pre treatments are more common when working with aluminium [30, 31, 32].

2.5.2 Electroless pre treatment

Chemical etching of the aluminium surface is a possibility for removing the oxide layer an/or corrosion products. The process creates a rough and adhesive surface by a combination of dipping aluminium in concentrated acids or bases and accelerate and aid controlled

corrosion of the aluminium surface [33]. Chemicals used for etching aluminium include NaOH and $FeCl_3$. A downside with chemical etching include re-formation of the oxide layer when the aluminium is exposed to the atmosphere [29].

Zincate treatment is another process used for creating an adhesive surface for the aluminium substrate, and further making electroplating more accessible [20, 30, 32, 33, 34]. The zincate bath mainly consists of sodium NaOH and ZnO creating an alkaline environment. Additional additives can be included in the bath to increase he adhesion of zinc to the surface like $FeCl_3$ and $CuSO_4 \cdot 5H_2O$ [35]. Immersing aluminium in the alkaline bath aids with removing the oxide layer as aluminium becomes chemically active, and a thin metallic zinc layer is subsequently deposited on the aluminium surface [36]. The redox reactions are as following [20]:

$$\mathrm{Al(s)} + 3\mathrm{OH^-\,(aq)} \longrightarrow \mathrm{Al(OH)_3\,(s)} + 3e^- \tag{2.8}$$

$$\mathrm{Zn^{2+}(aq)} + 2e^- \longrightarrow \mathrm{Zn\,(s)} \tag{2.9}$$

The zinc layer provides with better adhesion to the later deposited coating, and also prohibit the aluminium oxide to form again [20]. Single zincate process creates large zinc deposits and leads to non-uniform surface. A double zincate treatment is therefore used, where the dipping step occurs two times in between an acidic etching step. Removing the first zincate layer creates a rougher and more adhesive surface for the next zinc layer to lay upon. Hydrogen evolution may occur as a side reaction in the zincating process [20].

2.5.3 Prior results with electrodeposition on Al

Both copper and cobalt have been successfully deposited on aluminium as a substrate [37, 38]. Similar with both experiments are the aforementioned pre-treatment of the aluminium metal surface with both chemical etching and zincate step [37, 38]. The oxide layer was reported to decrease the cathodic current compared to the etched surface, due to the increased conductivity when the etched surface was exposed to the electrolyte [38]. Deposition of metal through the oxide layer depends on factors including electronic conductivity and migration and diffusion of ions, and is complicated to examine due to breakdown of the oxide layer when hydrogen evolves and increase the pH locally [39]. Local increase in pH also affect the flux of metal ions to the substrate and decrease the cathodic current as hydroxide compounds form, and subsequently the metal ions available for deposition decrease [37, 38].

2.6 Zn-Mn co-deposition

Zn-Mn co-deposition has been successfully deposited on carbon steel as substrate in both acidic and alkaline baths [6, 7, 9, 10, 21, 22, 23]. Zn-Mn co-deposition is of interest due to its synergistic effect regarding corrosion resistance and environmental friendly nature of the two metals [9, 23]. The deposited coating illustrate passivating behaviour under different corrosive environments [23]. Two standard electrolytic baths have been of significant interest for the electrodeposition process; acidic and alkaline bath. These baths contain

metal salts of Zn and Mn in addition to additives for improved properties for the coating [6, 7, 9, 10, 21, 22, 23]

2.6.1 Acidic electrolyte and deposition

The Pourbaix diagram for Mn and Zn predict an area at low pH and potential where metal ions reduces to solid metal, making acidic environment interesting for Zn-Mn co-deposition [7, 9, 10, 18, 22, 23]. Typical baths for acidic Zn-Mn deposition contain Zn and Mn salts (usually chloride- or sulphate based), additional salt for increased conductivity, chemical for pH buffer and hydrogen evolution-inhibitor and additional additives for increased adhesion or reduction of potential gap [7]. pH used for the baths range in the acidic area between 3-5, and room temperature is widely used as increased temperature was reported to inhibit inclusion of the less noble metal, Mn, in the coating [7, 9, 10, 22, 40]. A summary of the different roles for the chemicals are shown in Table 2.2.

Table 2.2: Example of bath setup for acidic Zn-Mn co-deposition [10, 22, 23]

Chemical	Role
$ZnCl_2$/$ZnSO_4$	Zn-source
$MnCl_2$/$MnSO_4$	Mn-source
KCl/Na_2SO_4	Conductivity
H_3BO_3	pH buffer
Additive	Improved adhesion, reduced H_2-evolution etc.

2.6.2 Results from acidic deposition

Several important conclusions have been made from acidic Zn-Mn deposition. Increased Mn content in the electrolytic bath enables faster reduction of Mn^{2+}-ions and acts as inhibitor for Zn deposition, enabling a standard in the baths to include higher concentrations of Mn compared to Zn [10]. Increase of current density illustrate the same property, according to previous reports [10]. Several reported $\frac{[\mathrm{Mn}^{2+}]}{[\mathrm{Zn}^{2+}]}$ ratios have been used both with and without commercial additives, ranging from 3-8, with associated Mn content in the coating ranging from 1-27 wt. $\%$ [7, 9, 10, 22, 23].

Changing the salt from chloride based to sulphate based lowers the current efficiency due to increased deposition overpotential, but in addition increase the Mn content in the coating and decrease the crystal size [5]. The reported microstructure and adhesion from sulphate based electrolytes show smooth deposits at low current densities and becomes more heterogeneous as current density increases, while acidic based electrolytes are more adhesive and compact in a larger range of current densities [5]. Current efficiencies for acidic Zn-Mn deposition range from 60-95 $\%$ as the parasitic hydrogen evolution reaction takes place during deposition [7, 9, 10, 22, 23].

Oxygen in the air or water have the potential to react with the deposited metals on the

substrate, thus oxidizing the metals [41]. Experiments done without purging the bath reports that oxidised Zn and Mn species, in addition to oxygen bonded to the substrate, are present in the final coating using acidic electrolyte [7, 41]. These include oxides like ZnO, MnO, Mn_2O_3, Mn_3O_4 and MnO_2 [41].

2.6.3 Alkaline electrolyte and deposition

Zn-Mn co-deposition has been achieved in alkaline environment mainly including sulphate based chemicals and additives [6, 21, 22, 23]. The main purpose of the additive is to decrease the potential gap between the metals and prohibit precipitation of hydroxides and oxides [21, 22, 23]. Some additives known to contain these properties are pyrophosphate ($K_4P_2O_7$) and citrates [21, 22]. pH ranges from 9-10 in these baths, and room temperature is again chosen because of the aforementioned drawback with increased temperatures [6, 21, 22, 23]. A summary of the different roles for the chemicals are shown in Table 2.3.

Table 2.3: Example of bath setup for alkaline Zn-Mn co-deposition [10, 22, 23]

Chemical	Role
$ZnCl_2$/$ZnSO_4$	Zn-source
$MnCl_2$/$MnSO_4$	Mn-source
$K_4P_2O_7$/citrate	Hydroxide/oxide formation inhibitor
Additives	Oxidation inhibitors, reduced H_2-evolution

2.6.4 Results from alkaline deposition

Pyrophosphate based baths needs to include a $\frac{[{P_2O_7}^{4-}]}{[Mn^{2+}]}$-ratio larger than 18 to avoid precipitation of Mn-pyrophosphate double salt [21]. Further it was reported that $\frac{[Mn^{2+}]}{[Zn^{2+}]}$-ratio in alkaline bath should be close to 1 to get larger Mn content in the coating, in addition to more adhesive coating to the substrate [21]. Prohibition and delaying of Mn oxidation in the electrolytic bath is achieved with inclusion of reducing agent (ascorbic acid, hydroxylamine, sulphite etc.) [21, 22]. Current efficiencies for alkaline deposition of Zn-Mn are reported in the region of 20-30 $\%$ due to hydrogen evolution being more excessive in this type of bath [22].

2.6.5 Morphology and phases of Zn-Mn deposit

The morphology of the Zn-Mn alloy deposit depends on the applied current density and electrolyte for the deposition and can be mono-, bi- and triphasic in nature [5, 7, 10]. The changes in phases are mainly the result of changes in manganese content, as reports have stated that adjustment of temperature and stirring only influence the peak intensity of the phases [42]. Previous results have stated that small inclusion of Mn in the Zn matrices greatly change the morphology of the deposit [7].

Most results from acidic baths using DC setup confirm that increased applied current densities, while increasing the Mn content in the coating, tends to form a porous deposit due to increased hydrogen evolution [9, 10, 23]. Dendrite formation is also likely at high current densities, given the nucleation and growth process being under diffusion control [10]. Lower current density application gravitate towards more homogeneous and uniform deposit, including hexagonal crystals typical for Zn deposits [9, 23, 43]. The drastic changes in morphology for different Zn-Mn phases are highlighted in Figure 2.3. The morphology changes from a flower-like structure in (a), with large pure Zn, content to a more fine granular shape when the current density increases [7].

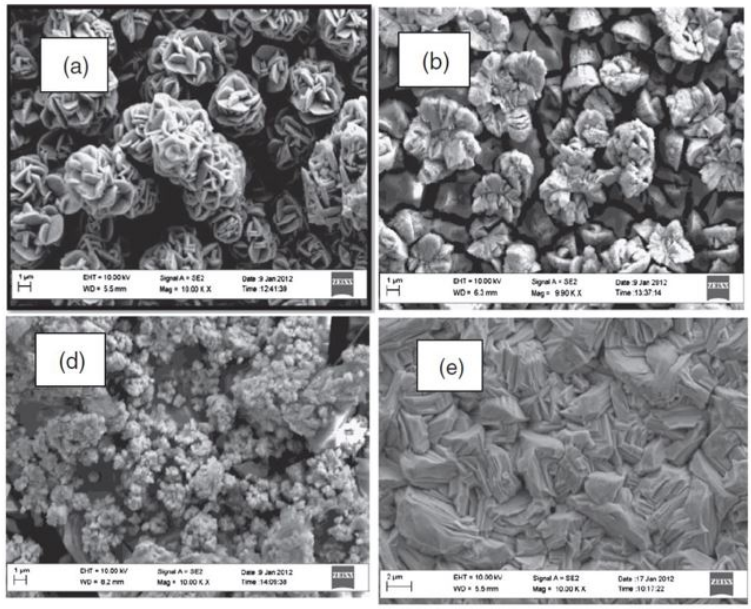

Figure 2.3: Scanning electron micrographs of Zn-Mn coatings deposited at various potentials from DC acidic chloride electrolyte (a) -1.65 V, (b) -1.7 V, (d) -1.75 V (all vs. SCE (sat.)) and (e) Zn deposit at current density of 15 $\mathrm{mA/cm^2}$ [7]

2.6.6 Zn-Mn deposition from pulse plating

Deposition of Zn and Zn alloys have been achieved with pulse plating before with carbon steel being applied as substrate [27, 42]. Pulse plating has been preferred over direct current as the high current densities needed in DC application for inclusion of relevant alloy metal, in this example Mn, leads to low current efficiencies [21, 23]. Both reduction potentials of Zn and Mn are below that of hydrogen evolution, so different pulse plating parameters are proposed for favouring the deposition of metal(s) [27]. Pulse plating reports for Zn-Mn deposition indicate monophasic alloy compared to bi-phasic deposit for direct current, and improved appearance compared to that of direct current [42]. Optimum properties from acidic EDTA-based Zn-Mn bath concluded that low pulse frequencies (10-

50 Hz), low duty cycles (0.25-0.5) and current densities over 20 $\mathrm{mA/cm^2}$ were needed for acceptable current efficiency and for inclusion of 25-40 wt $\%$ Mn [42].

2.6.7 Hydrogen evolution in pulse plating

The aforementioned hydrogen evolution competes with Zn and Mn deposition at higher current densities, and must be treated carefully for increased incorporation of wanted metal deposits [27]. Short pulses and low duty cycles are the factor contributing to pulse plating being a more beneficial deposition method, as less hydrogen is developed [44]. The anodic off-time eliminates the hydrogen, and with inclusion of $\mathrm{i_{an}}$ the hydrogen can be reduced within the deposited coating [27, 44].

2.7 Feasibility study of Zn-Mn deposition on aluminium

A feasibility study of whether co-deposition of Zn-Mn on aluminium was possible has been examined [45]. The study examined DC deposition for 60 s in two acidic and one alkaline bath. The chemical composition of the coating of the two acidic baths are shown in Table 2.4 and 2.5. The micrographs of the deposited coatings are shown in Figure 2.4 and 2.5. The alkaline bath showed no inclusion of either wanted metals [45].

Table 2.4: EDS elemental composition of deposited coating at centre at -1.50 V vs. Ag/AgCl (sat.) (DC) in acidic chloride electrolyte [45]

Element	Atomic percent [$\%$]
Al	0
Zn	59
Mn	6
O	35

Table 2.5: EDS elemental composition of deposited coating at centre at -1.50 V vs. Ag/AgCl (sat.) (DC) in acidic sulphate electrolyte [45]

Element	Atomic percent [$\%$]
Al	0
Zn	67
Mn	4
O	29

The Mn content from the study was lower than the reported Mn contents achieved using steel as a substrate with the similar bath [10, 46]. Large cathodic current applied for inclusion of Mn in the coating initiated large hydrogen bubble formation, leading to localised pH and what was thought of as hydroxide and oxide formation at the surface [45]. No further examination of the coating was done, leaving questions regarding the chemical composition of the deposits.

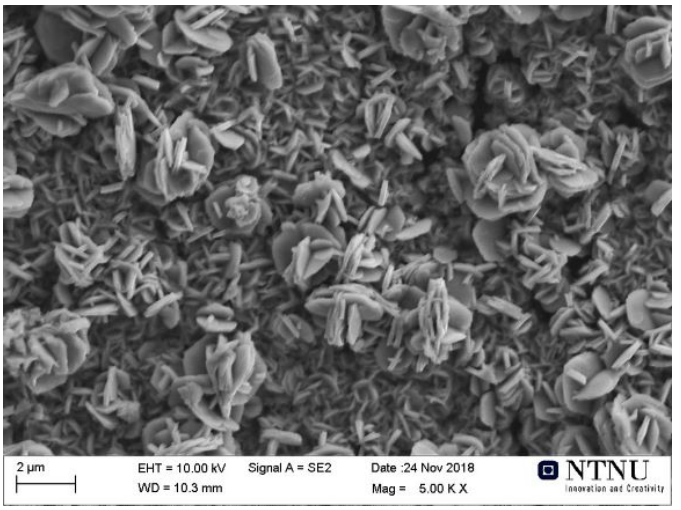

Figure 2.4: Scanning electron micrograph at the centre of deposited coating at -1.50 V vs. Ag/AgCl (sat.) (DC) in acidic chloride electrolyte (5KX) [45]

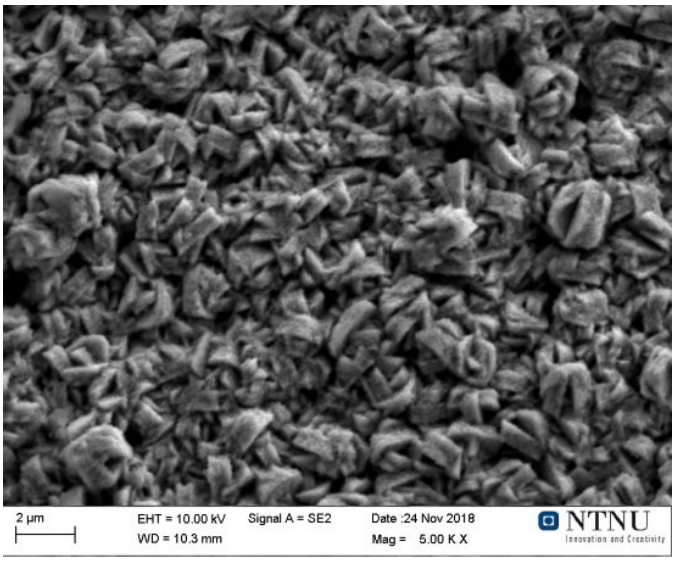

Figure 2.5: Scanning electron micrograph at the centre of deposited coating at -1.50 V vs. Ag/AgCl (sat.) (DC) in acidic sulphate electrolyte (5KX) [45]

Chapter 3

Experimental

3.1 Pre-treatment

The aluminium specimen used as substrate was made of the 9153 aluminium alloy. The chemical composition of the bulk given in wt. % is given in Table 3.1. The alloy was cut in the following dimension with a MiniTom cutter: 4 cm height x 2.5 cm length x 0.1 cm width.

Table 3.1: Chemical composition of 9153 aluminium alloy (wt. %)

Al	**Mn**	**Fe**	**Si**	**Ga**	**Zn**	**Ti**	**V**	**Zr**
98.88	0.91	0.09	0.04	0.02	0.02	0.02	0.01	0.01

The aluminium substrate was chemically etched with the aforementioned zincate method for obtaining zinc-rich adhesive surface properties. The zincate bath composition is displayed in Table 3.2. The zincating procedure was as following [36]:

- Dip in zincate bath for 30 s
- Rinse in distilled water
- Chemically etching in concentrated HNO_3 (60 %) for 60 s
- Rinse in distilled water
- Dip in zincate bath for 30 s
- Rinse in distilled water
- Blow dry at 50 °C

Table 3.2: Zincate bath [32]

Chemical	Concentration [mol/L]
NaOH	4.25
ZnO	0.61

The backside of the zincated aluminium surface was nail polished for smaller active surface area and thus easier control of deposition parameters. The nail polish was also applied below the sample to block the tube holes below, as illustrated in Figure 3.1, and further block a potential large surface area for deposition in addition to hindering hydrogen evolution inside the tube.

Figure 3.1: Multi-port extruded tubes [1]

3.2 Bath composition

Two baths were prepared as electrolytic baths for deposition: one alkaline and one acidic. All chemicals are laboratory grade, and the pH used for the baths is noted in the bath description.

3.2.1 Alkaline pyrophosphate based

The alkaline pyrophosphate bath is described in Table 3.3. pH was changed with H_2SO_4 [21].

Table 3.3: Alkaline pyrophosphate electrolyte at pH = 10 for Zn-Mn electrodeposition [21]

Chemical	Concentration [mol/L]
$ZnSO_4 \cdot 7H_2O$	0.05
$MnSO_4 \cdot H_2O$	0.05
$K_4P_2O_7$	1
L – ascorbic acid	0.01

3.2.2 Acidic sulphate based bath

The acidic sulphate bath is described in Table 3.4. pH was adjusted with H_2SO_4 [46].

Table 3.4: Acidic sulphate electrolyte at pH = 2 for Zn-Mn electrodeposition [46]

Chemical	Concentration [mol/L]
$ZnSO_4 \cdot 7\,H_2O$	0.3
$MnSO_4 \cdot H_2O$	1
Na_2SO_4	1.25
H_3BO_3	0.4

3.3 Cyclic voltammetry

Determination of electrode reactions at the aluminium surface were determined with the use of cyclic voltammetry. A Gamry Potentiostat with added program software was used for electrochemical measurements. The scanning rate chosen was 10 mV/s and the anode used was a zinc plate with similar dimensions as the cathode. For both baths the starting potential for the cathodic scan was chosen as -0.2 V vs. Ag/AgCl (sat.) since no reduction reaction was expected to take place [18]. The potential was swept down to -2.0 V vs. Ag/AgCl (sat.), or until maximum current possible to apply from the potentiostat (819 mA) was reached, before the potential was reversed back to -0.2 V vs. Ag/AgCl (sat.). The zincated part of the surface was the only part of the sample that was in contact with the electrolyte to try minimise corrosion of aluminium and mimimise introducing foreign ions [35].

3.4 Electrochemical deposition

Direct current deposition was realised with galvanostatic deposition software on the Gamry Potentiostat. The setup for pulse current was customized for the specific currents and duty cycles needed, and the setup is presented for each sample. The total pulse current was created by cycling the specific cathodic and anodic current until the designated deposition time was reached. The bath was stirred in between depositions for both current applications, but not during deposition. After deposition the samples were dried with a heat gun at 50°C for 2-3 min.

3.5 SEM and EDS

Zeiss Supra 55-VP Low Vacuum Field Emission Scanning Electron Microscopy (LVFE-SEM) was applied for morphological analysis of the deposited coating. The associated energy-dispersive x-ray spectroscopy (EDS) was utilized for chemical characterisation of the deposit. All micrographs and chemical analysis are from the Zeiss Supra 55-VP. The excitation energy chosen was 15 keV for all EDS analysis, given that aluminium, Zn and Mn all contained characteristic x-ray energies below this value [47]. Point analysis of the whole area displayed in the micrograph was chosen for analysing the recorded SEM micrograph, and the analysing time was set for 50 s for all samples.

3.6 GD-OES

The samples were analysed with a glow discharge optical emission spectroscopy (GD-OES) for chemical depth profile of the deposited coating on the aluminium surface. The samples were analysed for 3 min, and a customary Al-Zn standard for detection of the wanted elements was used for all samples.

3.7 Raman spectroscopy

Witech Alpha 300 Raman spectroscope was utilized for all documented Raman spectra. The laser power was set to 65 mW, and Zeiss EC Epiplan 50x lens and working distance of 1 mm was used for all samples. All Raman spectra arrives from the Witch spectroscope.

Chapter 4

Results and discussion

4.1 Method for analysing the results

Method used for analysing the results of the produced coatings are described below.

- Cyclic voltammetry (CV) of the chosen electrolyte is discussed, highlighting areas of interest for electrodeposition
- The current transient from deposition for the samples is commented
- The morphology and chemical composition (EDS) of the sample is displayed and analysed. All EDS spectra for analysed samples are placed in the Appendix. Foreign elements with detected at. $\%$ lower than 0.05 are neglected in the Tables highlighting the chemical composition.
- GDOES and Raman spectrum of interesting samples are shown and further discussed with regards to chemicals present in the coating. All Raman spectra and EDS analysis are taken from an area right beside the hole created by the sputtering argon ions from the GDOES analysis
- Current efficiency (CE) and thickness of coating are commented. All CE calculation are based on 100 $\%$ deposited Zn for simplicity, and are shown in the Appendix
- Plating processes for the different electrolytes are discussed, and both electrolytes and plating processes are compared at the end

All pulse current samples and resulting Figures/Tables are presented with the constructed i_{avg}. DC samples are presented with the initial potential chosen for deposition. If not stated, the area analysed is taken from the centre.

4.2 Zincate pre treatment

The zincating step, conducted as described in Section 3.1, was analysed for determination of contribution of chemical composition underneath the later deposited coating. Morphological analysis of the surface was established by the author in a previous study using similar pre treatment setup. A qualitative measurement of the chemical composition was therefore done with EDS, GDOES and Raman spectroscopy. Chemical composition of the zincated surface is shown in Table 4.1, and GDOES and Raman spectrum of the zincated sample are displayed in Figure 4.1 and 4.2

Table 4.1: EDS elemental composition of the zincated surface

Element	Atomic percent [%]
Al	83
Zn	4
Mn	0
O	13

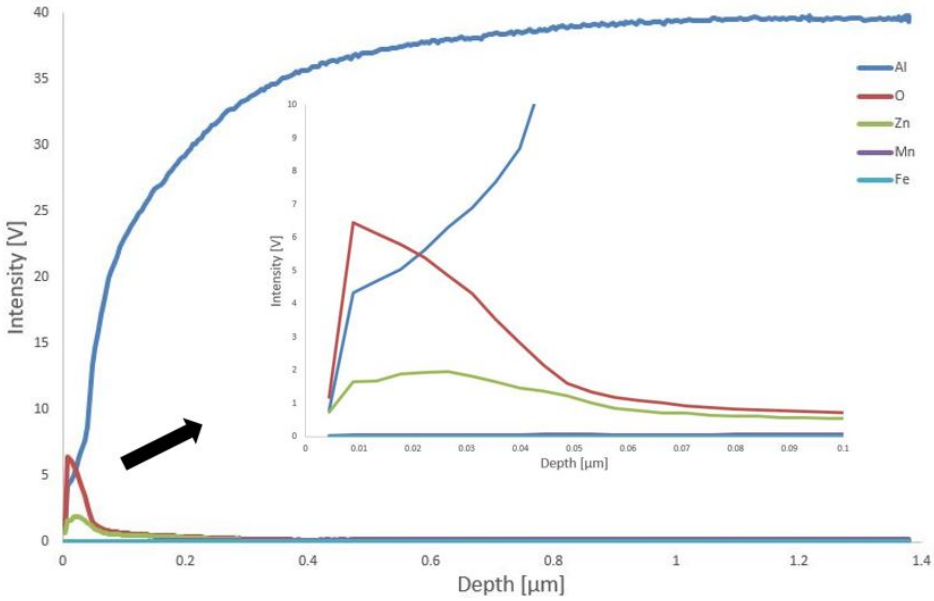

Figure 4.1: GDOES elemental depth profile of zincated aluminium sample

The ratio between Zn and oxygen is around 1:3, shown in Table 4.1, indicating that oxygen rich compounds have deposited on the surface. Hydroxide could be a compound, as deposit at the aluminium surface is a result of hydrogen evolution, creating high local pH at the surface and further formation of hydroxide [9, 43]. GDOES analysis shown in Figure 4.1 confirm that the deposited zinc from the zincate step have oxidised, as the oxygen

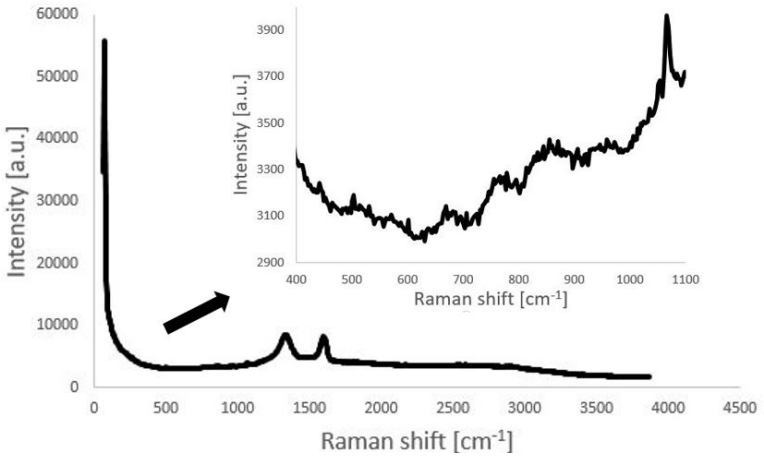

Figure 4.2: Raman spectrum of zincated aluminium surface

and zinc profile follows the same pattern to a depth of around 0.3 μm. Reduction of Zn concentration in the zincate bath is factor playing into this as the bath was reused several times for zincating several samples. Reduction of zinc concentration in the bath leads to oxidation of Al to $\mathrm{Al(OH)_3}$ being the dominating reaction at surface and could explain the high oxygen level found from the EDS analysis in Table 4.1 [35, 36].

Raman spectrum shown in Figure 4.2 illustrates two large peaks at around 1380 and 1590 $\mathrm{cm^{-1}}$ are correlated to amorphous sp2-containing carbon components [48]. This is a result from degradation of carbon from the nail polished coating, as some coating was observed to be torn down during electrodeposition, or degradation of $\mathrm{CO_2}$ in the electrolyte [48]. The enhanced figure shows several smaller peaks in the range of 500-1100, showing possibilities for ZnO composited deposit [49, 50]. Hydroxides are not a dominant species on the surface according to the Raman spectrum, as hydroxides typically show peaks in ranges of 3100 $\mathrm{cm^{-1}}$ and up [49, 51]. The results does not rule out the possibility of hydroxides in the coating, but suggest that the thickness of chemical concentration is too low to be detected by the Raman setup. No dominant peaks in the range between 400-570 $\mathrm{cm^{-1}}$ also rule out $\mathrm{Al_2O_3}$ [52], thus highlighting that the pre treatment have worked. The spectra makes it difficult to pinpoint exact chemical composition on the surface of the zincated surface, but for further examination of the coated samples a coating thickness of 0.3 $\mu\mathrm{m}$ was established as base from the zincated surface.

4.3 Alkaline pyrophosphate electrolyte

4.3.1 Visual inspection of electrolyte and CV scan

Visual inspection of the two samples with same electrolyte after different time had passed are shown in Figure 4.3 and 4.4. The inspection illustrated a problem with Mn based electrolyte, namely oxidation of Mn^{2+} to Mn^{3+} [21]. This further leads creation of Mn^{3+}-pyrophosphate complexes, as they are stable in most Mn concentrations and pH [53]. The problem was solved by using L-ascorbic acid as reducing agent in the electrolyte [21].

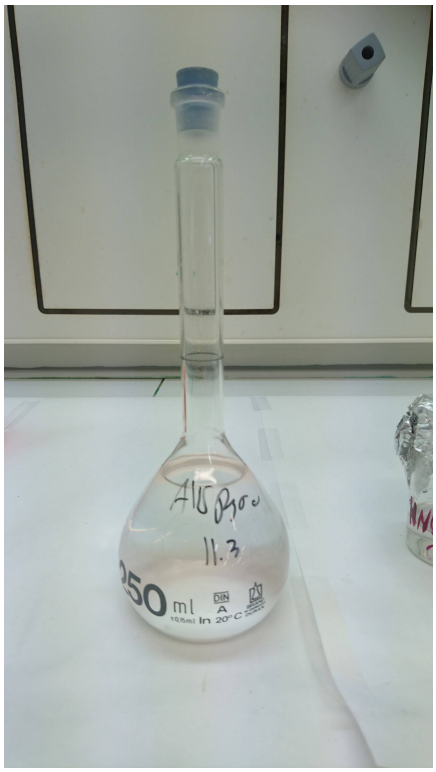

Figure 4.3: Visual inspection of bath a) after 1 day

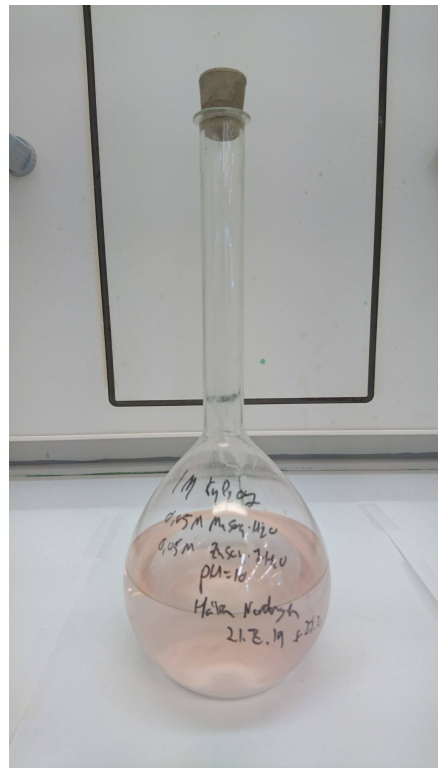

Figure 4.4: Visual inspection of bath b) after 1 month

CV scan of the zincated aluminium sample was conducted in alkaline pyrophosphate electrolyte for determination of potential deposition range for Zn and Mn deposition. Two electrolytes were compared to each other; one electrolyte that had stood out for a day (bath a)) and one for a month (bath b)). The voltammogram is shown in Figure 4.5.
Change in chemical composition in the electrolyte illustrates the effect of complex formation on deposition factors. The 1 month old electrolyte (bath b)) shows a steeper increase in current densities for lower potentials than that of the 1 day old electrolyte (bath a)). For

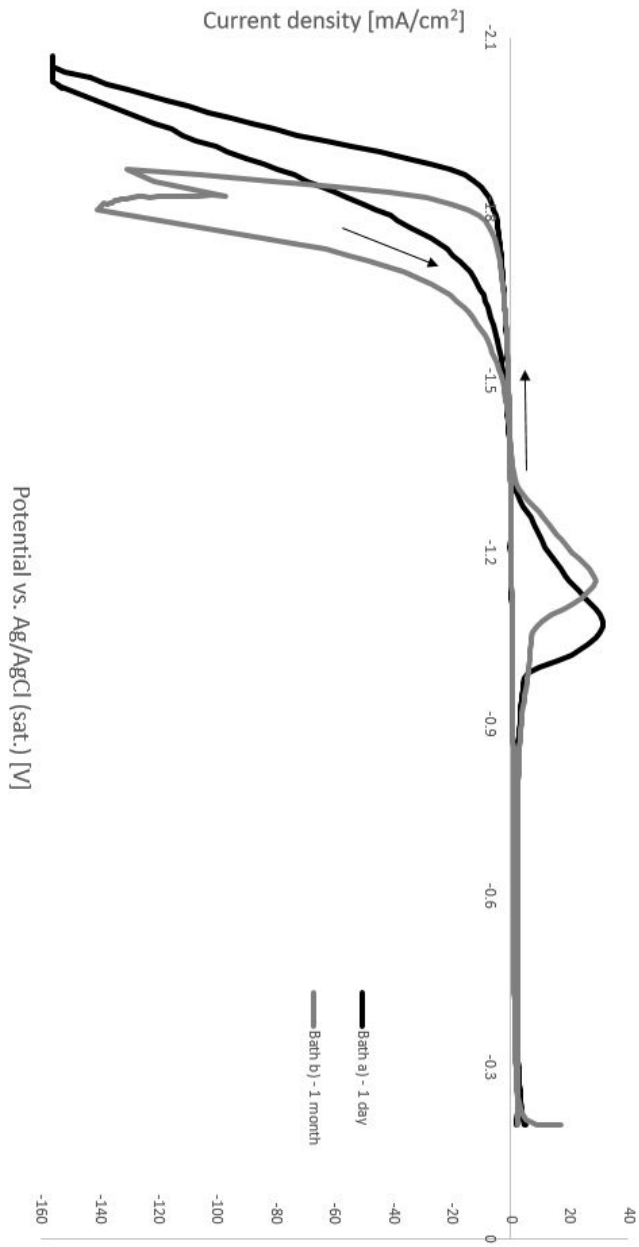

Figure 4.5: CV scan of zincated aluminum sample in alkaline pyrophosphate electrolyte

the deposition potential of Zn in alkaline environment at pH = 10 (-1.40 V vs. Ag/AgCl (sat.)) both electrolytes illustrate increased cathodic current density as Zn deposition is initiated. Increased current density initiate proton reduction and hydrogen evolution [21].

Availability for Mn^{2+}-ions available for reduction in bath b) is lower given the complex formation [53]. This result factors into bias for proton reduction and hydrogen evolution at lower potentials, thus drastically increasing the current density at lower potentials for the Mn^{2+}-limited bath b). The trend have been reported before when changing with the concentration of metal ions [10].

No clear reduction peaks are observed in the voltammogram, thus making the choice for potential selection tricky. However several studies analysing Zn-Mn cyclic voltammograms have stated that the Mn reduction peak is hiding behind the drastic cathodic current increase constructed by hydrogen evolution [10, 21]. Potentials chosen for deposition, and the associated cathodic current densities, were therefore chosen from the Mn^{2+}-rich bath a) at potentials lower than -1.70 V vs. Ag/AgCl (sat.). The potential is close to the one found in the same electrolyte on steel substrate at -1.65 V vs. Ag/AgCl (sat.) [21]. Recorded anodic peaks from the anodic scan suggest that the cathodic current applied initiated deposit of several phases during DC application [9, 21, 46].

Observation of deposited coating after deposition

A macroscopic illustration of the deposited coating on the zincated aluminium substrate is illustrated in Figure 4.6.

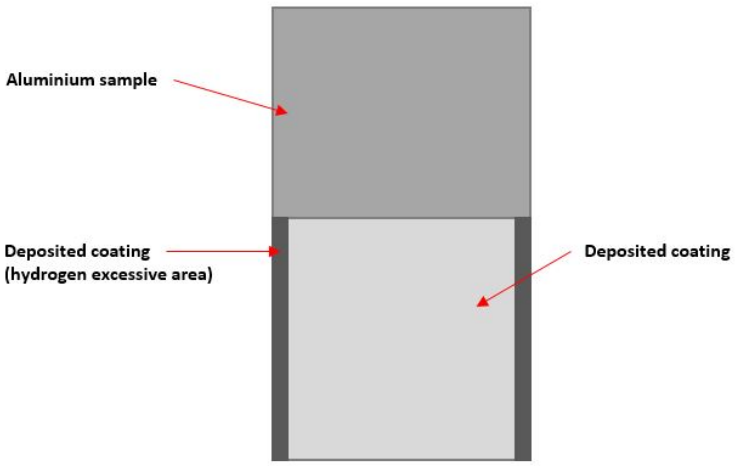

Figure 4.6: Schematic of deposited coating on zincated aluminium substrate

Hydrogen evolution was mostly excessive during the deposition at the edges of the sample, illustrated in the Figure 4.6 with dark coloring. The centre experienced less hydrogen evolution, and was the reference for all measurements with the Ag/AgCl (sat.) reference electrode. Observation of this change in color, and change in chemical composition, points to an estimated error for the documented current densities over the whole sample. Increased current density leads to larger hydrogen evolution, thus suggesting that the edges of the

sample experience larger current densities than the centre [12]. Similar observation was also made for the acidic sulphate electrolyte.

4.3.2 Direct current (DC)

Testing of plating techniques in alkaline pyrophosphate electrolyte (bath a) were conducted, starting with direct current (DC). Two samples was made with DC application for alkaline pyrophosphate electrolyte. The deposition time was set for 60 s, and the potential used were chosen in the hydrogen dominant region of the fresh electrolyte from the CV scan in Figure 4.5 where the Mn-deposition was believed to be masked. All results from the DC application in this setup are taken from the centre of the sample (illustrated in Figure 4.6).

Sample 1: -1.80 V vs. Ag/AgCl (sat.) (DC)

The current transient for DC deposition at -1.80 V vs. Ag/AgCl (sat.) is shown in Figure 4.7.

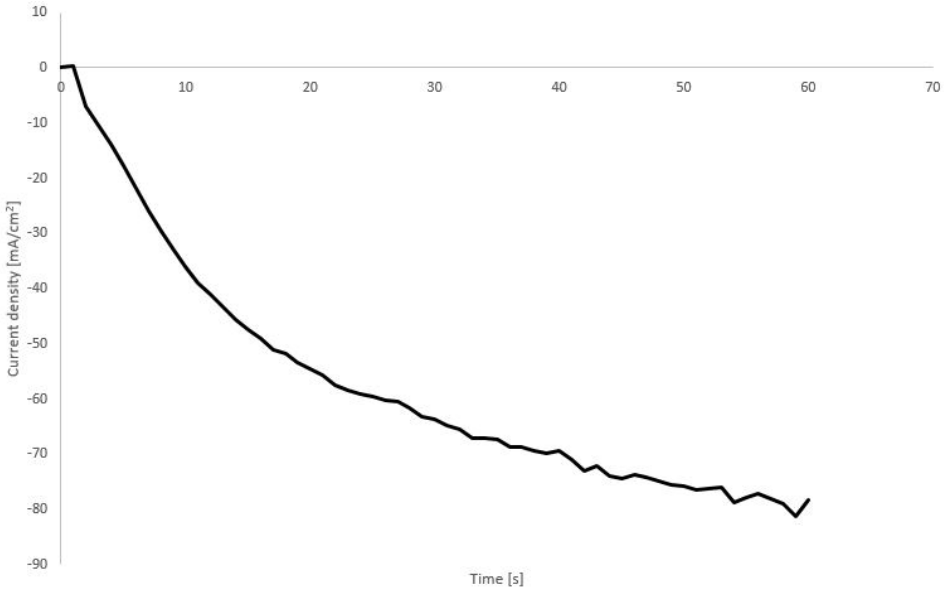

Figure 4.7: Current transient of direct current deposition in alkaline pyrophosphate electrolyte at -1.80 V vs. Ag/AgCl (sat.)

Observation of heavy hydrogen evolution at the left and right side of the aluminium sample, and low hydrogen evolution at the centre of the sample, was made for this deposition. Current transient was recorded from the centre of the sample. The current density documented exceeds the value related to -1.80 V vs. Ag/AgCl (sat.) found from the CV scan in Figure 4.5 (around 50 $\mathrm{mA/cm^2}$).

Initial decreasing trend for the curve comes from charging the double layer [7]. However a maximum current density in the cathodic direction, and subsequently a plateau which is typical for diffusion limited deposition, is not present indicating that Zn and Mn may not co-deposit. The steadily increased current density during deposition indicate formation of oxygen rich compounds like hydroxides and oxides, and Mn^{3+}-pyrophosphate complexes, making the electrolyte inaccessible for steadily deposit Zn. For the exact same electrolyte it was reported that potentials below -1.70 V vs. Ag/AgCl (sat.) was needed for Zn-Mn co-deposition, with only 0.5 at. % of Mn reported in the coating [21].

The deposited coating was examined at the centre with SEM, EDS, GDOES and Raman spectroscopy. The SEM micrograph, EDS analysis, GDOES and Raman spectrum are shown in Figure 4.8, Table 4.2, Figure 4.9 and Figure 4.10 respectively.

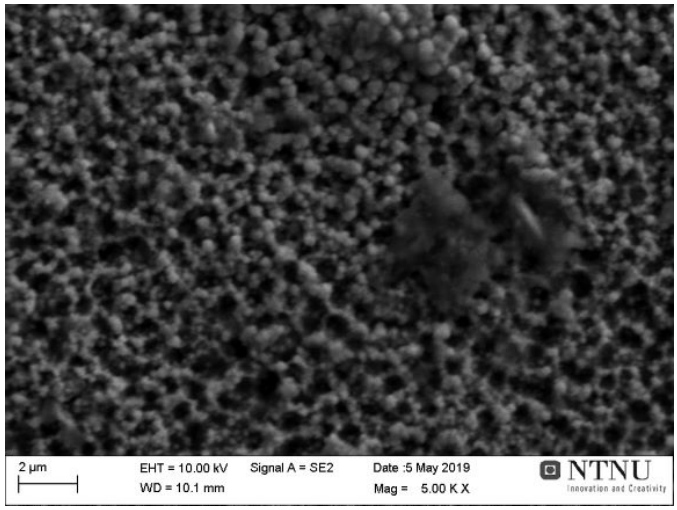

Figure 4.8: Scanning electron micrograph at the centre of deposited coating at -1.80 V vs. Ag/AgCl (sat.) (DC) in alkaline pyrophosphate electrolyte (5KX)

Table 4.2: EDS elemental composition of deposited coating at the centre at -1.80 V vs. Ag/AgCl (sat.) (DC) in alkaline pyrophosphate electrolyte

Element	**Atomic percent w/ Al [%]**	**Atomic percent wo/ Al [%]**
Al	31	0
Zn	28	41
Mn	11	16
O	27	39
K	3	4

Deposits of small, even sized deposits make up the deposit illustrated in Figure 4.8. Clusters of deposits are observed, and some pore formation indicate non-compact coating [21].

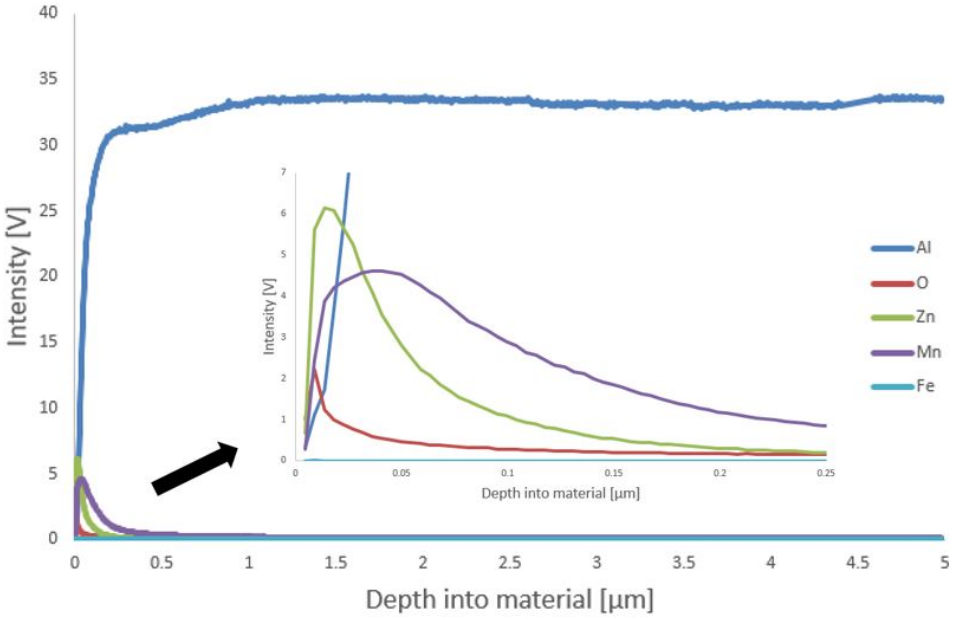

Figure 4.9: GDOES elemental depth profile of deposited coating at the centre at -1.80 V vs. Ag/AgCl (sat.) (DC) in alkaline pyrophosphate electrolyte

EDS analysis, displayed in Table 4.2, confirm that complex formation and oxygen-rich deposits have been deposited in the coating with the inclusion of oxygen and K. Different phases predicted deposited by the anodic CV scan are confirmed as Zn, Mn, oxygen and potassium have been included in the final coating. Potassium arrive from pyrophosphate complex, mainly from reaction with Mn to form Mn-pyrophosphate complexes [53]. Inclusion of complex formation at the coating surface act as inhibitor for further growth of nuclei, forcing new nuclei to form instead [54].

GDOES analysis illustrated in Figure 4.9 shows that the oxygen deposited is mainly located at the top surface showing a peak at around 0.01 μm. Oxidation of Zn or Mn is the reason for this trend since both metals follow the the oxygen profile at the coating surface [55]. Mn have been reported to be easily oxidise in electrolytes containing oxygen, and in addition to the darker color at the edge support the metal oxidation claim [7, 10]. Mn content is present throughout the entire coating, indicating that Mn have been deposited in between the Zn deposits and not only at the top surface.

Raman spectroscopy shown in Figure 4.10 shows, in addition to the aforementioned carbon peaks at 1380 and 1590 cm^{-1}, one large peak at around 660 cm^{-1}. The peak pinpoints towards Mn-O bonds, more specifically $\mathrm{Mn_3O_4}$ [56, 57, 58]. This corresponds well with the Mn content found, depth profile shown in Figure 4.9 and previous resulted oxidation properties for Mn [41].

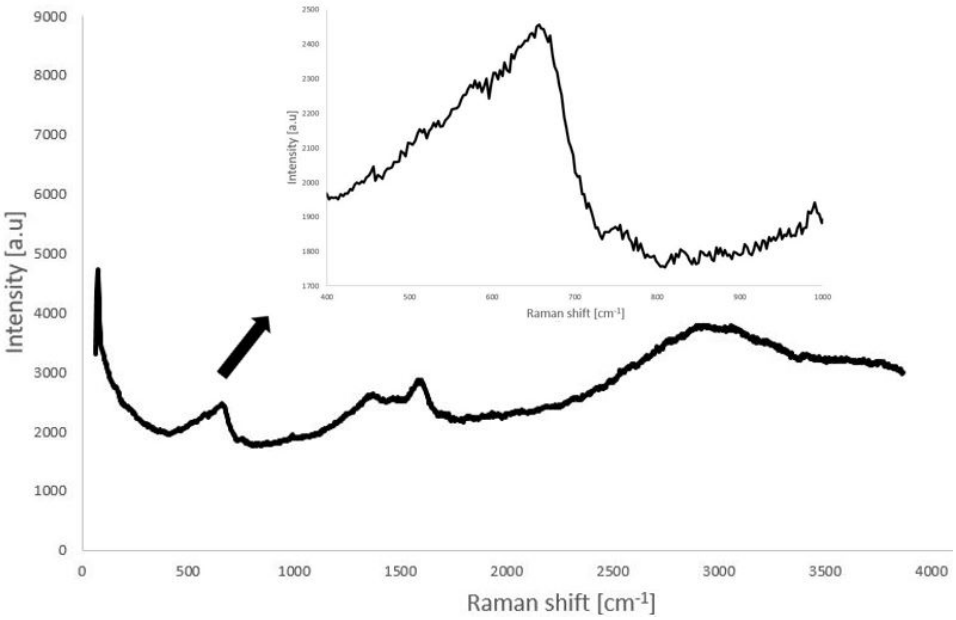

Figure 4.10: Raman spectrum of deposited coating at the centre at -1.80 V vs. Ag/AgCl (sat.) (DC) in alkaline pyrophosphate electrolyte

Factors contributing to a current efficiency (CE) of 51 $\%$, found from calculation in the Appendix, include hydrogen evolution at longer time, complex formation and thus further inhibition of metal deposit and growth [6, 21]. CE found suggest that the zincated surface pre treatment applied on the substrate aided with adhesion of new deposits. Theoretical thickness of 1.15 μm and an approximate thickness of around 1.1 μm correlate closely to the CE found. Inclusion of oxygen bound components in the coating contribute to the error in the coating thickness, as the calculation of pure Zn was used [24].

Sample 2: -1.90 V vs. Ag/AgCl (sat.) (DC)

The current transient for DC deposition at -1.90 V vs. Ag/AgCl (sat.) is shown in Figure 4.11.

Initial decrease in current density is from charging the double layer at the metal surface. The constant region at -155 $\mathrm{mA/cm^2}$ is due to the program reaching the maximal current possible, indicating that for the chosen potential a sharp decrease for lower potentials was tried to be achieved. Further decrease in cathodic current density results from growth of phases and increase in nuclei at the substrate surface [10]. Cathodic current density does not reach a diffusion-controlled plateau during the 60 s of deposition which corresponds to around -100 $\mathrm{mA/cm^2}$ found from the CV in Figure 4.5. A rough Zn-Mn deposited coating is a possible result for this sample as near maximum cathodic current achievable

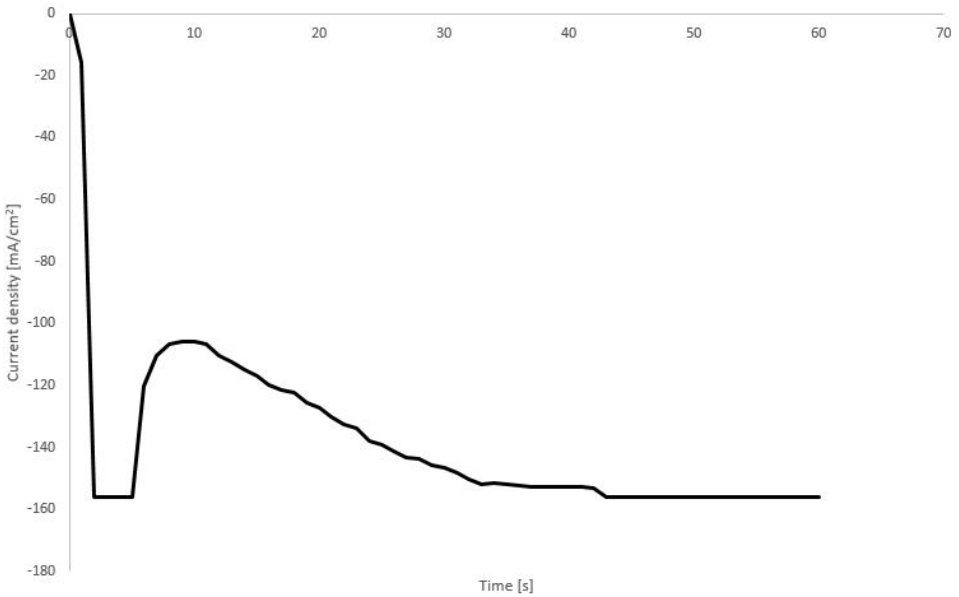

Figure 4.11: Current transient of direct current deposition in alkaline pyrophosphate electrolyte at -1.90 V vs. Ag/AgCl (sat.)

is utilised during the current transient [5].

SEM micrograph, EDS analysis, GDOES and Raman spectrum of the sample are shown in Figure 4.12, Table 4.3, Figure 4.13 and Figure 4.14 respectively.

Table 4.3: EDS elemental composition of deposited coating at the centre at -1.90 V vs. Ag/AgCl (sat.) (DC) in alkaline pyrophosphate electrolyte

Element	**Atomic percent w/ Al [%]**	**Atomic percent wo/ Al [%]**
Al	24	0
Zn	46	61
Mn	9	12
O	20	27
K	0	0

Morphology of the deposit, displayed in Figure 4.13, shows more uneven distribution for deposition sizes in the coating. The deposits also displays larger degree of clustering compared to Sample 1. Change in morphology compared to Sample 1 suggest that Zn-Mn have co-deposited [7]. Influence of hydrogen bubbles on disturbance of uniform distribution of deposits have been reported for the similar electrolyte before, and also explain the unevenness [23]. The coating is expected to be less compact and uniform when compared to Sample 1 as the deposits are more clustered.

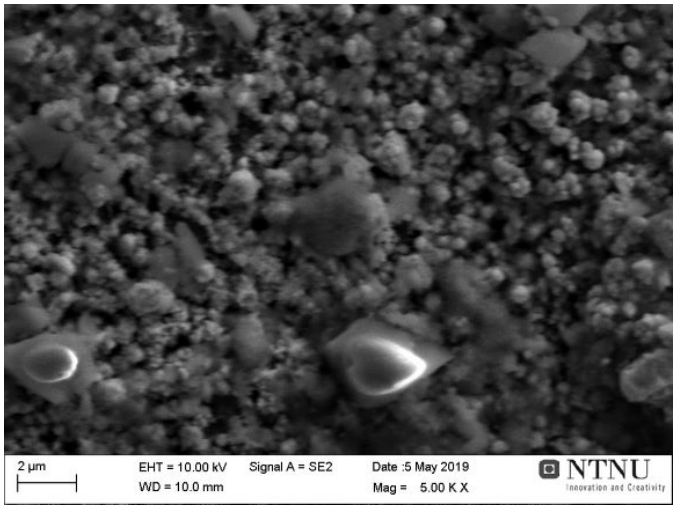

Figure 4.12: Scanning electron micrograph at the centre of deposited coating at -1.90 V vs. Ag/AgCl (sat.) (DC) in alkaline pyrophosphate electrolyte (5KX)

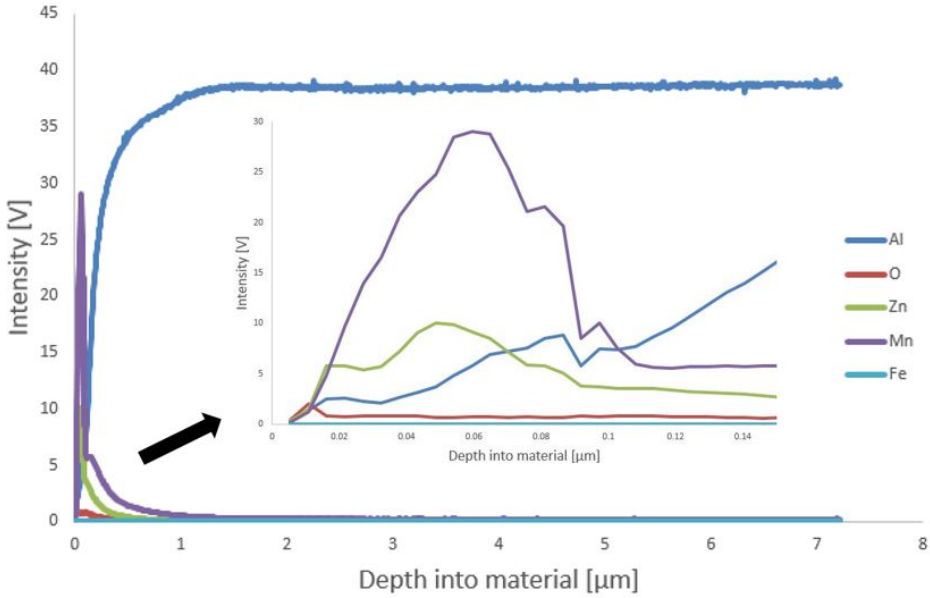

Figure 4.13: GDOES elemental depth profile of deposited coating at the centre at -1.90 V vs. Ag/AgCl (sat.) (DC) in alkaline pyrophosphate electrolyte

EDS analysis from Table 4.3 highlight several changes when compared to Table 4.2. Firstly the Al content have decreased, and thus illustrating a thicker coating. This is to

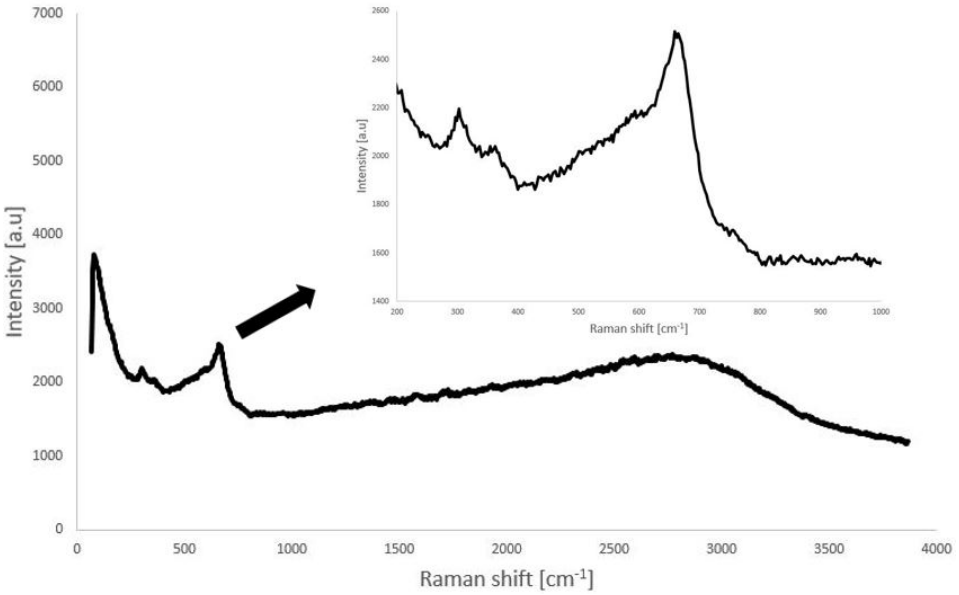

Figure 4.14: Raman spectrum of deposited coating at the centre at -1.90 V vs. Ag/AgCl (sat.) (DC) in alkaline pyrophosphate electrolyte

be expected by applying larger current densities in relation with Faradays law showed in Equation 2.4 [24].

Increased applied cathodic current density have lead to increased Zn content and decreased Mn content, according to Table 4.3. This result has been reported before and is attributed to inhibition effect from the hydrogen evolution reaction [7, 10, 21]. Reports also suggest that Mn content remain stable at high current densities, and that detachment of Zn-Mn alloys in form of powder is evident as the CE decrease at large applied cathodic current densities [7, 10]. Increased Zn content arrive from Zn-Mn co-deposition and the aforementioned Mn content limitation, explaining the reduced oxygen content as less Mn have oxidised at the coating surface [7, 10, 21, 41].

Results from GDOES analysis shown in Figure 4.13 illustrate a coherent trend between Zn and Mn, as both metals peak at around 0.05 μm into the coating [59]. This indicate co-deposition of the two metals, as similar GDOES trend has been observed for alloy coatings [55]. The concentration profile of Mn does not correlate with the chemical composition of the coating found in Table 4.3. The Mn profile suggest far larger Mn content than Zn, and much lower oxygen content than displayed in the GDOES analysis. GDOES analysis in Figure 4.13 shows that Al content does not reach bulk concentration before 1 μm, and that Al is integrated into the coating. A possibility for this incoherence is large chemical difference between GDOES analysis and the spot analysed from EDS. The thickness of the coating is around 1.3 μm, and does not correlate well with the theoretical thickness of

1.82 μm calculated from CE of 32 %. Uncertainty from the validity of the GDOES analysis is factoring this error. Decreased CE compared to the other DC sample is expected as a result from the increased hydrogen evolution occurring at the higher current densities [23].

No carbon peaks are observed from the Raman spectrum in Figure 4.14, but several peaks are observed at the Raman shift range of 300-700 cm^{-1}. The large peak at approximately 660 cm^{-1} correlates to the $\mathrm{Mn_3O_4}$ as with the previous case [46, 56, 57, 58]. Two peaks, at 300 and 350 cm^{-1}, were not present in the previous DC sample in alkaline pyrophosphate electrolyte. $\mathrm{MnO_2}$ peaks are dominant in this range and can, together with the oxygen content found from the EDS analysis, explain why the new dominant peaks have arrived [60]. The result from these peaks and the EDS analysis emphasizes that the GDOES analysis shown in Figure 4.13 is incorrect, or do not represent the analysed area.

Comparison between DC samples in alkaline pyrophosphate electrolyte

Alkaline pyrophosphate electrolyte have successfully included Mn during DC deposition, but the oxygen content still remains as a parasitic intruder in the coating. Current densities applied for the electrolytes are sufficient for Mn inclusion, but at a cost of low current efficiencies as a result of the parasitic hydrogen evolution reaction (51 % and 32 % for Sample 1 and 2 respectively).

As with previous results for the same electrolyte the Mn inclusion reaches a maximum content. For this setup that current density is lower than 140 $\mathrm{mA/cm}^2$. Additional Mn is included in the coating by analysing cathodic current densities between 60 and 140 $\mathrm{mA/cm}^2$. Non uniformity of the coating illustrated in Figure 4.12 from the SEM micrograph for Sample 2 suggest less homogeneous and rough coating for larger $\mathrm{i_{cath}}$ applied. Change in morphology from Mn inclusion in Zn matrix have been reported before, and together with the GDOES trend of Zn and Mn suggest Zn-Mn co-deposition [21].

Inclusion of the pyrophosphate in the electrolyte provided several challenges. Potassium in it self may be included in the final coating and hinder growth the deposits, as shown with Sample 1 in Figure 4.8. However it was a necessity to include pyrophosphate in the electrolyte for preventing hydroxide formation. Overall the inclusion can be justified as Zn and Mn were able to be deposited.

Deposition time of 20 s was used for the rest of the samples, partly to decrease the effect hydrogen had on the substrate in addition to closely simulate realistic deposition time.

4.3.3 Pulse plating (PC) - changing frequency

Reportedly less hydrogen exposure on the substrate, in addition to the proposed advantages using pulse plating, made this setup an interesting choice for electrodeposition [27, 42]. Frequencies for good Zn-Mn inclusion in deposited coating in acidic electrolyte was reported between 10-50 Hz [42]. Four experiments were conducted in alkaline pyrophosphate electrolyte to see if Zn and Mn were able to be included in similar fashion. The two first samples (Sample 3 and 4) looked at different frequencies.

Sample 3: 48 mA/cm^2 (PC, 10 Hz)

The first sample used a pulse frequency of 10 Hz. PC setup for the deposition is displayed in Figure 4.15, showing two cycles. Cathodic current density chosen was expected to include Mn following the behaviour from the CV scan in Figure 4.5. Key deposition parameters are shown in Table 4.4. All average current densities were calculated using Equation 2.7. Deposition setup was cycled 200 times giving a deposition time of 20 s.

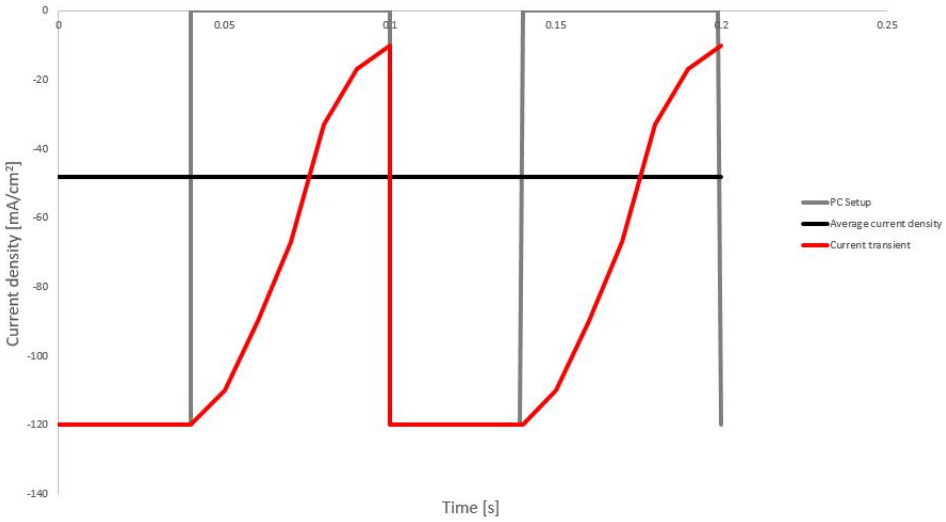

Figure 4.15: Setup for PC plating at 48 $\mathrm{mA/cm^2}$ (10 Hz) in alkaline pyrophosphate electrolyte

Table 4.4: Key values for PC setup giving i_{avg} = 48 $\mathrm{mA/cm^2}$ (10 Hz) in alkaline pyrophosphate electrolyte

t_{off} [s]	t_{on} [s]	t_{cycle} [s]	i_{an} [$\mathrm{mA/cm^2}$]	i_{cath} [$\mathrm{mA/cm^2}$]	i_{avg} [$\mathrm{mA/cm^2}$]
0.06	0.04	0.1	0	-120	-48

The current transient shown in Figure 4.15 shows the limitation of the setup with Gamry Potentiostat with setting up pulse plating. The potentiostat needs longer t_{off} to reach the anodic current density. The proposed current density experienced for this sample is therefore larger than the constructed one. Lower anodic currents at longer t_{off} have been reported to favour incorporation of the both metals as refilling of metal ions of the cathode surface is favoured [42, 54].

SEM micrograph of the deposited coating is shown in Figure 4.16. The EDS analysis and GDOES depth profile is displayed in Table 4.5 and Figure 4.17 respectively.
The SEM micrograph in Figure 4.16 clearly shows large hexagonal plates, which is associated with pure Zn deposits [21, 23, 43]. Pores and uneven clustered sizes are present at the coating surface. The fact that the deposition never reaches the anodic current density

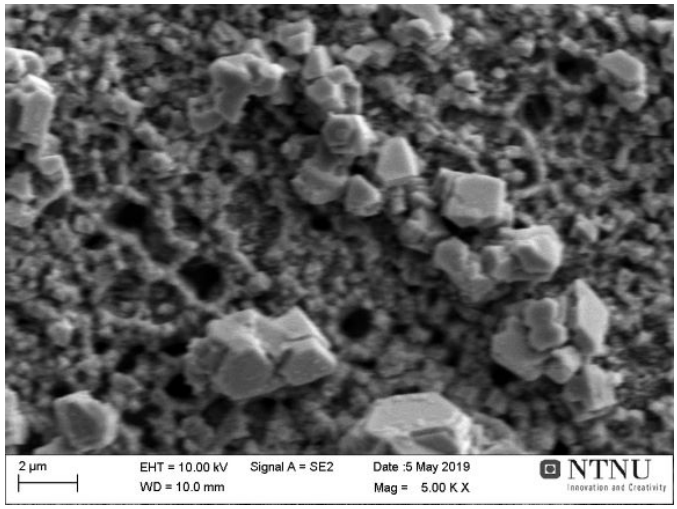

Figure 4.16: Scanning electron micrograph at the centre of deposited coating at 48 $\mathrm{mA/cm^2}$ (sat.) (PC, 10 Hz) in alkaline pyrophosphate electrolyte (5KX)

Table 4.5: EDS elemental composition of deposited coating at the centre at 48 $\mathrm{mA/cm^2}$ (PC, 10 Hz) in alkaline pyrophosphate electrolyte

Element	Atomic percent w/ Al [%]	Atomic percent wo/ Al [%]
Al	34	0
Zn	45	68
Mn	0	0
O	21	32
K	0	0

leads to the deposits experiencing less $\mathrm{i_{an}}$ and further lead to insufficient growth of the particles [26, 54].

Mn content in the coating is non-existent, as shown in Table 4.5. Results from the DC application from the same electrolyte proposed that cathodic current density larger than 60 $\mathrm{mA/cm^2}$ was sufficient to include Mn. This setup confirms that $\mathrm{i_{an}}$ and $\mathrm{t_{off}}$ applied are insufficient for the less noble metal to be incorporated [26, 54]. The large Zn content in the coating is expected to arrive mainly from pure Zn deposits and some oxide formation at the coating surface, given the large oxygen content found.

GDOES confirms that no Mn have been deposited as the depth concentration keeps the same bulk concentration throughout the analysis. Some oxidised Zn at the coating surface is displayed as the oxygen peaks at around 0.01 $\mu\mathrm{m}$. 70 % CE indicate more optimal deposition, even though it can not be directly compared to the DC for several reasons. Theoretical coating thickness of 0.7 $\mu\mathrm{m}$ is close to the observed coating thickness found

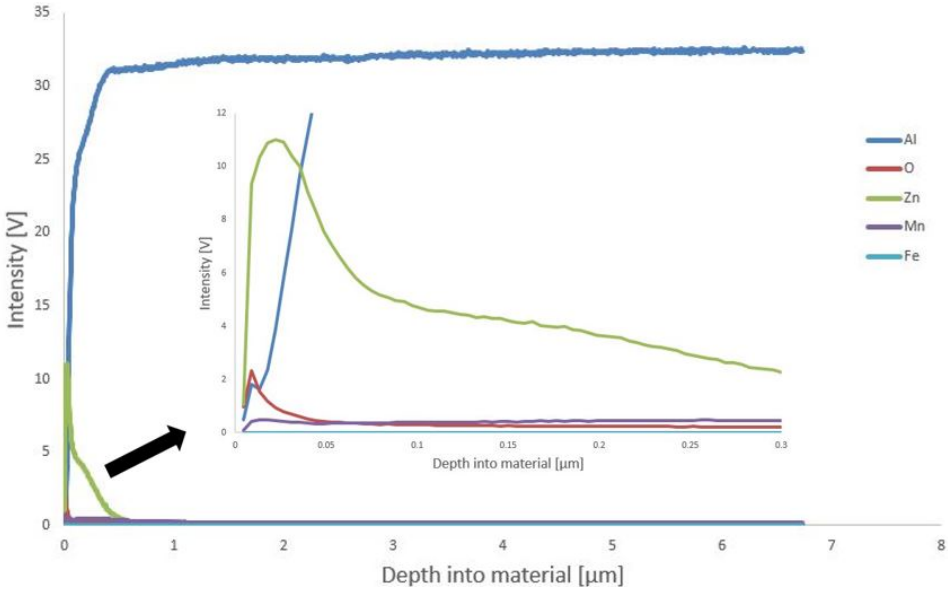

Figure 4.17: GDOES elemental depth profile of deposited coating at the centre at 48 $\mathrm{mA/cm^2}$ (PC, 10 Hz) in alkaline pyrophosphate electrolyte

from GDOES analysis in Figure 4.17. Zn approximation for coating thickness is the main contributor to this fact, as no Mn was detected. No Raman spectrum was conducted for this sample given the nonexistent Mn content.

Sample 4: 48 mA/cm^2 (PC, 20 Hz)

Another sample with increased pulse frequency, f = 20 Hz, was in addition conducted for analysis. The setup for the deposition is shown in Figure 4.15, showing two cycles. Key deposition parameters are shown in Table 4.6. Deposition setup was cycled 400 times giving a deposition time of 20 s.

Table 4.6: Key values for PC setup giving $\mathrm{i_{avg}}$ = 48 $\mathrm{mA/cm^2}$ (20 Hz) in alkaline pyrophosphate electrolyte

$\mathrm{t_{off}}$ [s]	$\mathrm{t_{on}}$ **[s]**	$\mathrm{t_{cycle}}$ **[s]**	$\mathrm{i_{an}}$ **[mA/cm^2]**	$\mathrm{i_{cath}}$ **[mA/cm^2]**	$\mathrm{i_{avg}}$ **[mA/cm^2]**
0.03	0.02	0.05	0	-120	-48

The anodic time was not sufficient, when comparing to the setup in Figure 4.15, to reach the anodic current density. Shorter pulses, as a result of shorter $\mathrm{t_{off}}$ and $\mathrm{t_{on}}$, have been reported to reduce hydrogen evolution and adsorption, form a less porous surface and incorporate more of Mn in alloy deposition [42].

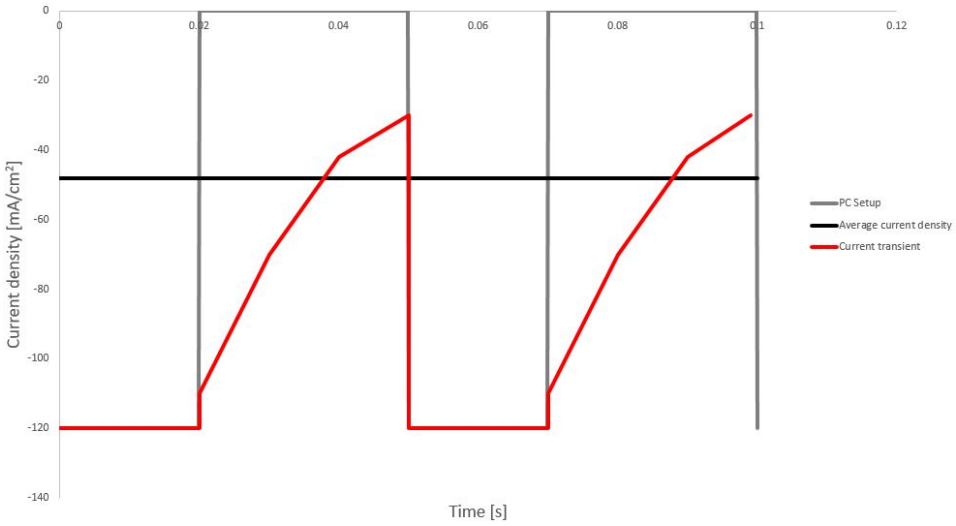

Figure 4.18: Setup for PC plating at 48 $\mathrm{mA/cm^2}$ (20 Hz) in alkaline pyrophosphate electrolyte

SEM micrograph, EDS analysis and GDOES analysis are displayed in Figure 4.19, Table 4.7 and Figure 4.20 respectively.

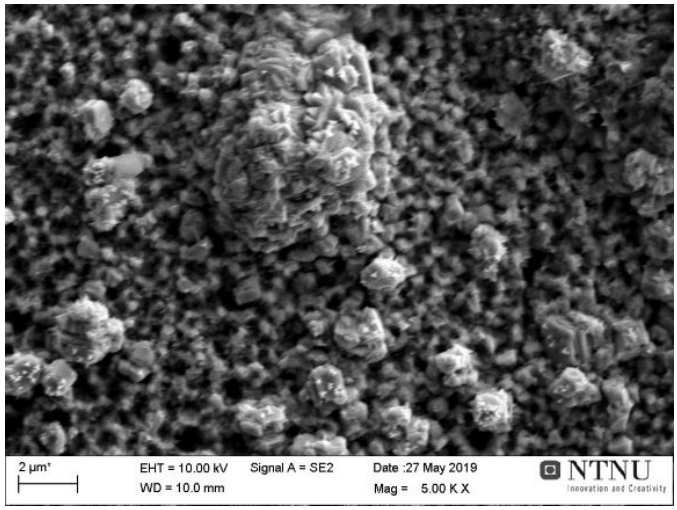

Figure 4.19: Scanning electron micrograph at the centre of deposited coating at 48 $\mathrm{mA/cm^2}$ (sat.) (PC, 20 Hz) in alkaline pyrophosphate electrolyte (5KX)

The deposited coating for this setup display smaller particles when compared to the SEM micrograph in Figure 4.16. This tendency has been reported before as lower value of $\mathrm{t_{on}}$ when applying similar $\mathrm{i_{cath}}$ prohibit nuclei growth [54, 61]. A large ”deposit tower” is displayed in the upper centre of the micrograph. The micrograph also shows reduced

Table 4.7: EDS elemental composition of deposited coating at the centre at 48 $\mathrm{mA/cm^2}$ (PC, 20 Hz) in alkaline pyrophosphate electrolyte

Element	Atomic percent w/ Al [%]	Atomic percent wo/ Al [%]
Al	41	0
Zn	33	56
Mn	2	3
O	23	39
K	1	2

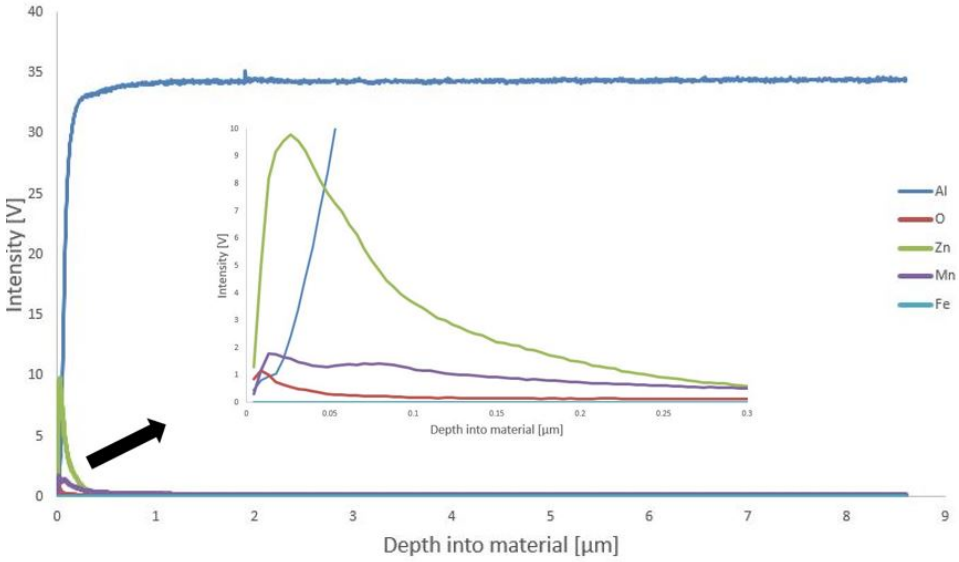

Figure 4.20: GDOES elemental depth profile of deposited coating at the centre at 48 $\mathrm{mA/cm^2}$ (PC, 20 Hz) in alkaline pyrophosphate electrolyte

grain size, and is a result of the increased cycles forming new grains more frequently [61]. Uneven sizes (together with the "deposit tower") arrive from inhibiting foreign species adsorbing on the surface and blocking growth centers, forcing growth of new nuclei at every new pulse [62].

EDS analysis from Table 4.7 show that potassium have been introduced in the coating, explaining an intruder hindering even size distribution. Mn content was expected to be larger by reducing $\mathrm{t_{off}}$ (and increasing the frequency), but in contrast be hindered by the increased $\mathrm{i_{an}}$ shown in Figure 4.18 when compared to Sample 3 [42]. In the end Mn have been successfully deposited in the coating with the setup, even though the atomic percent is small according to the EDS analysis. Larger experienced $\mathrm{i_{cath}}$ overall is the reason for the larger Mn content included [42]. Zn content have decreased and Al content have increased, even though this samples should perceive larger $\mathrm{i_{avg}}$ than Sample 3. Inhibition of

Zn deposition from inclusion of Mn and potassium is factoring this result [9, 21, 43].

GDOES layout in Figure 4.20 clearly illustrates deposition of Mn, as the Mn profile lowers does not remain constant. However the GDOES profile exhibit larger Mn content and lower oxygen profile than expected when comparing with the contents found in Table 4.7. The large oxygen content and depth profile found in this sample does not correlate with the profile found in Figure 4.20. As Al was detected it is to be assumed that the entire coating was analysed, so the excitation energy utilised was sufficient for detecting the chemical composition. Oxygen peaks at the coating surface of around 0.01 $\mu\mathrm{m}$, and must be the detected oxygen from the EDS sample. Previously stated Mn oxidation contribute to the larger oxygen content.

Higher $\mathrm{i_{avg}}$ experienced by this sample compared to Sample 3 should lead to thicker coating, in correlation with Faraday's law [23]. This is not the case when comparing GDOES Figures 4.20 with 4.17. CE at 65 $\%$ is lower than the same sample with lower frequency (10 Hz). This trend has been reported before and is related to the relationship between Mn content and current density as they are inversely proportional during plating processes [42].

Thickness of the coating found from the GDOES profile in Figure 4.20 (around 0.5 $\mu\mathrm{m}$) is not close to the theoretical thickness (0.79 $\mu\mathrm{m}$). In addition the thickness of the coating was supposed to be larger when compared to the 10 Hz sample given the larger $\mathrm{i_{avg}}$ [25]. Non uniform current distribution, insufficient anodic time and foreign atom inclusion contributes to this deviation.

Effect of frequency change in alkaline pyrophosphate electrolyte

Sample 3 and 4 highlighted several parameters that are of interest for further pulse plating. Difference in Mn content indicate that a combination of either larger $\mathrm{i_{avg}}$ or longer $\mathrm{t_{on}}$ are necessary. The setup highlighted that lower frequencies are necessary for the potentiostat to reach the anodic parameters, and could further lead to inclusion of more Mn.

Uncertainty regarding pulse setup for the high frequencies, $\mathrm{i_{avg}}$, thickness for two presumably similar setups and anodic current density and time tends to an investigation for the same electrolyte with shorter pulses and more controlled anodic parameters. Rest of the PC samples were analysed at both the centre and the edge, as suspicion of chemical differences arose given the overall low Mn content for Sample 3 and 4.

4.3.4 Pulse plating (PC) - changing current density

Two average current densities of 48 and 60 $\mathrm{mA/cm^2}$ were constructed with θ = 40 $\%$ and f = 4 Hz for examining the effect of lower frequency. Current density was chosen in the region where Mn was believed to be deposited (potentials lower than -1.80 V vs. Ag/AgCl (sat.), predicted by the alkaline pyrophosphate CV).

Sample 5: 48 mA/cm^2 (PC, 4 Hz)

PC setup for achieving an average current density of 48 $\mathrm{mA/cm^2}$ is illustrated in Figure 4.21, showing two cycles. Key values from the pulse setup are shown in Table 4.8. Total deposition time was set for 20 s, meaning one pulse cycle had to be done 80 times with the setup.

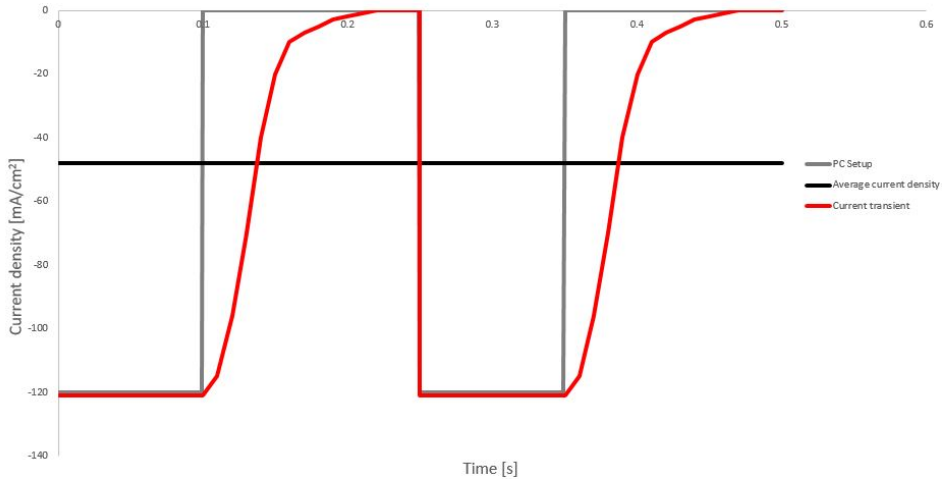

Figure 4.21: Setup for PC plating at 48 $\mathrm{mA/cm^2}$ (4 Hz) in alkaline pyrophosphate electrolyte

Table 4.8: Key values for PC setup giving $\mathrm{i_{avg}}$ = 48 $\mathrm{mA/cm^2}$ (4 Hz) in alkaline pyrophosphate electrolyte

$\mathrm{t_{off}}$ [s]	$\mathrm{t_{cat}}$ [s]	$\mathrm{t_{cycle}}$ [s]	$\mathrm{i_{an}}$ [$\mathrm{mA/cm^2}$]	$\mathrm{i_{cat}}$ [$\mathrm{mA/cm^2}$]	$\mathrm{i_{avg}}$ [$\mathrm{mA/cm^2}$]
0.15	0.1	0.25	0	-120	-48

The setup for pulse plating is still not completely perfect, but by decreasing the frequency the anodic parameters are reached earlier and promote inclusion of Mn. Lower $\mathrm{i_{avg}}$ experienced might, in contrast, reduce Mn content in the coating [42].

Two areas were analysed: centre end the edge as depicted in Figure 4.6. The centre was analysed first. SEM micrograph, EDS analysis, GDOES profile and Raman spectrum are shown in Figure 4.22, Table 4.9, Figure 4.23 and Figure 4.24 respectively.
The SEM micrograph of deposits showed in Figure 4.22 shows larger deposit sizes and less clustering when compared to Sample 3 and 4 with larger frequencies. Larger deposits are a result of longer $\mathrm{t_{on}}$, thus leaving the potential for nuclei growth larger [27]. Lower frequency exhibited on the sample have lead to less clustering [54]. EDS analysis shows no sign of Mn inclusion in the coating. Lower overall $\mathrm{i_{avg}}$ inhibits inclusion of Mn in this case, even though $\mathrm{t_{off}}$ have increased. The total sum of the forces at play results in no Mn being included in the coating.

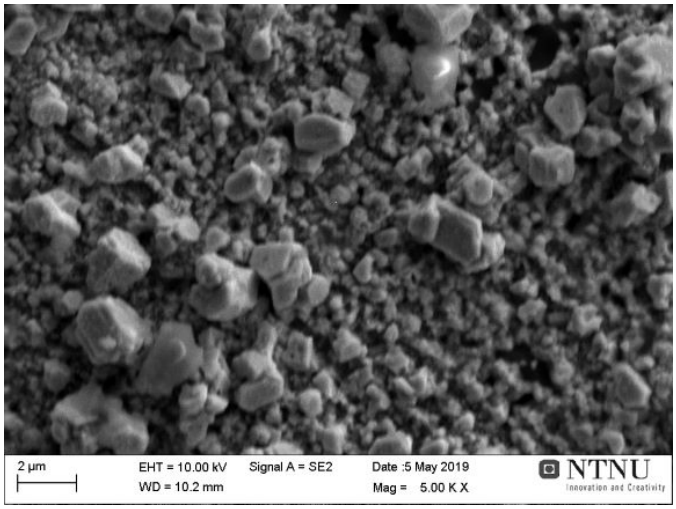

Figure 4.22: Scanning electron micrograph at the centre of deposited coating at 48 $\mathrm{mA/cm^2}$ (sat.) (PC, 4 Hz) in alkaline pyrophosphate electrolyte (5KX)

Table 4.9: EDS elemental composition of deposited coating at the centre at 48 $\mathrm{mA/cm^2}$ (PC, 4 Hz) in alkaline pyrophosphate electrolyte

Element	Atomic percent w/ Al [%]	Atomic percent wo/ Al [%]
Al	38	0
Zn	42	68
Mn	0	0
O	17	27
K	3	5

Oxygen content found in the coating results from oxidation at the coating surface following the trend from oxygen and Zn illustrated from the GDOES analysis from Figure 4.23. It could also arrive from $\mathrm{Al(OH)_3}$ from the zincate pre treatment. Figure 4.23 also confirms that no Mn have been deposited. Oxygen linked with Zn is related to ZnO and its peak at around 550 $\mathrm{cm^{-1}}$, as shown from the Raman spectrum in Figure 4.24 [49, 50, 63]. Increased CE of 80 % correlates well with the lower $\mathrm{i_{avg}}$ experienced for this sample when compared to Sample 3 and 4 [42, 61]. Thickness of 0.8 $\mu\mathrm{m}$ is larger than the theoretical coating thickness of 0.67 $\mu\mathrm{m}$. Inclusion of oxygen contribute to this deviation.

The edge was analysed in similar fashion as the centre in hopes of explaining the changes between observed macroscopic differences. SEM micrograph, EDS analysis, GDOES profile and Raman spectrum are shown in Figure 4.25, Table 4.10, Figure 4.26 and Figure 4.27 respectively.

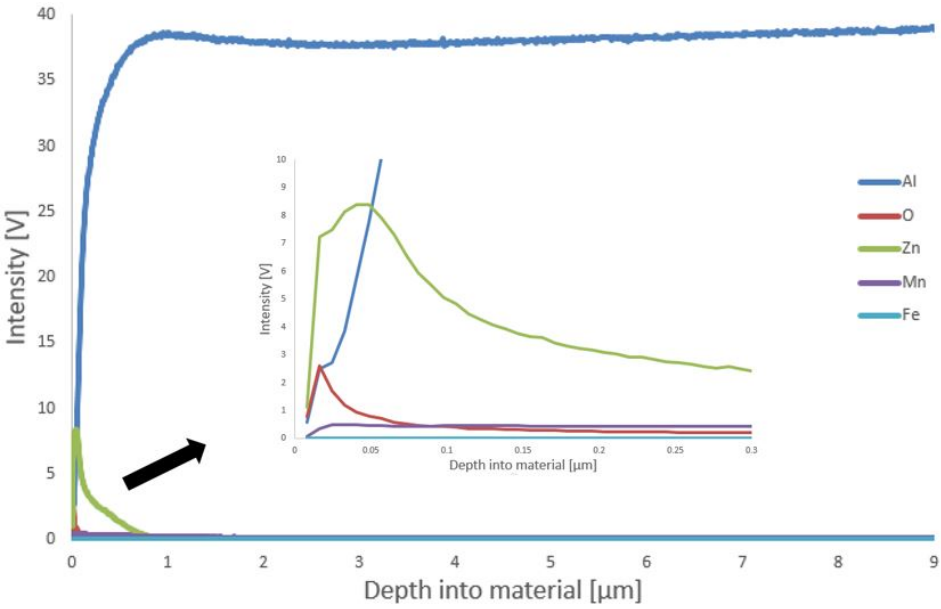

Figure 4.23: GDOES elemental depth profile of deposited coating at the centre at 48 $\mathrm{mA/cm^2}$ (PC, 4 Hz) in alkaline pyrophosphate electrolyte

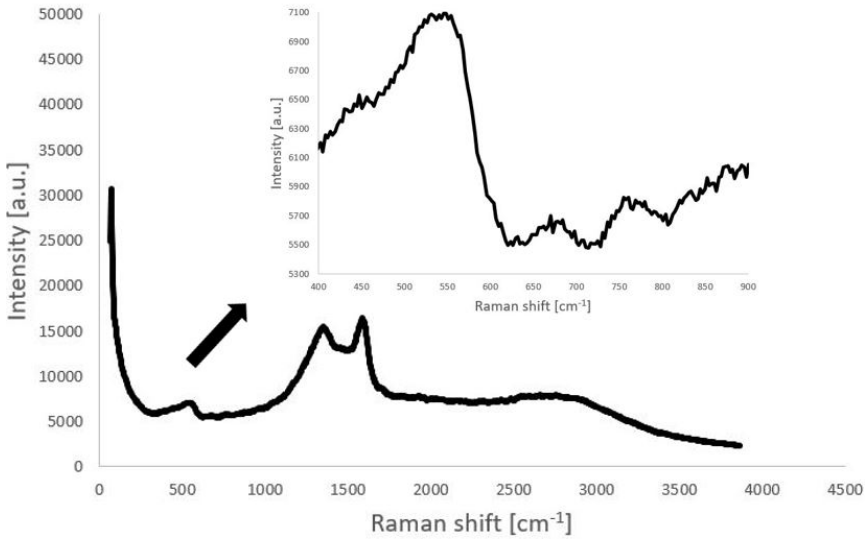

Figure 4.24: Raman spectrum of deposited coating at the centre at 48 $\mathrm{mA/cm^2}$ (PC, 4 Hz) in alkaline pyrophosphate electrolyte

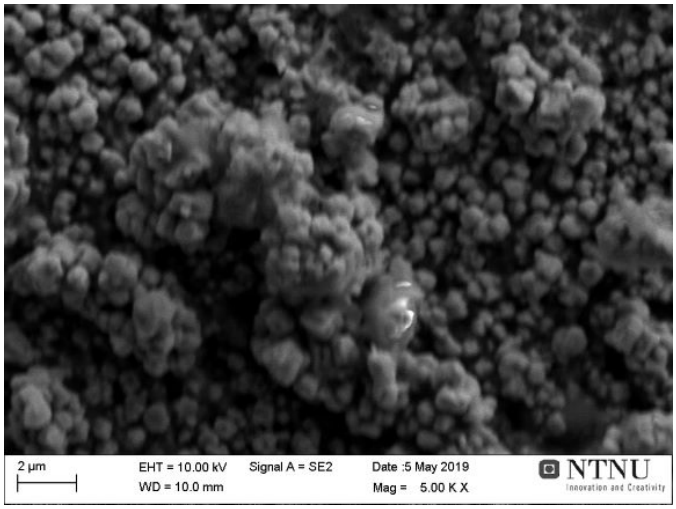

Figure 4.25: Scanning electron micrograph at the edge of deposited coating at 48 $\mathrm{mA/cm^2}$ (sat.) (PC, 10 Hz) in alkaline pyrophosphate electrolyte (5KX)

Table 4.10: EDS elemental composition of deposited coating at the edge at 48 $\mathrm{mA/cm^2}$ (PC, 4 Hz) in alkaline pyrophosphate electrolyte

Element	Atomic percent w/ Al [%]	Atomic percent wo/ Al [%]
Al	39	0
Zn	43	69
Mn	12	19
O	6	10
K	1	2

The exact current density experienced at the edge is uncertain as no additional current transient was recorded at the mentioned area. SEM micrograph shown in Figure 4.25 clearly shows more clustering of deposits and more depth when compared to the centre. Increased cathodic current density will lead to increased overpotential and further higher nucleation rates, thus forming coatings with smaller grain sizes [14, 27]. Increased nuclei formation indicate that the edge have experienced larger current density than the centre. While the Al content stays the same for the centre and the edge, the EDS analysis still suggest that larger current density have been experienced as Mn have been successfully deposited. Mn inclusion have hindered Zn deposition, and explain why the Zn content has not increased when the current density was increased [21, 23]. Relative atomic weight of Zn and Mn also explain the decrease in atomic ratio of oxygen [17]. Zn and Mn share the same depth profile trend until a peak is reached at around 0.025 μm, which suggest co-deposition at the coating surface [59].

The GDOES profile confirms that Mn have been deposited, and that oxygen mainly con-

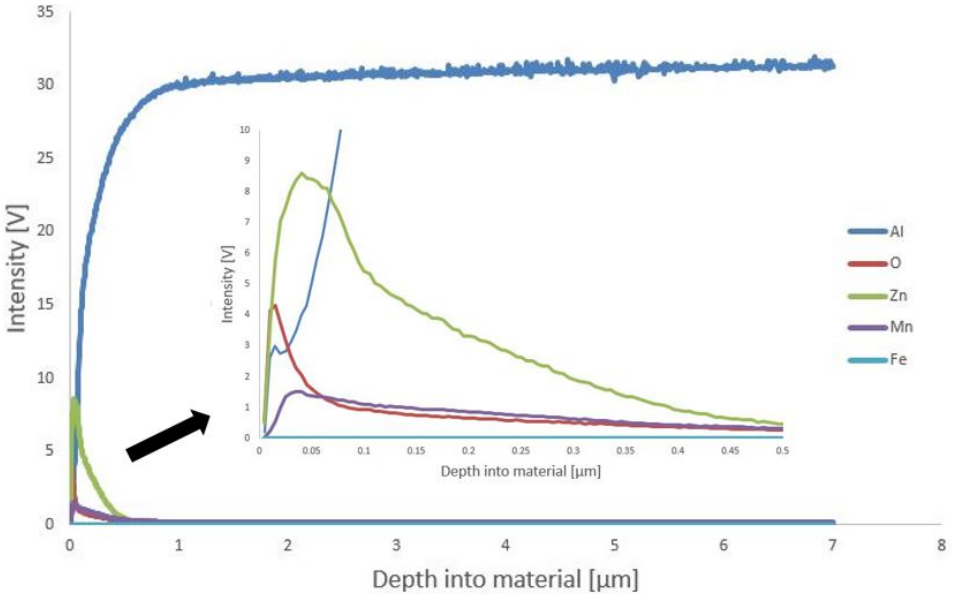

Figure 4.26: GDOES elemental depth profile of deposited coating at the edge at 48 $\mathrm{mA/cm^2}$ (PC, 4 Hz) in alkaline pyrophosphate electrolyte

sists at the top of the coating. Raman spectrum shows a large peak from the aforementioned ZnO area and a small peak around 660 $\mathrm{cm^{-1}}$, indicating that the Mn deposited have been oxidised to $\mathrm{Mn_3O_4}$ [56, 58].

The thickness of the coating at the edge is similar to that of the centre at around 0.7-0.8 $\mu\mathrm{m}$. Reduction of Zn and inclusion of Mn in the coating attribute to this similarity of thickness. The result demonstrates that edges of the samples with larger frequencies could contain larger Mn content than first proclaimed.

Sample 6: 60 mA/cm^2 (PC, 4 Hz)

A similar analysis was done with the same frequency and duty cycle, but now with increased $\mathrm{i_{cath}}$. PC setup is shown in Table 4.11, showing two cycles. Current transient is shown in Figure 4.28.

Table 4.11: Key values for PC setup giving $\mathrm{i_{avg}}$ = 60 $\mathrm{mA/cm^2}$ (4 Hz) in alkaline pyrophosphate electrolyte

$\mathrm{t_{off}}$ [s]	$\mathrm{t_{on}}$ [s]	$\mathrm{t_{cycle}}$ [s]	$\mathrm{i_{an}}$ [$\mathrm{mA/cm^2}$]	$\mathrm{i_{cath}}$ [$\mathrm{mA/cm^2}$]	$\mathrm{i_{avg}}$ [$\mathrm{mA/cm^2}$]
0.15	0.1	0.25	0	-150	-60

Recorded current transient from the pulse plating setup does not reach completely anodic

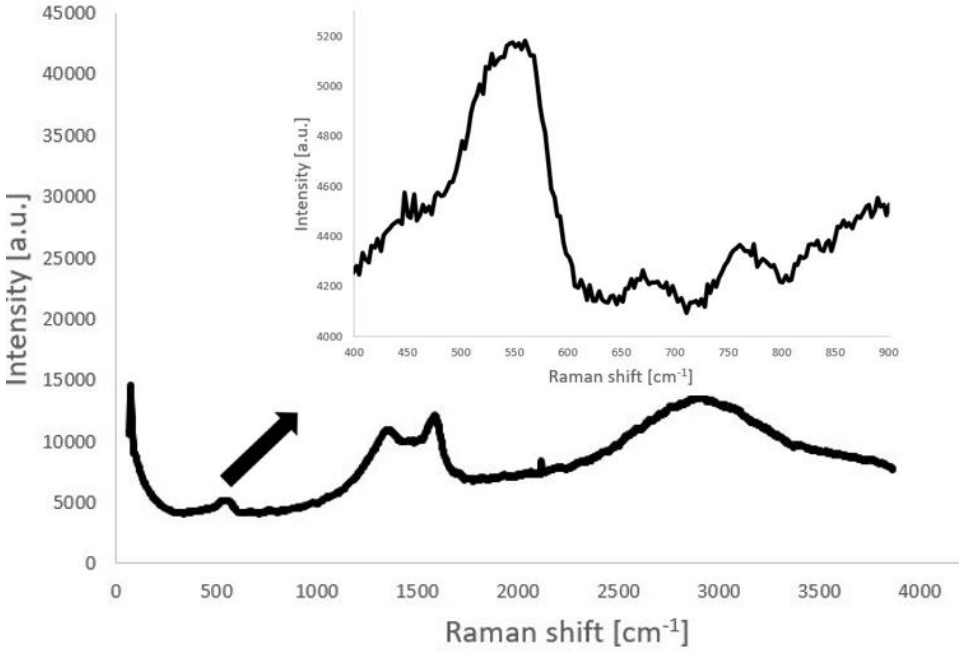

Figure 4.27: Raman spectrum of deposited coating at the edge at 48 $\mathrm{mA/cm^2}$ (PC, 4 Hz) in alkaline pyrophosphate electrolyte

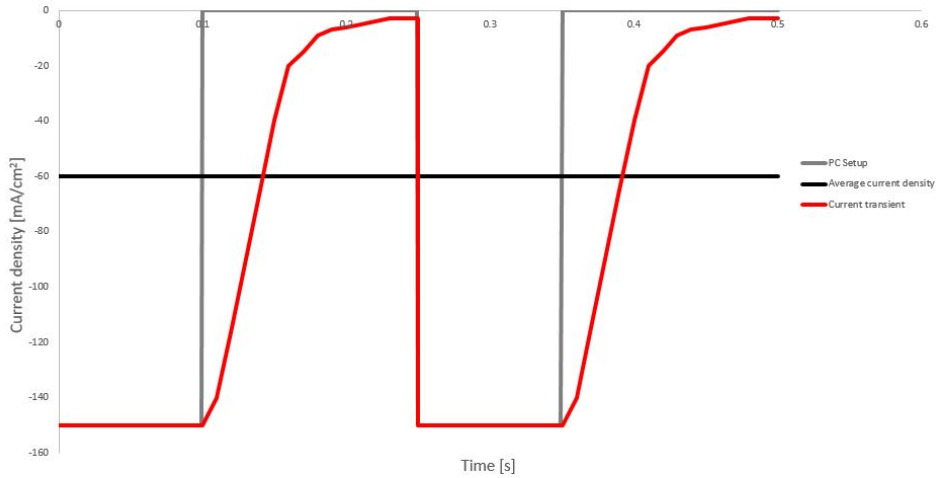

Figure 4.28: Setup for PC plating at 60 $\mathrm{mA/cm^2}$ (4 Hz) in alkaline pyrophosphate electrolyte

current density from the $\mathrm{t_{off}}$ applied. The increased difference between $\mathrm{i_{cath}}$ and $\mathrm{i_{an}}$ is factoring this trend, as increased $\mathrm{t_{off}}$ should been used for reaching 0 $\mathrm{mA/cm^2}$.

Firstly the centre of the sample was analysed. The SEM micrograph, EDS analysis, GDOES profile and Raman spectrum are shown in Figure 4.29, Table 4.12, Figure 4.30 and 4.31.

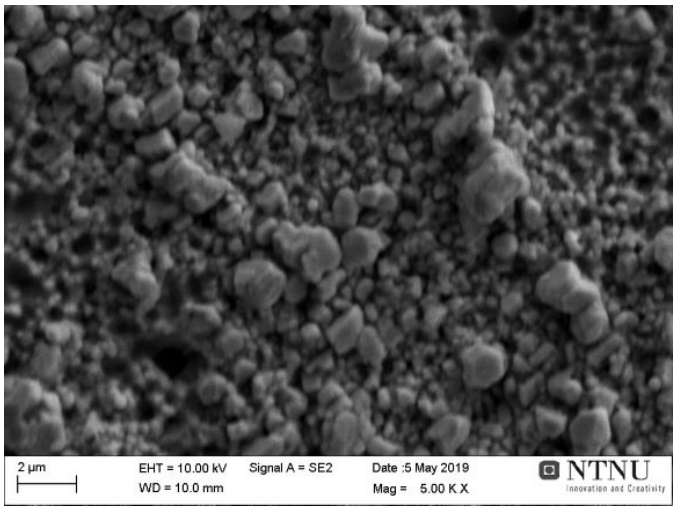

Figure 4.29: Scanning electron micrograph at the centre of deposited coating at 60 $\mathrm{mA/cm^2}$ (sat.) (PC, 4 Hz) in alkaline pyrophosphate electrolyte (5KX)

Table 4.12: EDS elemental composition of deposited coating at the centre at 60 $\mathrm{mA/cm^2}$ (PC, 4 Hz) in alkaline pyrophosphate electrolyte

Element	**Atomic percent w/ Al [%]**	**Atomic percent wo/ Al [%]**
Al	57	0
Zn	35	81
Mn	1	2
O	6	15
K	1	2

Increase in $\mathrm{i_{avg}}$ was expected to reduce grain size and form more nuclei due to the increased nucleation rate given the larger overpotential [54, 64]. Deposits overall are smaller than the ones from the centre of the previous PC samples. Growth of nuclei is impeded when nucleation is the dominating factor, and previous reports have stated that at "large current densities" the agglomeration of nuclei will be dominating [64]. This is not the case for the chosen $\mathrm{i_{avg}}$, but in turn will make the coating more compact.

Mn have deposited at small quantities according to the EDS analysis from Table 4.12. More depletion of $\mathrm{Zn^{2+}}$ at the cathode surface at larger $\mathrm{i_{cath}}$ allow more $\mathrm{Mn^{2+}}$ to be reduced, and thus enable Mn reduction at the surface [42, 54]. However given the larger Al

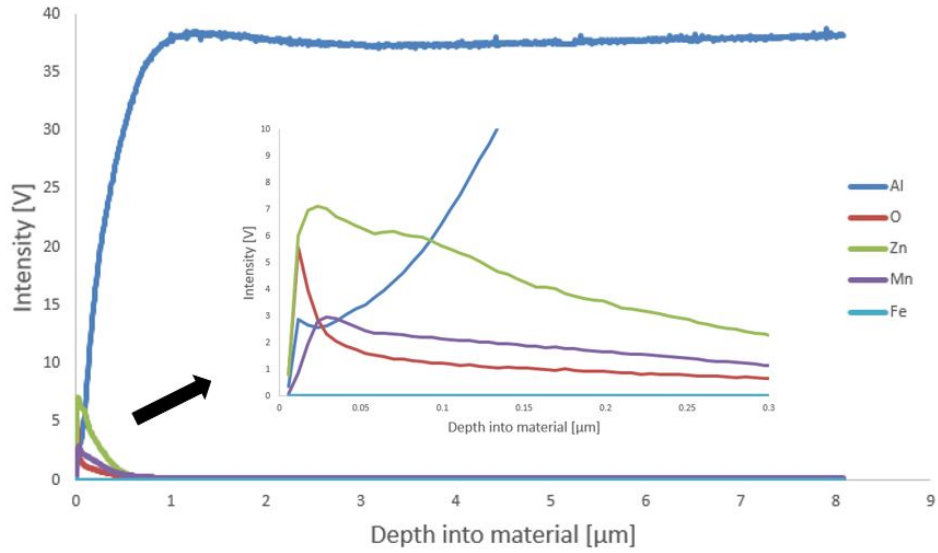

Figure 4.30: GDOES elemental depth profile of deposited coating at the centre at 60 $\mathrm{mA/cm^2}$ (PC, 4 Hz) in alkaline pyrophosphate electrolyte

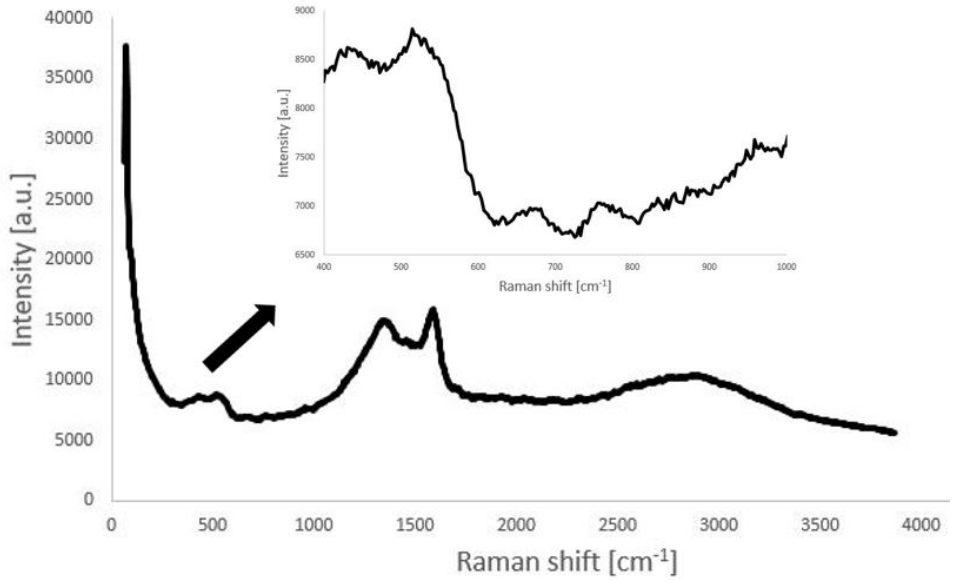

Figure 4.31: Raman spectrum of deposited coating at the centre at 60 $\mathrm{mA/cm^2}$ (PC, 4 Hz) in alkaline pyrophosphate electrolyte

content found in the coating, the Mn content could also arrive from the bulk concentration of the surface. Larger Al content is not to be expected given the larger current density applied for this sample [42, 43, 54]. Zn make up most of the coating, thus hinting towards insufficient current density applied for Mn incorporation. Deposited Mn also arrives from complex formation with potassium, which has been incorporated in the coating [53].

GDOES analysis does not correlate with the concentration of Mn found in the EDS analysis. The concentration profile for Mn clearly shows deposition, and the intensity peak is larger than the edge of the 48 $\mathrm{mA/cm^2}$ (4 Hz) which in contrast contained around 12 at. $\%$ Mn. Local chemical differences in the coating have to be the reason for the inconsistency when comparing EDS analysis with the GDOES profile. Mn GDOES profile also follows the Zn profile until 0.06 $\mu\mathrm{m}$, indicating that the applied current density was sufficient for co-deposition of the metals [55, 59].

CE at 60 $\%$ is lower than Sample 5 with lower $\mathrm{i_{cath}}$. Incorporation of Mn adds uncertainty and error for the estimated efficiency, which is based on 100 $\%$ Zn. However the decreasing trend have been reported before and is due to the increased hydrogen bubble formation at larger $\mathrm{i_{cath}}$ [42]. This uncertainty spread to the theoretical thickness approximation of 0.65 $\mu\mathrm{m}$, which is lower than the thickness found from GDOES at around 0.8 $\mu\mathrm{m}$. Reasons for this deviation are, other than the approximation of 100 $\%$ deposited Zn, larger $\mathrm{i_{avg}}$ applied and foreign atoms included providing larger coating.

Zn peaks at the Raman spectrum were expected, taking into consideration the concentration profile found in Figure 4.30. Two peaks at 450 and 510 $\mathrm{cm^{-1}}$ are associated with ZnO peaks, and correlate well with the oxygen and zinc profile found in the GDOES analysis [49]. The contradicting information regarding Mn content in the coating made analysis of the edge interesting.

Information from the edge of Sample 6 are shown in Figure 4.32, Table 4.13, Figure 4.33 and Figure 4.34.

Table 4.13: EDS elemental composition of deposited coating at the edge at 60 $\mathrm{mA/cm^2}$ (PC, 4 Hz) in alkaline pyrophosphate electrolyte

Element	**Atomic percent w/ Al [$\%$]**	**Atomic percent wo/ Al [$\%$]**
Al	13	0
Zn	56	64
Mn	14	16
O	14	16
K	3	4

Smaller deposits and larger amount of clustering are evident when comparing the SEM micrograph at the edge to the centre. Larger nucleation rate, as a result from larger $\mathrm{i_{cath}}$ and subsequent larger overpotential, is expected for this edge analysis as well [54, 64]. Larger current density experienced is confirmed as the Al content found in Table 4.13 is

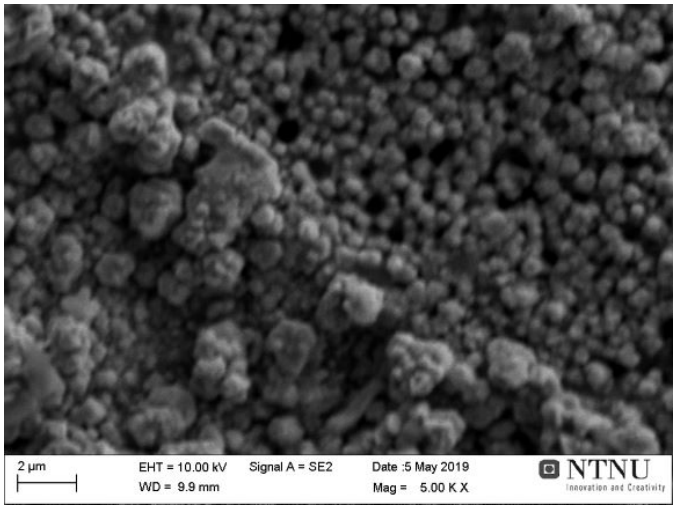

Figure 4.32: Scanning electron micrograph at the edge of deposited coating at 60 $\mathrm{mA/cm^2}$ (sat.) (PC, 4 Hz) in alkaline pyrophosphate electrolyte (5KX)

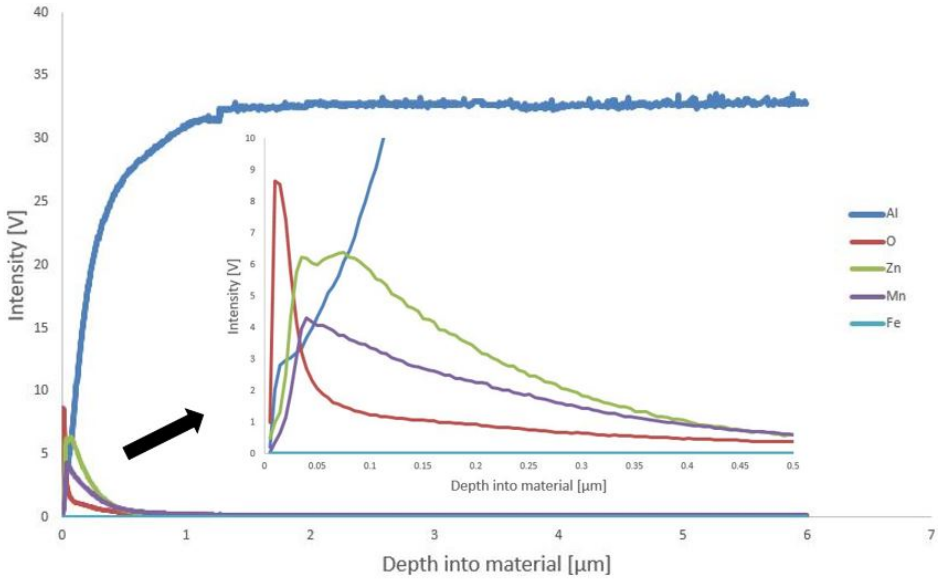

Figure 4.33: GDOES elemental depth profile of deposited coating at the edge at 60 $\mathrm{mA/cm^2}$ (PC, 4 Hz) in alkaline pyrophosphate electrolyte

lower than the one found at the centre. Inclusion and adsorption of potassium in the coating, most likely from Mn-pyrophosphate complex, also explains the low nuclei sizes [62]. Increase in Mn content was to be expected with the previous results leaning towards higher

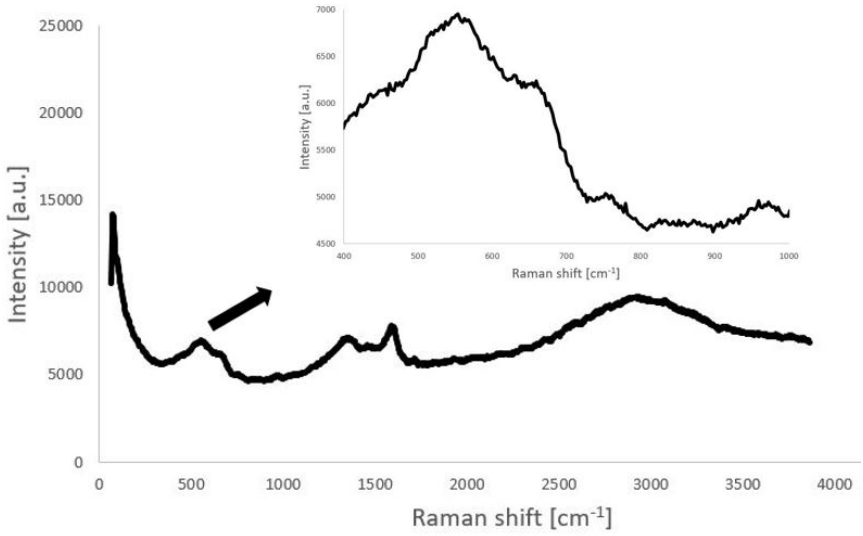

Figure 4.34: Raman spectrum of deposited coating at the edge at 60 $\mathrm{mA/cm^2}$ (PC, 4 Hz) in alkaline pyrophosphate electrolyte

$\mathrm{i_{avg}}$ experienced at the edge, which in turn enable Mn deposition [9, 10, 43].

Oxygen content have also increased and is, according to the EDS analysis shown in Figure 4.33 attributed to oxidation of both metals at the coating surface. Lower Zn ratio in the coating is attributed to Mn inclusion and further inhibition of Zn deposition [10, 23, 42]. EDS analysis shows correlation between Zn and Mn again, indicating co-deposition of the metals. Coherence between the EDS and GDOES profile at the edge suggest that the centre EDS analysis was incorrect, or that the local chemical differences considered were larger than expected. The thickness of the coating at the edge is not so dissimilar to that of the centre, even though the Al content found at the aforementioned areas should suggest otherwise.

The Raman spectrum shows relative larger intensity peaks, and 550 and 660 $\mathrm{cm^{-1}}$ compared to the centre. Peak at 660 $\mathrm{cm^{-1}}$ should be associated with $\mathrm{Mn_3O_4}$, considering the large Mn content found in this area [56, 57, 58]. A peak around 550 $\mathrm{cm^{-1}}$ should relate to areas for Zn-oxide bonding [63, 65].

Effect of current density change in alkaline pyrophosphate electrolyte

Discovery of larger amounts of Mn, and different chemical composition, at the edge of the samples hints towards possible Mn inclusion for Sample 3 and 4 as well at the edges. However the inconsistent setup for those samples, most notably with the anodic parameters, imply that further improvements towards the pulse setup can be done for additional inclusion of Mn [42]. The morphology of Sample 5 and 6 confirmed that larger $\mathrm{i_{cath}}$ pro-

duced more homogeneous and rough coating as a result of increased nucleation rate and clustering.

The change in i_{cath} for PC deposition showed potential for incorporation of increased Mn inclusion in the coating. The decreasing CE value, from 80 to 60 $\%$ by increasing the i_{cath} and i_{avg}, was in accordance with experiments previously done changing i_{cath} [42, 44, 54]. Increasing the i_{cath} from 120 to 150 mA/cm^2 aided the driving force towards deposition of Mn, and is heavily implied from the reduction of Zn at the edges for Sample 5 and 6. Co-deposition is hinted by the GDOES trends of Zn Mn at the edges, specially for Sample 6 at both centre and edge [59].

The inclusion of potassium was inconsistent when comparing centre to centre and edge to edge for both samples. Inclusion of reducing agent and the chosen concentration of pyrophosphate was supposed to inhibit formation of any pyrophosphate complexes with Mn, so adsorption of potassium at the coating surface is causing this result. Reports have been made from Zn-pyrophosphate complex formation in alkaline pyrophosphate electrolyte using DC application [21]. However inclusion of potassium and reduction of Zn-complexes to Zn^{2+} have been reported to occur at high cathodic current densities over longer deposition time [21, 66].

Effect of plating setups in alkaline pyrophosphate electrolyte

The electrolytic alkaline pyrophosphate electrolyte shows great potential as a candidate of choice for Zn and Mn inclusion. The DC samples showed Mn content ranging between 12 and 16 at. $\%$ at recorded current densities between 60 and 140 mA/cm^2. More samples can be recorded between the current density applied since previous results have shown that non homogeneous and powdery Mn deposits occur at too high current densities [21, 42]. The at. $\%$ of Mn in the coating naturally increase when the oxygen content is reduced, so monitoring the samples for inhibition of oxide formation is important for a more compact and chemical interesting coating [6, 9, 21]. CE should also be taken into consideration. The higher current density applied favour incorporation of more Mn, but at a cost of lower CE this consideration should be evaluated carefully.

PC samples exhibited higher current efficiencies than the DC samples. This is mainly attributed to the overall lower i_{avg} experienced, particularly in relation with t_{off}. All samples for PC followed the same trend as the DC samples; increased i_{avg} lead to lower current density. Metal rich edges for Sample 5 and 6 showed Mn content ranging from 16 to 19 at. $\%$, but in addition large oxygen content at the coating surface. Oxidation of metal at the surface is the main contributor to this result, and is clearly evident at the Zn and Mn rich areas.

4.4 Acidic sulphate electrolyte

4.4.1 CV scan

A CV scan was constructed in similar fashion for the acidic sulphate electrolyte as for the alkaline pyrophosphate electrolyte. The voltammogram is shown in Figure 4.35.
Current density stays put at 0 $\mathrm{mA/cm^2}$ for the forward scan at potentials ranging from -0.50 to -1.20 V vs. Ag/AgCl (sat.), corresponding to potentials where no significant metal deposit. The current density increase in the cathodic direction until a small kink is observed at -1.30 V vs. Ag/AgCl (sat.). Deposition of Zn is the main factor contributing to this trend, starting at a potential lower than the theoretical reduction potential for Zn in acidic environment (-1.00 V vs. Ag/AgCl (sat.)) [18].

Bubble formation due to hydrogen evolution at the electrode surface becomes excessive at potentials lower than -1.40 V vs. Ag/AgCl (sat.). The current behaviour for deposition of Mn is again masked [7, 10, 67]. This trend has been reported before with exact same electrolyte composition using steel as substrate [46]. The reverse scan in anodic direction shows several small dissolution peak between -0.85 V and -0.65 V vs. Ag/AgCl (sat.), indicating deposition of several phases during the forward scan [13]. Rapid electrochemical dissolution of Mn in acidic electrolyte can factor in towards the smaller peaks observed at -0.70 V vs. Ag/AgCl (sat.) [10].

4.4.2 Direct current (DC)

Testing of direct current (DC) application of acidic sulphate electrolyte was conducted in similar fashion as the alkaline pyrophosphate electrolyte. Previous study of the electrolyte using DC application indicated that some Mn have been deposited, but this study lacked depth profile and Raman spectrum [45]. A similar setup was conducted for pinpointing the chemical composition. The deposition time was set for 20 s for later comparison with pulse setup for the same electrolyte. The potential chosen was -1.50 V vs. Ag/AgCl (sat.).

Sample 7: -1.50 V vs. Ag/AgCl (sat.) (DC)

The current transient for direct current application at -1.50 V vs. Ag/AgCl (sat.) is shown in Figure 4.36.

The current transient starts in similar fashion as the alkaline pyrophosphate sample with DC deposition; sharp increase in cathodic current due to charging of the double layer. The increase in current is a result of growth and nucleation of metal deposit at the coating surface [5]. The maximum current density recorded is larger than the recorded current density during the CV scan in Figure 4.35, alluding towards increased nuclei and phase growth [10]. The curve shows typical current transient for metal deposition process [10, 38].

The SEM micrograph, EDS analysis, GDOES and Raman analysis are shown in Figure 4.37, Table 4.37, Figure 4.38 and Figure 4.39 respectively.

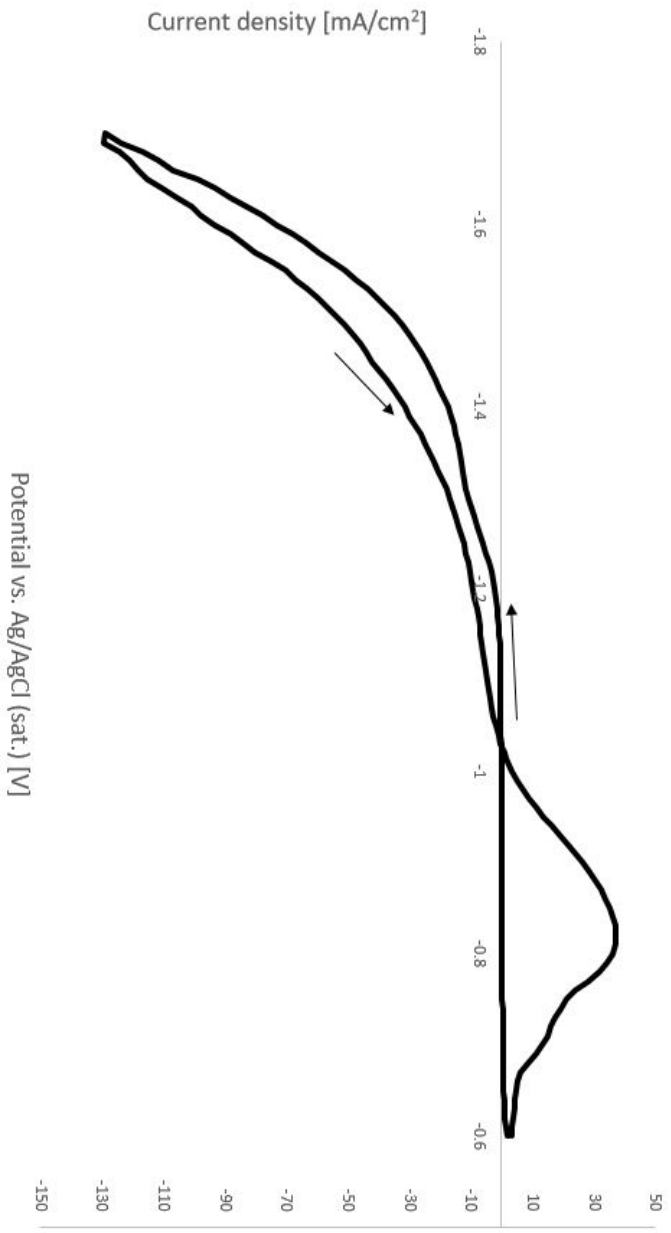

Figure 4.35: CV scan of zincated aluminum sample in acidic sulphate electrolyte

The deposited metals does not cover the entire surface, suggesting that the applied current density and time was not sufficient at the centre for efficient deposition. The morphology appears as hexagonal deposits, indicating Zn deposits [43]. Current transient alluded to-

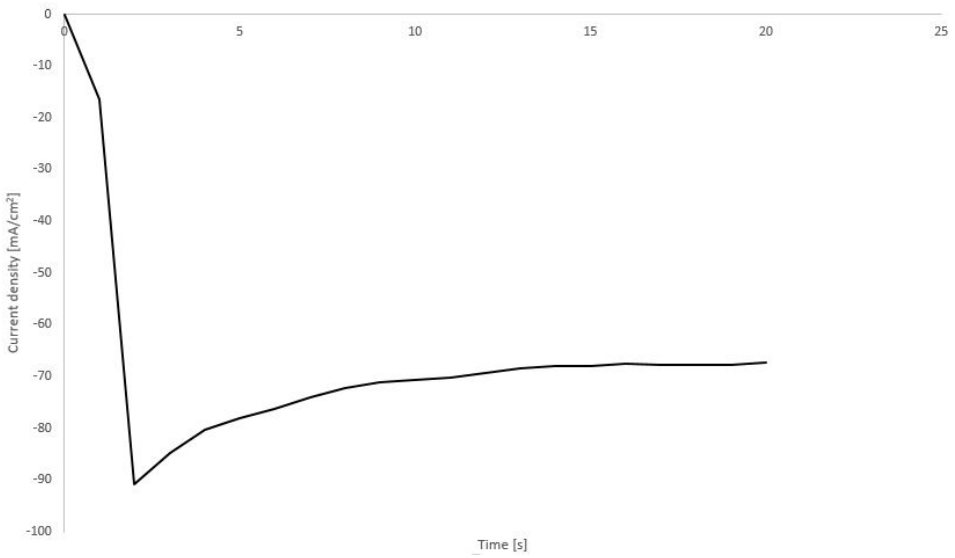

Figure 4.36: Current transient of direct current deposition in acidic sulphate electrolyte at -1.50 V vs. Ag/AgCl (sat.)

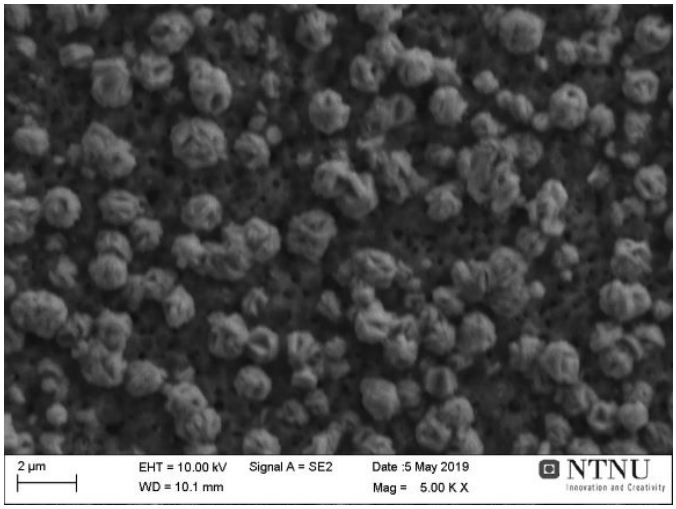

Figure 4.37: Scanning electron micrograph at the centre of deposited coating at -1.50 V vs. Ag/AgCl (sat.) (DC) in acidic sulphate electrolyte (5KX)

wards larger phase formation, but this is not observed from the related micrograph. Reduction of Al content and increased Zn content shown in Table 4.14, when compared with the zincated composition in Table 4.1, indicate Zn deposition have occurred during deposition. The high Al content shown in Table 4.14 makes the determination of where the Mn arrives

Table 4.14: EDS elemental composition of deposited coating at the centre at -1.50 V vs. Ag/AgCl (sat.) (DC) in acidic sulphate electrolyte

Element	Atomic percent w/ Al [%]	Atomic percent wo/ Al [%]
Al	73	0
Zn	13	48
Mn	1	4
O	12	44
S	1	4

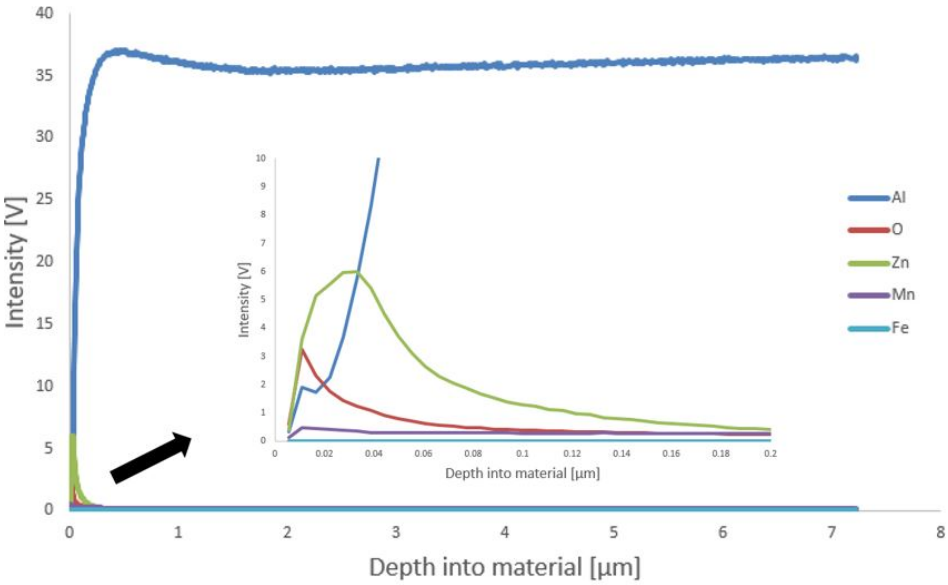

Figure 4.38: GDOES elemental depth profile of deposited coating at the centre at -1.50 V vs. Ag/AgCl (sat.) (DC) in acidic sulphate electrolyte

from difficult, but a small peak around 0.01 μm and a downwards trend to 0.04 μm in the GDOES analysis from Figure 4.38 reveals that some Mn have been deposited. Larger current densities could be applied for increased Mn content for this setup [9]. GDOES analysing reveals that some of the deposited Zn have been oxidised at the coating surface following the correlating concentration trends for Zn and oxygen until 0.01 μm.

The CE at 35 % is higher than the same efficiency for 60 s deposition time (29 %) [45]. Less hydrogen evolution due to lower deposition time contributes to this result [9]. Dominant peaks around 400-600 cm^{-1} were Zn-O bonds was to be expected given chemical concentration and depth profile [49, 68]. Two peaks at approximately 440 and 550 cm^{-1} corresponds to peaks related to ZnO, confirming that the oxygen content comes from oxidation of metal [50, 63, 65]. No dominant $\mathrm{Mn_3O_4}$ peaks are present in the Raman given

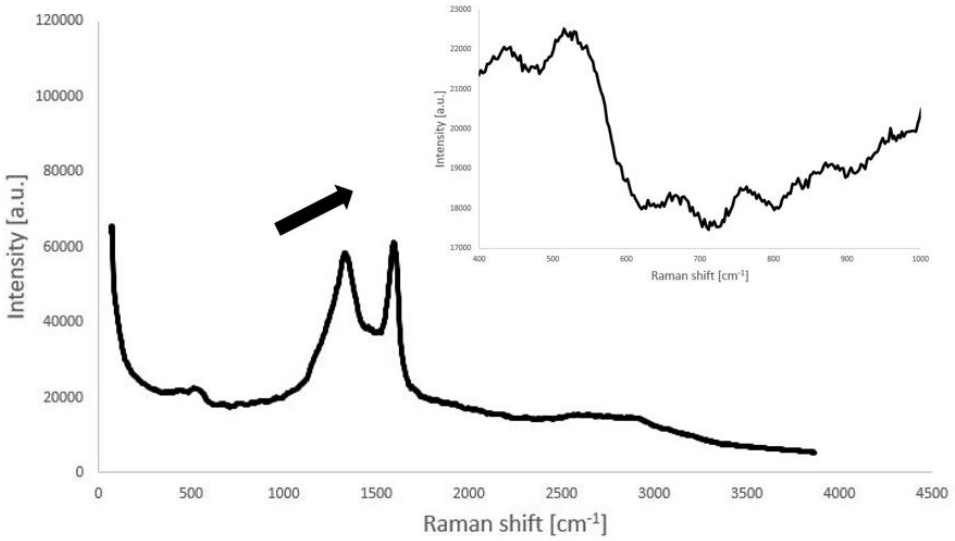

Figure 4.39: Raman spectrum of deposited coating at the centre at -1.50 V vs. Ag/AgCl (sat.) (DC) in acidic sulphate electrolyte

the low Mn concentration found.

Reports of 4 at. % Mn from similar setup are similar to the 4 at. % found in the coating for same setup with 60 s deposition time [45]. However the Zn content was lower and deposit sizes were smaller for this setup, mainly due to the lower deposition time applied [12]. The oxygen found in the previous study is, after reviewing the results, most likely arriving from oxidised Zn or Mn, and not hydroxide formation as first believed.

4.4.3 Pulse plating (PC) - changing current density

Pulse plating (PC) technique was done in a similar fashion with acidic sulphate electrolyte as with the alkaline sulphate electrolyte. Two samples with i_{cath} below the associated current density at -1.50 V vs. Ag/AgCl (sat.) was prepared for analysing. The two samples were constructed to achieve i_{avg} of 32 and 36 mA/cm^2 respectively, in addition to θ = 40 % and f = 4 Hz.

Sample 8: 32 mA/cm^2 (PC, 4 Hz)

PC setup for sample achieving 32 mA/cm^2 in acidic sulphate electrolyte is illustrated in Figure 4.40, showing two cycles. Key parameters for deposition are shown in Table 4.15. The current setup reaches the desired anodic current density, 0 mA/cm^2, for the setup constructed. The sample experience larger i_{avg} than the constructed 32 mA/cm^2 in accordance with previous stated trends for the PC setup.

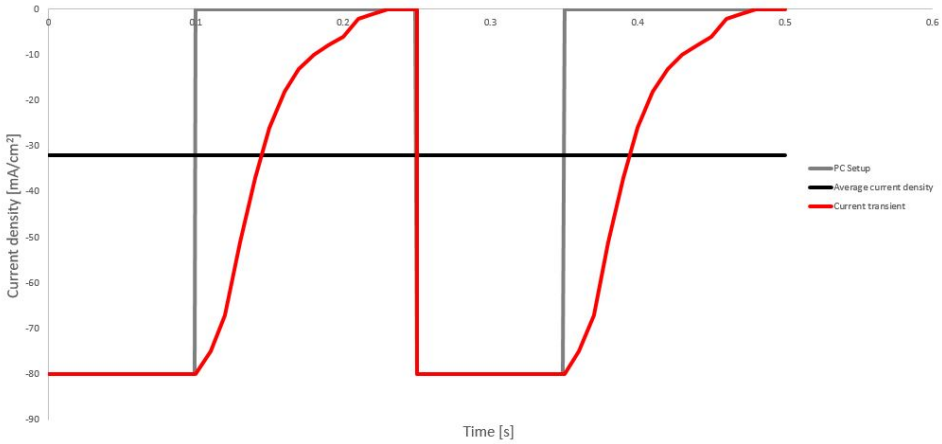

Figure 4.40: Setup for PC plating at 32 $\mathrm{mA/cm^2}$ (4 Hz) in acidic sulphate electrolyte

Table 4.15: Key values for PC setup giving i_{avg} = 32 $\mathrm{mA/cm^2}$ (4 Hz) in acidic sulphate electrolyte

t_{off} [s]	t_{on} [s]	t_{cycle} [s]	i_{an} [$\mathrm{mA/cm^2}$]	i_{cath} [$\mathrm{mA/cm^2}$]	i_{avg} [$\mathrm{mA/cm^2}$]
0.15	0.1	0.25	0	-80	-32

The SEM micrograph of the centre and the EDS analysis are displayed in Figure 4.41 and Table 4.16 respectively. The GDOES analysis is shown in Figure 4.42 and the Raman spectrum is shown in Figure 4.43.

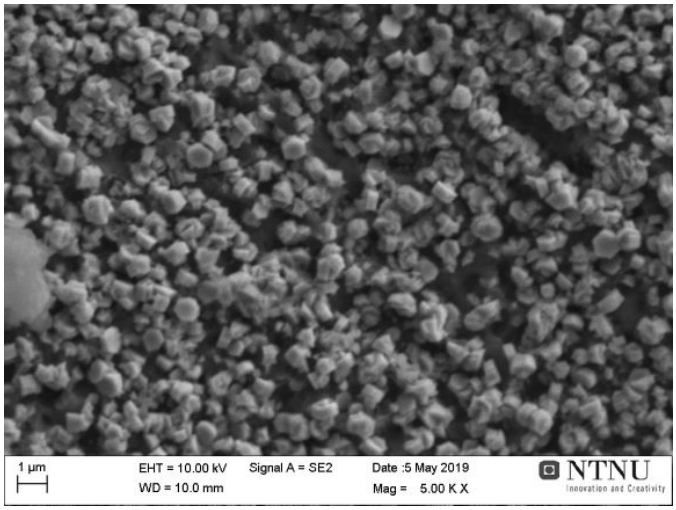

Figure 4.41: Scanning electron micrograph at the centre of deposited coating at 32 $\mathrm{mA/cm^2}$ (sat.) (PC, 4 Hz) in alkaline pyrophosphate electrolyte (5KX)

Table 4.16: EDS elemental composition of deposited coating at the centre at 32 $\mathrm{mA/cm^2}$ (PC, 4 Hz) in acidic sulphate electrolyte

Element	Atomic percent w/ Al [%]	Atomic percent wo/ Al [%]
Al	15	0
Zn	55	66
Mn	12	14
O	16	19
S	1	1

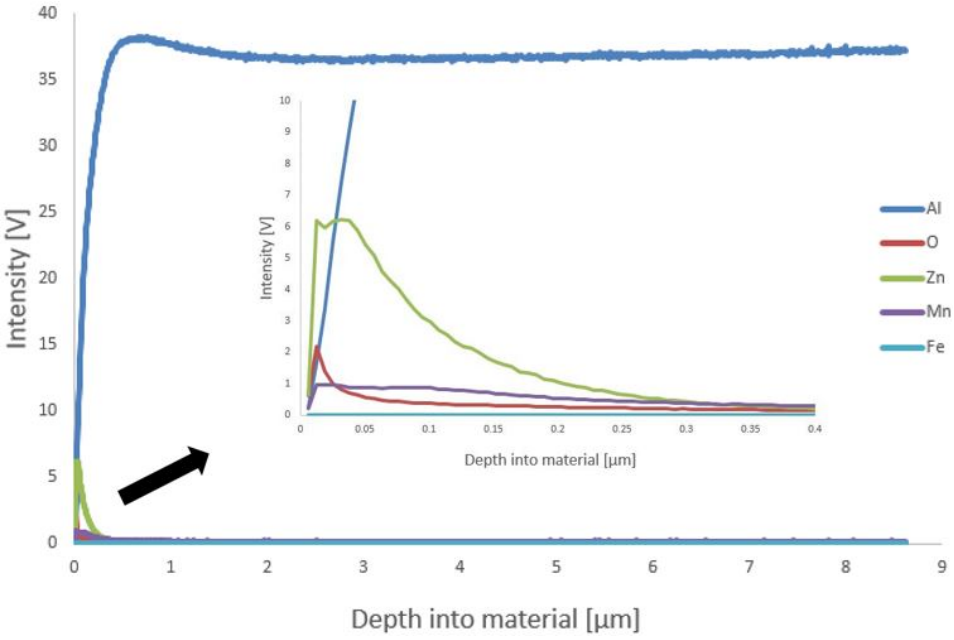

Figure 4.42: GDOES elemental depth profile of deposited coating at the centre at 32 $\mathrm{mA/cm^2}$ (PC, 4 Hz) in acidic sulphate electrolyte

Deposits shown in Figure 4.41 are smaller and more evenly distributed over the coating surface when compared to the deposit from DC sample in the same electrolyte. The pulse setup and current density applied favour nucleation rate for each pulse, as observed with the alkaline pyrophosphate electrolyte [42, 54]. Inclusion of sulphate, either from adsorption on the substrate surface or deposit of complex, also factor towards the lower sizes of the deposits [62].

Several hexagonal plates are observed, indicating that Zn is the major contributor for the electrodeposited coating [7]. This is confirmed from the EDS analysis from Table 4.16. The $\mathrm{i_{avg}}$ applied for the pulse setup have lead to lower detected Al content in the sample compared to the DC sample. Non compact deposit distribution (the zincated surface can

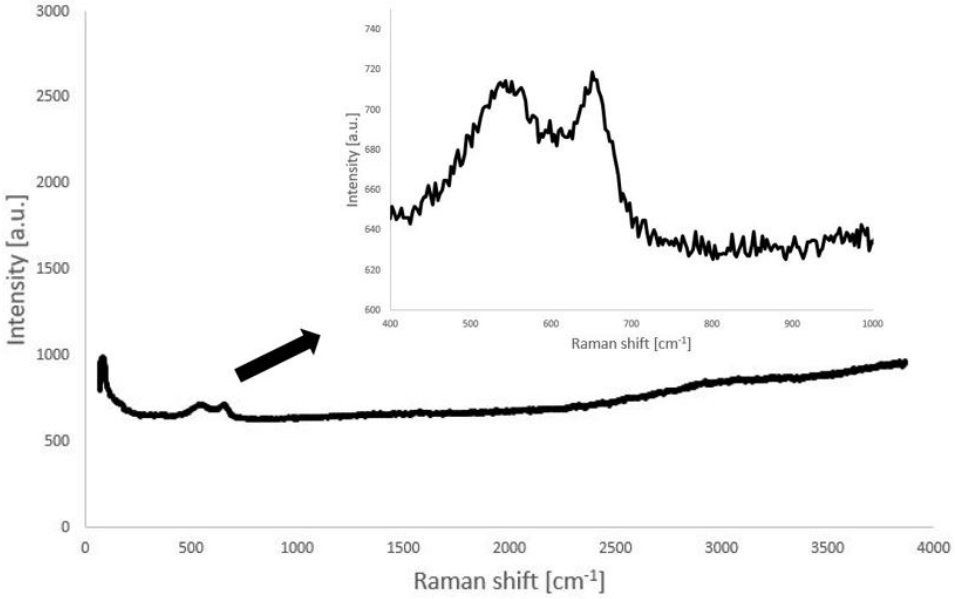

Figure 4.43: Raman spectrum of deposited coating at the centre at 32 $\mathrm{mA/cm^2}$ (PC, 4 Hz) in acidic sulphate electrolyte

be observed) for the DC deposit shown in Figure 4.37 must be factoring towards this observation [42]. The lower Al content found for the pulse setup was not expected, and leads to further uncertainty to the DC setup as the analysed surface must have experienced lower current density than what was recorded. Inclusion of Mn in the coating for a cathodic current density chosen at 80 $\mathrm{mA/cm^2}$ either leans towards 70 $\mathrm{mA/cm^2}$ being too low of a current density for Mn incorporation, or that Mn have deposited other places for Sample 7.

Mn concentration profile from GDOES depth profile in Figure 4.42 displays Mn deposition throughout the coating. Zn is the major contributor to the coating, as displayed in Table 4.16. The oxygen arrives yet again from oxidised metals, which correlates well with the Raman spectrum peaks shown in Figure 4.43 showing Zn-O and Mn-O bound peaks [56, 63]. 49 $\%$ CE is lower than the pulse setup for the alkaline pyrophosphate electrolyte where the current density applied were up to 150 $\mathrm{mA/cm^2}$. The larger current density needed was factored by the Pourbaix-pH relationship and choosing pyrophosphate as an additive, as the additive shift the reduction potential for $\mathrm{Zn^{2+}}$ and $\mathrm{Mn^{2+}}$ towards lower potentials and thus higher cathodic current densities [6, 18, 21]. Considering the pulse setup and the current efficiencies calculated, it can be suggested that pyrophosphate aids the electrolyte better than boric acid and sulphate salt in regards towards hydrogen evolution inhibition and lowering reduction potential gap difference for PC setup.

The edge of the sample was analysed in similar fashion. The SEM micrograph and EDS analysis are shown in Figure 4.44 and Table 4.17 respectively. The GDOES depth profile

is displayed in Figure 4.45 and Raman spectroscopy is shown in Figure 4.46.

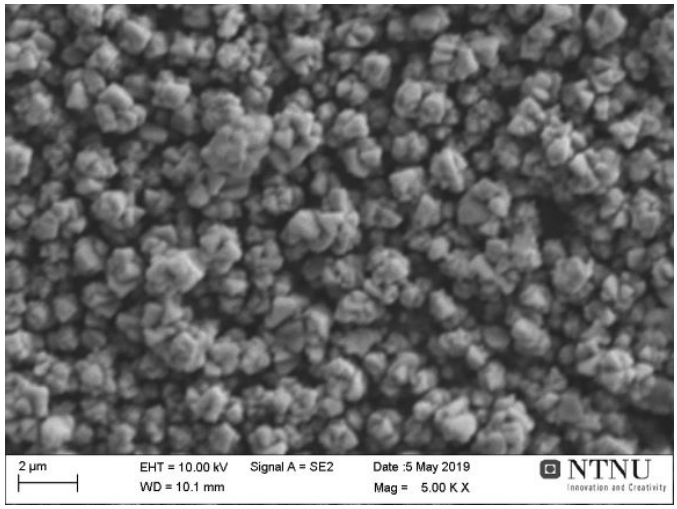

Figure 4.44: Scanning electron micrograph at the edge of deposited coating at 32 $\mathrm{mA/cm^2}$ (sat.) (PC, 4 Hz) in alkaline pyrophosphate electrolyte (5KX)

Table 4.17: EDS elemental composition of deposited coating at the edge at 32 $\mathrm{mA/cm^2}$ (PC, 4 Hz) in acidic sulphate electrolyte

Element	**Atomic percent w/ Al [%]**	**Atomic percent wo/ Al [%]**
Al	3	0
Zn	76	78
Mn	14	15
O	7	7
S	0	0

The deposit shown in the micrograph in Figure 4.44 shows a more compact and layered deposit distribution with decreased pores and conglomerated particles. It is also showing less single hexagonal particles compared to the morphology at the centre. The larger particle sizes are to be expected from the trend at higher current density experienced at the edge. The change in morphology suggest Zn-Mn co-deposition [10, 43, 46].

The coating consists mainly of Zn and Mn, with smaller oxygen content at the edge than at the centre, as depicted in Table 4.17. The coating is also thicker at the edge given the lower concentration of Al detected. The result shows that favourably incorporating Mn in the deposit is by applying higher current density, making Mn a more dominant element in the coating [10, 21, 43, 46]. Incorporation of more Mn and generally thicker coating also explain the lower content of sulphur at the edge compared to that of the centre of the sample [46].

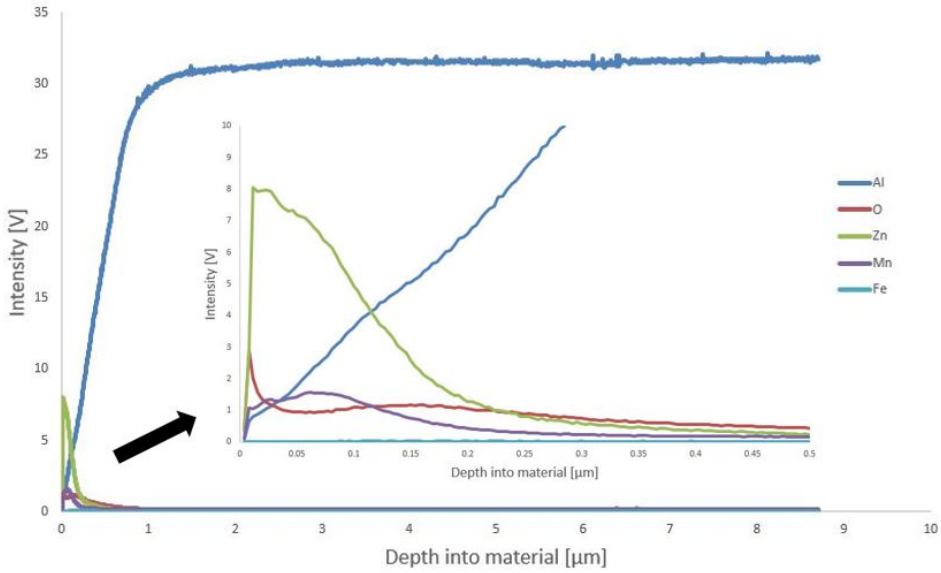

Figure 4.45: GDOES elemental depth profile of deposited coating at the edge at 32 $\mathrm{mA/cm^2}$ (PC, 4 Hz) in acidic sulphate electrolyte

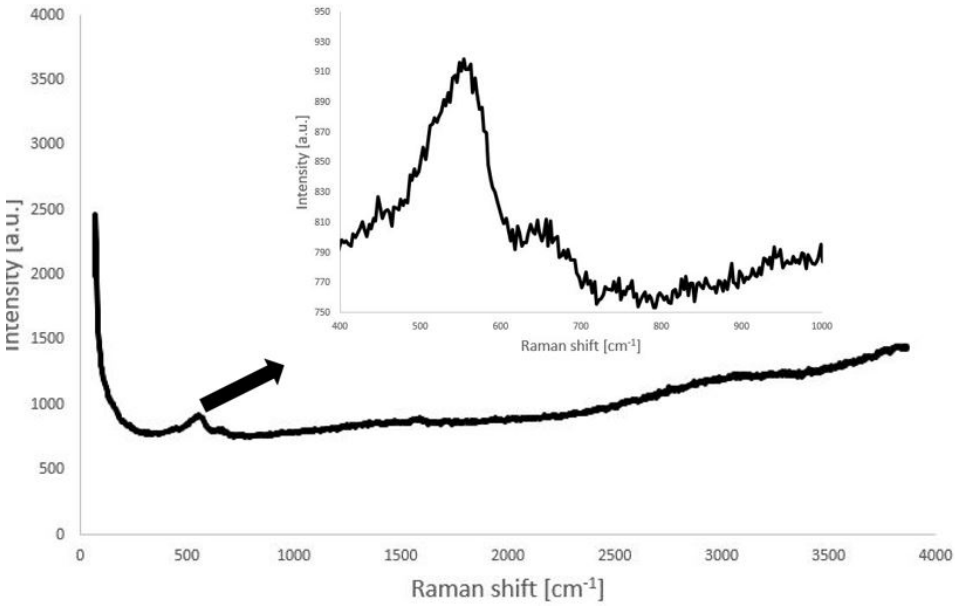

Figure 4.46: Raman spectrum of deposited coating at the edge at 32 $\mathrm{mA/cm^2}$ (PC, 4 Hz) in acidic sulphate electrolyte

Previous trends have, however, stated that increased Zn and Mn tends to increase the oxygen content as well. This is not the case for this sample, as the oxygen content have decreased while the Zn and Mn content have increased. Factors playing in to this result is more Mn content inside the coating, and less oxidised metal at the coating surface. This is confirmed following the increased concentration of Mn inside the coating until 0.075 μm shown in Figure 4.45. Co-deposition have occurred inside the coating for this sample, given the

No Mn-O bonding peaks are dominating in the Raman spectrum of the edge shown in Figure 4.46, as the peak is correlated to ZnO [56, 63]. The result strengthens the claim that pure Mn or Zn-Mn deposits are present in the coating, and that oxidation of the Mn at the coating surface is a large contributor to the oxygen content in the coating.

Sample 9: 36 mA/cm^2 (PC, 4 Hz)

The final sample analysed was with acidic sulphate electrolyte and increasing the $\mathrm{i_{cath}}$ from 80 to 90 $\mathrm{mA/cm^2}$, achieving $\mathrm{i_{avg}}$ of 36 $\mathrm{mA/cm^2}$. PC setup is shown in Figure 4.47, showing two cycles. Key parameters are shown in Table 4.18. The setup reaches 0 $\mathrm{mA/cm^2}$ slower than the setup achieving 32 $\mathrm{mA/cm^2}$, showing similar behaviour as the alkaline pyrophosphate electrolyte when increasing $\mathrm{i_{cath}}$. The average current density is also here larger than constructed. SEM micrograph, EDS analysis, GDOES concentration profile and Raman spectrum are displayed in Figure 4.48, Table 4.19, Figure 4.49 and 4.50 respectively.

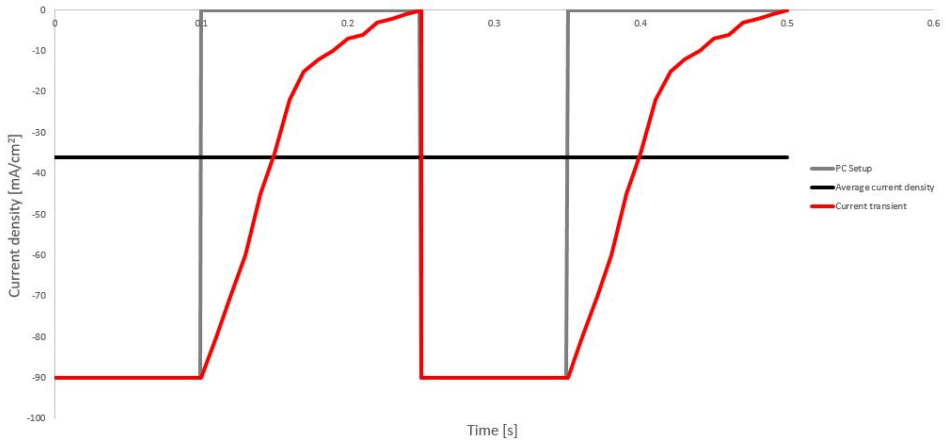

Figure 4.47: Setup for PC plating at 36 $\mathrm{mA/cm^2}$ (4 Hz) in acidic sulphate electrolyte

A more compact layer is presented in Figure 4.48 when comparing with the centre of Sample 8. The increased current density have, as expected, enhanced the nucleation rate for deposits [64]. Larger oxygen content have been found on the coating surface, as shown in Table 4.20. Mn content have decreased at the centre, mainly since the detected oxygen

Table 4.18: Key values for PC setup giving i_{avg} = 36 mA/cm^2 (4 Hz) in acidic sulphate electrolyte

t_{off} [s]	t_{on} **[s]**	t_{cycle} **[s]**	i_{an} **[**mA/cm^2**]**	i_{cath} **[**mA/cm^2**]**	i_{avg} **[**mA/cm^2**]**
0.15	0.1	0.25	0	-90	-36

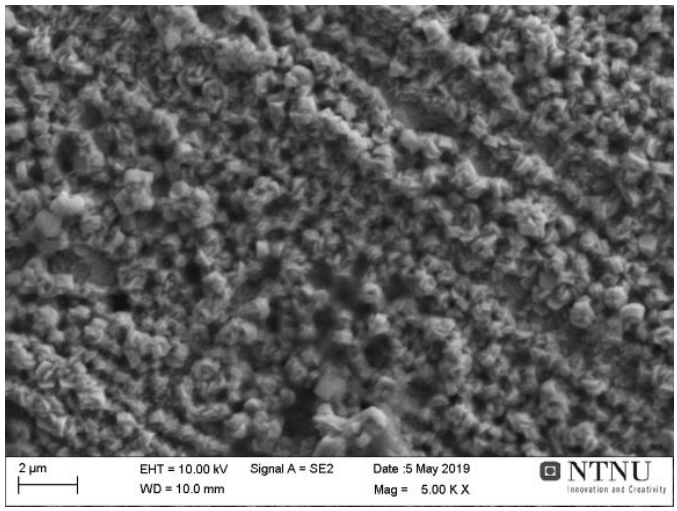

Figure 4.48: Scanning electron micrograph at the centre of deposited coating at 36 mA/cm^2 (sat.) (PC, 4 Hz) in acidic sulphate electrolyte (5KX)

Table 4.19: EDS elemental composition of deposited coating at the centre at 36 mA/cm^2 (PC, 4 Hz) in acidic sulphate electrolyte

Element	**Atomic percent w/ Al [%]**	**Atomic percent wo/ Al [%]**
Al	6	0
Zn	56	60
Mn	8	9
O	30	31
S	0	0

content have increased drastically. The GDOES profile in Figure 4.49 confirms this trend for oxygen. More metal have oxidised at the surface as the peak for both Zn and Mn are larger than at the centre for Sample 8 with lower i_{avg}. Comparing Mn content for the different samples then becomes difficult, as the oxygen content included drastically alters the final value for Mn in the EDS result. The trend between Zn and Mn confirm that some co-deposition have deposited inside the coating.

The aforementioned oxidation peaks for Mn and Zn are present in the Raman spectrum range at 550 and 660 cm^{-1}. The peak at around 310 cm^{-1}, indicating Mn_2O_3 incorpo-

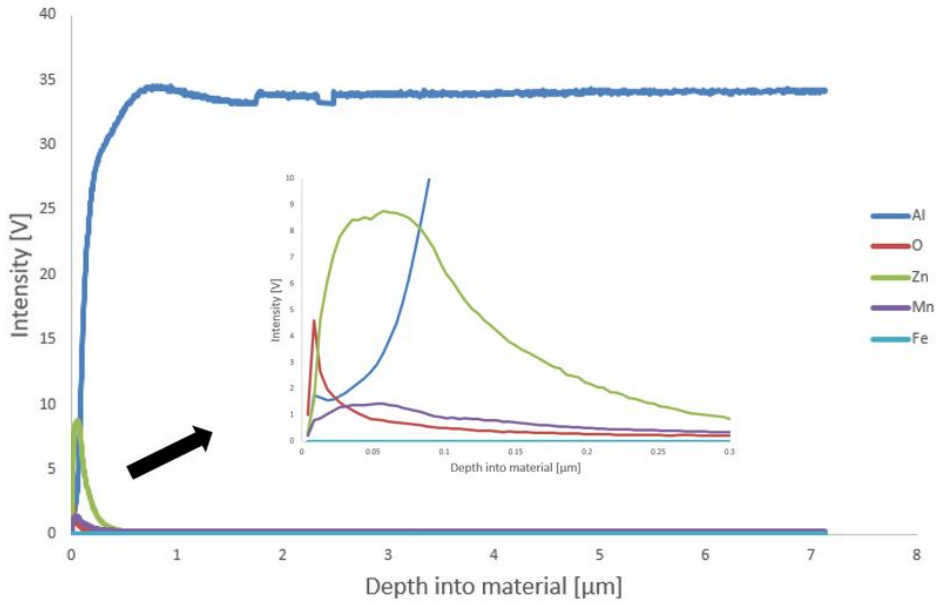

Figure 4.49: GDOES elemental depth profile of deposited coating at the centre at 36 $\mathrm{mA/cm^2}$ (PC, 4 Hz) in acidic sulphate electrolyte

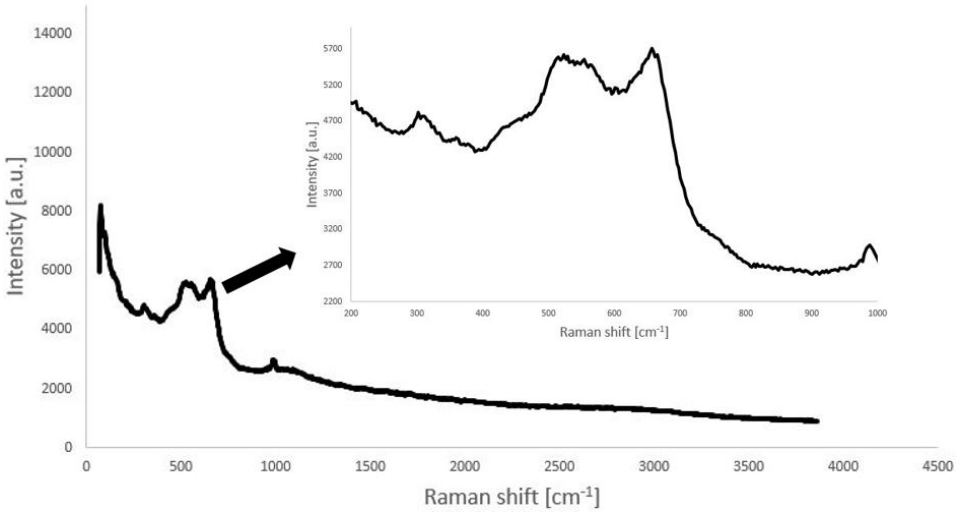

Figure 4.50: Raman spectrum of deposited coating at the centre at 36 $\mathrm{mA/cm^2}$ (PC, 4 Hz) in acidic sulphate electrolyte

ration, contributes to the large oxygen peak in the GDOES profile shown in Figure 4.49 [41, 56]. CE of 44 %, lower than the Sample 8 with lower $\mathrm{i_{avg}}$, was expected following the

trends for samples from alkaline pyrophosphate electrolytes and documented results from acidic sulphate electrolyte [23].

The results of the edge for the same sample are shown in Figure 4.51, Table 4.20, Figure 4.53 and Figure 4.52.

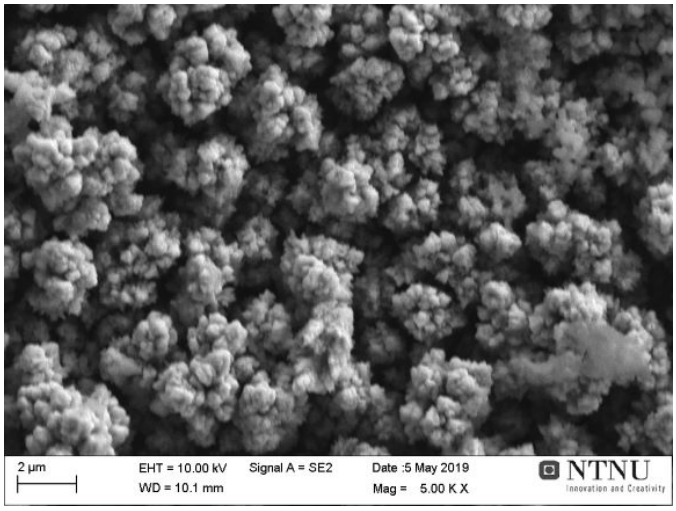

Figure 4.51: Scanning electron micrograph at the edge of deposited coating at 36 $\mathrm{mA/cm^2}$ (sat.) (PC, 4 Hz) in acidic sulphate electrolyte (5KX)

Table 4.20: EDS elemental composition of deposited coating at the edge at 36 $\mathrm{mA/cm^2}$ (PC, 4 Hz) in acidic sulphate electrolyte

Element	Atomic percent w/ Al [%]	Atomic percent wo/ Al [%]
Al	0	0
Zn	44	44
Mn	13	13
O	38	38
S	5	5

Sprouts of deposits make up the coating shown in Figure 4.51. The chosen current densities favours nucleation formation as clusters have been deposited in larger quantities [42, 54]. The GDOES profile in Figure 4.53 demonstrates large amounts of Mn deposited in the coating, and confirms that the EDS analysis is not able to predict Mn content alone. Mn content for 13 at. % is accompanied with 38 at. % oxygen, and the GDOES analysis clearly demonstrates the relationship between deposited Mn and oxidation which has been reported before [41]. The Mn and Zn profiles clearly shows an linear trend until around 0.025 μm, indicating that co-deposition have occurred. The larger Zn content found from the EDS analysis, even though the GDOES profile hints towards larger Mn content, largely

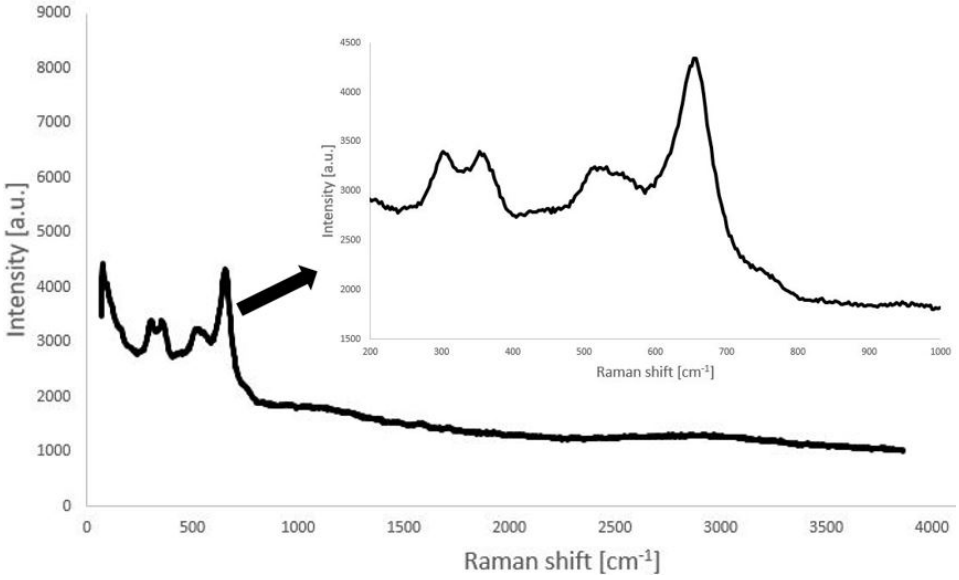

Figure 4.52: Raman spectrum of deposited coating at the edge at 36 $\mathrm{mA/cm^2}$ (PC, 4 Hz) in acidic sulphate electrolyte

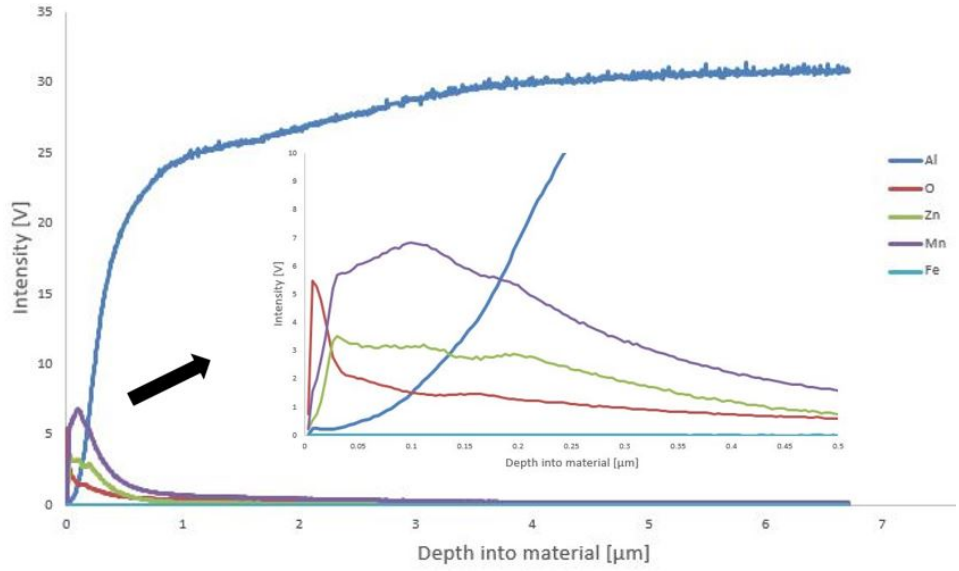

Figure 4.53: GDOES elemental depth profile of deposited coating at the edge at 36 $\mathrm{mA/cm^2}$ (PC, 4 Hz) in acidic sulphate electrolyte

originate from Zn deposition inside the coating.

All the previous peaks related to Mn-O bonds from Raman spectrum are present in Figure 4.52. Peaks at 310, 350 and 660 cm^{-1} corresponds to $\mathrm{MnO_2}$-species and $\mathrm{Mn_3O_4}$ [56, 58, 60]. The Mn peaks are to be expected as a result from the increased Mn showed in the GDOES profile.

Effect of plating setups in acidic sulphate electrolyte

DC application for the acidic sulphate electrolyte showed low Mn content at the centre, but since the edge was not analysed nor larger $\mathrm{i_{cath}}$ was applied no definitive answer can be given for the application. CE for the process was estimated to 35 $\%$, as compared to 32 and 51 $\%$ for the DC samples in alkaline pyrophosphate electrolyte with longer deposition time. As larger current densities is needed for incorporation of Mn for the DC application, the process will head towards lower efficiencies resulting from the larger amount of hydrogen evolution developed.

Sample 8 and 9, with chosen $\mathrm{i_{cath}}$ at 80 and 90 $\mathrm{mA/cm^2}$ respectively, all showed inclusion of Mn in some fashion. These were also the only samples where the content of Mn was larger 2 at. $\%$ at the centre, showing 12 and 8 at. $\%$ respectively. Oxidation of metal all occurred at these samples as well, and were included in such a fashion that the Mn content is not well reflected in the EDS Tables. The GDOES analysis for the samples highlighted exemplified this trend, as Mn content was largest at the 36 $\mathrm{mA/cm^2}$ edge sample but in addition the oxygen content was largest here.

At the edge of Sample 8 the Mn was able to be deposited inside the coating, and the lower Mn metal at the coating surface reduced the oxygen content. Deposition parameters need to enhance Mn deposit further below the coating, as oxidation of metal prevent only metal containing deposit. This trend have been reported before, and have been provided with purging the electrolyte [41]. Disadvantage with this electrolyte include the lower current efficiencies (44-49 $\%$ in acidic sulphate electrolyte, and 60-80 $\%$ in alkaline pyrophosphate electrolyte), even though lower current densities were applied. Inclusion of sulphur was kept to a minimal, and was most notably at higher current densities at the edges. Overall pulse plating provides the coating with larger Mn content and higher current efficiencies, thus making this plating setup superior compared to the DC sample for Zn-Mn co-deposition.

4.5 Comparison between electrolytes

4.5.1 DC

Compact and deposit rich coating was achieved with the alkaline electrolyte for the DC samples. The result is coloured by larger deposition time for the alkaline electrolyte. Higher current efficiencies for larger current densities applied for the alkaline bath gives insight into the reported properties pyrophosphate provides electrolyte [21, 23]. The unevenness and non uniform distribution of the deposit for large current densities and excessive hydrogen evolution, as shown with Sample 2 (-1.90 V vs. Ag/AgCl (sat.) in alkaline pyrophosphate electrolyte) leads to a more rougher coating. The rougher morphology comes in contrast to the increased Mn content in the deposit, as 11 and 9 at. $\%$ was included in the coating for Sample 1 and 2 respectively.

i_{cath} plays a major part into the Mn inclusion of DC setup in the coating. Usage of DC setup achieved Mn inclusion in the coating for both alkaline samples, but for the acidic sulphate electrolyte sample the current density applied was not adequate for incorporation of Mn. GDOES results indicate large Mn content inclusion in the alkaline pyrophosphate electrolyte by increasing the current density from 60 to 155 $\mathrm{mA/cm^2}$. Even though the EDS analysis indicated otherwise for Sample 2, as shown in Table 4.3, the Raman and GDOES analysis showed Mn rich coating for the largest possible i_{cath} possible for the potentiostat used. Lower CE for acidic sulphate electrolyte, even with lower deposition time compared with Sample 1 and 2, indicate that the alkaline electrolyte is superior for incorporation of Mn in the coating and with better efficiency.

4.5.2 Pulse plating

Pulse setup for both baths included more clustered deposits when compared to the DC samples, a result expected from the previous pulse plating setups [42, 54, 61]. Generally smaller deposits were observed for the alkaline pyrophosphate based samples utilising larger frequencies. Larger frequencies are expected to produce a more uniform and compact coating. However as seen in the SEM micrograph in Figure 4.16 with Sample 3 (48 $\mathrm{mA/cm^2}$, 10 Hz) some deposits have the same size as the sample utilising lower frequency (4 Hz). Flaws with the pulse setup and non ideal current transient leads to larger perceived current densities for the samples with larger frequencies, possibly assist in nucleation growth. Compactness and uniform deposit size can be easier controlled with more advanced pulse current machines.

The centre of the samples in alkaline pyrophosphate electrolyte illustrated low inclusion of Mn, ranging from 0 to 2 at. $\%$. The decrease in frequency change did not aid in Mn deposition at the centre of the samples. However the edges of Sample 3 and 4 (48 $\mathrm{mA/cm^2}$ using 10 Hz and 20 Hz respectively) could contain additional information as additional Mn was found at the edges for Sample 5 and 6 (both utilising 4 Hz and 48 and 60 $\mathrm{mA/cm^2}$ respectively).

Sample 8 and Sample 9 (32 and 36 $\mathrm{mA/cm^2}$ in acidic sulphate electrolyte respectively)

displayed increased Mn content throughout the coating, as displayed in Figure 4.45 and 4.49. Edge analysis of Sample 8 in particular illustrated that the chemical composition of the coating surface is a major contributor to the oxygen content included; larger Zn incorporation at the surface aids the coating with covering up the deposited Mn and protecting it from oxidation. Oxidation of Zn was found in close to all samples. However oxidation of Mn was the major contributor to oxygen increase. This result was highlighted in Sample 9 at the edge, as the highest Mn peak for PC deposition was found in the GDOES analysis in Figure 4.53.

Increased i_{cath} lead to larger Mn content in the coating in accordance with GDOES results for all acidic sulphate samples. The trend was also applicable for increased Zn concentration, as expected from previous result using acidic electrolytes [7, 9, 10, 22, 23]. The only sample not following this trend was the edge of Sample 9, which had deposited larger quantities of Mn compared to Zn. Maximum content previously found in acidic based baths for Zn-Mn electro co-deposition applying DC application was reported to be 27 wt. $\%$ [7]. However the pulse setup hints towards larger ratios, in contrast to what the EDS analysis in Table 4.20 for Sample 9 at the edge documented. Sample 9 experienced the highest i_{avg} for all the acidic pulse plating samples. Inclusion of oxygen makes direct comparison of at. or wt. $\%$ of Zn-Mn complicated, but the GDOES illustration in Figure 4.53 leans to the fact that Zn-Mn co-deposition have occurred given the concentration trend for both Mn and Zn. The dominating peaks found in the Raman spectrum for these samples were primarily related to Mn-O peaks, and corresponds well with previous Mn oxides found from Zn-Mn deposition [23, 56, 58, 60].

CE was larger for samples in alkaline pyrophosphate electrolyte, ranging from 60 to 80 $\%$. The high current densities necessary for reduction of the metals generated large amounts of hydrogen bubbles, but was contributor towards disturbance of uniform deposit [23]. Lower current efficiency, in a region between 44 to 49 $\%$, was documented in the acidic sulphate electrolyte. The inconsistency for uniform deposit is a result from large hydrogen evolution at the applied currents, which again is reflected in the values for current efficiency. GDOES and SEM micrographs from the PC samples also highlights that the pulse setup leaves a more compact and uniform coating at the centre, and rough and uneven structure on the edges.

4.6 Co-deposition of Zn-Mn

Morphology nor the EDS analysis has given enough information for prediction of Zn-Mn co-deposition for the different samples. The Raman spectra has not demonstrated dominated peaks for $ZnMn_2O_4$ around 320 cm^{-1}, thus highlighting that oxidized Zn-Mn co-deposit is not located at the coating surface. No regular Zn-Mn was expected to be deposited at the surface as well, given the general oxygen trend and content found in the GDOES and EDS analysis and from the found oxygen bound peaks. However the GDOES analysis showed signs of co-deposit given the aforementioned Zn-Mn trend profile. Both centre and edge for Sample 6, highlighted in Figure 4.30 and 4.33, exhibited this trend with similar increase and decrease of intensity. Similar trend was showed for

Sample 9 at the edge in Figure 4.53 and Sample 2 with the DC deposition, according to the GDOES spectrum in Figure 4.13. As with previous results trying co-deposition of Zn-Mn the samples with largest i_{cath} are the ones exhibiting Zn-Mn co-deposition trends [6, 7, 9, 10, 21, 22, 23].

Chapter 5

Conclusion

On the basis of the results presented it can be concluded that Zn and Mn can deposited using electrodeposition in both alkaline pyrophosphate and acidic sulphate electrolytes. The alkaline pyrophosphate electrolyte included Mn at. $\%$ in the following atomic ratios: 9-11 using DC setup with i_{avg} ranging from 60-155 mA/cm^2 and 0-14 at. $\%$ using PC setup with frequencies ranging from 4-20 and i_{avg} ranging from 48-60 to mA/cm^2. Morphology for the PC samples varied from compact and uniform for the PC samples at the centre, to more clustered, non uniform and rough deposit distribution at the edges. Increased i_{cath} lead to less uniform deposit distribution for DC samples. CE ranged from 32-51 $\%$ for DC samples and 60-80 $\%$ for PC samples, and all samples exhibited lower CE when i_{avg} was increased.

The acidic sulphate electrolyte displayed Mn at. $\%$ in the following atomic ratios: 1 at. $\%$ for DC setup utilising i_{avg} of 70 mA/cm^2 and 8-14 at. $\%$ for PC setup with frequency of 4 and i_{avg} ranging from 32-36 mA/cm^2. Morphology for the deposits for the DC and PC setup in acidic sulphate electrolyte displayed the same trend as the alkaline pyrophosphate electrolyte. CE for the DC sample was 35 $\%$, while it ranged from 45-49 $\%$ for the PC samples. PC samples at the edge (Sample 6 for alkaline and Sample 9 for acidic) incorporated largest amounts of M. Higher CE for the alkaline pyrophosphate electrolyte makes the electrolyte more efficient than the acidic electrolyte for both current application, and therefore the most promising electrolyte for Zn-Mn co-deposition.

GDOES analysis showed that the main Zn-Mn co-deposited phases was formed inside the coating, and for the PC samples utilising the largest i_{cath}. Oxidised specimens of Zn and Mn analysed from Raman spectra, like ZnO, Mn_3O_4 and MnO_2, made up most of the deposits on the coating surface from both electrolytes and was the major contributor to the oxygen found for all coatings.

Chapter 6

Further work

Improvements can be done for both deposition methods for less oxidation of surface metal and more incorporation of co deposited Zn-Mn. Additives in the zincate bath, like $FeCl_3$, can be added for even more adhesive substrate surface which might change the CE values found [36]. Smaller area should be utilised for more controlled electrochemical reactions on the aluminium surface. Several areas from the analysed samples were not analysed, leaving potential for more Mn deposited. Sample 3 and 4 (PC, 10 and 20 Hz respectively) in particular could exhibit more Zn and Mn than from the centre analysed. The area restriction also makes it more effective towards analysing the deposits.

Utilisation of improved instruments regarding PC setup can be applied for better anodic parameter control of t_{off} and i_{an}, providing better uniformity and compactness of the coating [42, 54, 61]. More samples can be studied for determining the maximum i_{cath} at which Mn gets incorporated in the coating at DC setup, and further optimizing CE in the process. The PRC setup can also be considered as plating setup, since previous studies suggest more uniform and compact coating for a price of lower CE. PRC setup can aid towards removing the oxidised layer on the surface [25].

Other electrolytes may be analysed for improved CE and incorporation of Zn-Mn co deposition, like acidic chloride electrolyte [5, 6, 10]. Additional additives can be looked at for the two tested electrolytes. Parameters not examined, like temperature dependence, pH dependence, stirring or purging, can be looked at for optimalisation of Zn-Mn incorporation on the aluminium substrate. X-ray diffraction (XRD) examination can be done on the deposits for a more qualitative analysis of exact phases deposited. Further investigation of the phases can be done for determination of which phases aids towards improved corrosion resistance in the diffusion coating. The deposited coatings on the aluminium substrate can be heat treated, and accelerated corrosion testing in seawater can be looked at for corrosion parameters characterisation like corrosion potential.

Bibliography

[1] M. Stepanova. *Zinc-rich coatings for improved corrosion resistance of extruded aluminium heatexchange tubing in acidified chloride solution*. PhD thesis, NTNU, 2017.

[2] G. Heidari, M. Mosavi-khoie, A. Hasanzadeh, P. Marashi, H. Keshmiri, and A. Shahosseini. Investigation of zinc thermal diffused coatings by solid state diffusion method. *Mater. Sci. Technol.*, pages 1462–1472, 2008.

[3] X.I. Zhang, S.L. Russo, A. Miotello, and L.A. Guzmán. The corrosion behavior of Zn coatings on Al3103 alloy. *Surf. Coat. Technol. 141*, pages 187–193, 2001.

[4] J.C.S Fernandes and M.G.S. Ferreira. Corrosion behaviour of physically vapour deposited Al-Zn coatings on 7075 aluminium alloy. *Surf. Coat. Technol. 53*, pages 99–100, 1992.

[5] M. Bucko, J. Rogan, S.I. Stevanovic, S. Staknovic, and J.B. Bajat. The influence of anion type in electrolyte on the properties of electrodeposited Zn-Mn alloy coatings. *Surf. Coat. Technol. 228*, pages 221–228, 2013.

[6] D. Sylla, C. Rebere, M. Gadouleau, C. Savall, J. Creus, and PH. Refait. Electrodeposition of Zn-Mn alloys in acidic and alkaline baths. influence of additives on the morphological and structural properties. *J. Appl. Electrochem. 35*, pages 1133–1139, 2005.

[7] S. Ganesan, G. Prabhu, and B.N Popov. Electrodeposition and characterization of Zn-Mn coatings for corrosion protection. *Surf. Coat. Technol. 238*, pages 143–151, 2014.

[8] N. Boshkov, K. Petrov, and S. Vitkova. Corrosion products of Zn-Mn coatings - part 3: double-protective action of manganese. *Met. Finish. 100*, pages 98–102, 2002.

[9] D. Close, N. Stein, N. Allain, A. Tidu, E. Drynski, M. Merklein, and R. Lallement. Electrodeposition, microstructural characterization and anticorrosive properties of Zn-Mn alloy coatings from acidic chloride electrolyte containing 4-hydroxybenzaldehyde and ammonium thiocyanate. *Surf. Coat. Technol. 298*, pages 73–82, 2016.

[10] N. Loukil and M. Feki. Zn-Mn alloy coatings from acidic chloride bath: Effect of deposition conditions on the Zn-Mn electrodeposition-morphological and structiral characterization. *Appl. Surf. Sci. 410*, pages 574–584, 2017.

[11] L. Pawlowski. *The Science and engineering of thermal spray coatings*. Wiley: USA, 1995.

[12] N. Kanani. *Electroplating: Basic Principles, Processes and Practice*. Elsevier Advanced Technology: UK, 2004.

[13] K.B. Oldham, J.C. Myland, and A.M. Bond. *Electrochemical science and technology*. John Wiley and Sons:UK, 2012.

[14] C.H. Hamann, A. Hamnett, and W. Vielstich. *Electrochemistry*. Wiley-VCH:Germany, 2007.

[15] J. Thonstad. *Fag 53541 Elektrolyseprosesser*. Institutt for teknisk elektrokjemi, Norges teknisk-naturvitenskapelige universitet:Norway, 1998.

[16] R.H. Petrucci, F.G. Herring, J.D. Madura, and C. Bissonnette. *General Chemistry: Principles and Modern Applications*. Peason:US, 2011.

[17] A.G. Blackman and L.R Gahan. *Aylward and Findlay's SI chemical data*. Wiley and Sons:Australia, 7.th edition, 2014.

[18] M. Pourbaix. *Atlas of electrochemical equilibria in equeous solutions*. Pergamon Press:USA, 1966.

[19] M.J. Rahman, S.R. Sen, and M. Moniruzzaman. Morphology and properties of electrodeposited Zn-Ni alloy coating on mild steel. *J. Mech. Eng. Sci. 40*, pages 9–14, 2009.

[20] S. Kunze and D. Schlettwein. Electrochemical and electroless deposition of porous zinc oxide on aluminium. *Electrochim. Acta. 128*, pages 360–367, 2014.

[21] D. Sylla, C. Savall, M. Gadouleau, C. Rebere, J. Creus, and P.H. Refait. Electrodeposition of Zn-Mn alloys on steel using an alkaline pyrophosphate-based electrolytic bath. *Surf. Coat. Technol. 200*, pages 2137–2145, 2004.

[22] M.V. Tomic, M.M. Bucko, M.G. Pavlovic, and J.B. Bajat. Corrosion stability of electrochemically deposited Zn-Mn alloy coatings. *Contemp. Mater. 1*, pages 87–93, 2010.

[23] M. Bucko, J. ROgan, S.I. Stevanovic, A. Peric-Grujic, and J.B. Bajat. Initial corrosion protection of Zn-Mn alloys electrodeposited from alkaline solution. *Corros. Sci. 53*, pages 2861–2871, 2011.

[24] S. Kumar, S. Pande, and P. Verma. Factor effecting electro-deposition process. *Int. J. Curr. Eng. Technol. 55*, pages 700–703, 2015.

[25] M.S Chandrasekar and M. Pushpavanam. Pulse and pulse reversing plating - conceptual, advantages and applications. *Electrochim. Acta 53*, pages 3313–3322, 2008.

[26] J.Y. Fei and G.D. Wilcox. Electrodeposition of Zn-Co alloys with pulse containing reverse current. *Electrochim. Acta. 50*, pages 2693–2698, 2005.

[27] W.E.G. Hansal and S. Roy. *Pulse Plating*. Eugen G. Leuze Verlag KG:Germany, 2012.

[28] Y. Addi and A. Khouider. Electrodeposition of Ni-Zn alloys on steel from acidic solution in presence of boric acid. *J. Electrochem. Soc. 45*, pages 79–85, 2013.

[29] K. Wefers and C. Misra. Oxides and hydroxides of aluminium. *Tech. Pap. - Alcoa Res. Lab. 19*, pages 143–151, 1987.

[30] A. Raveh, Z.K. Tsameret, and E. Grossman. Surface characterization of thin layers of aluminium oxide. *Surf. Coat. Technol. 88*, pages 103–111, 1996.

[31] M. Sait, T. Maegawa, and T. Homma. Electrochemical analysis of zincate treatments for Al and Al alloy films. *Electrochim. Acta 51*, pages 1017–1020, 2005.

[32] S. Egoshi, K. Azumi, H. Konno, B. Ebihara, and Y. Taguchi. Effects of minor elements in Al alloy on zincate pretreatment. *Appl. Surf. Sci. 261*, pages 567–573, 2012.

[33] O. Cakir. Chemical etching of aluminium. *J. Mater. Process. Technol. 199*, pages 337–340, 2008.

[34] M. Ardelean, S. Lascau, E. rdelean, and A. Josan. Surface treatments for aluminium alloys. *IOP Conf. Ser.: Mater. Sci. Eng. 294*, pages 1–11, 2018.

[35] A. Farzaneh, M. Sarvari, M. Ehteshamzadeh, and O. Mermer. Effect of zincating bath additives on structural and electrochemical properties of electroless Ni-P coating on aa6061. *Int. J. Electrochem. Sci. 11*, pages 9676–9686, 2016.

[36] M.H. Hafiz and B.S. Mahdi. Surface preparation of aluminium for plating by zincating. *J. Eng. Mater. Technol. 10*, pages 1184–1193, 2007.

[37] A. Augustin, B.U. Bhat, K.R. Udupa, and A.C. Hegde. Electron microscopic study of nodules formed during electrodeposition of copper on aluminium. *Mater. Sci. Forum. 830*, pages 371–374, 2015.

[38] P.G. Schiavi, P. Altimari, F. Pagnanelli, E. Moscardini, and L. Toro. Synthesis of cobalt nanoparticles by electrodeposition onto aluminium foils. *Chem. Eng. Trans. 43*, pages 673–678, 2015.

[39] J. Gruberger and E. Gileadi. Plating on anodized aluminium-I. the mechanism of charge transfer across the barrier-layer oxide film on 1100 aluminium. *Electrochim. Acta. 31*, pages 1531–1540, 1986.

[40] G.D. Wilcox and D.R. Gabe. Electrodeposited zinc alloy coatings. *Corros. Sci. 35*, pages 1251–1258, 1993.

[41] B. Bozzini, E. Griskonis, A. Fanigliulo, and A. Sulcius. Electrodeposition of Zn-Mn alloys in the presence of thiocarbamide. *Surf. Coat. Technol. 154*, pages 294–303, 2002.

[42] C. Muller, M. Sarret, and T. Andreau. Electrodeposition of ZnMn alloys with pulse plating. *J. Electrochem. Soc 150*, pages 772–776, 2003.

[43] P.S. da Silva, E.P. Schmitz, A. Spinelli, and J.R. Garcia. Electrodeposition of Zn and Zn-Mn alloy coatings from an electrolytic bath prepared by recovery of exhausted zinc-carbon batteries. *J. Power Sources 210*, pages 116–121, 2012.

[44] A. Stankeviciute, K. Leinartas, G. Bikulcius, D. Virbalyte, A. Sudavicius, and E. Juzeliunas. Deposition of Zn-Co by constant and pulsed current. *J. Appl. Electrochem. 28*, pages 89–95, 1998.

[45] H. Nordengen. Feasibility study of Zn-Mn electro co-deposition on aluminium, 2018.

[46] D. Thippeswamy and Y. Nayaka Arthoba. Electrochemical studies of Zn-Mn alloy plating from acid sulphate bath using condensation product 4-chloro-2-nitro-n-phenyl methylidene aniline using as a brightener. *J. Chem. Pharm. Res. 9*, pages 146–153, 2017.

[47] J. Hjelen. *Scanning elektron-mikroskopi*. SINTEF, Avdeling for metallurgi:NOR, 1986.

[48] A.C. Ferrari. Raman spectroscopy of graphene and graphite: disorder, electro-phonon coupling, doping and nonadiabatic effects. *Solid State Commun. 143*, pages 47–57, 207.

[49] M.C. Bernard, A.H. Le Goff, and N. Phillips. In situ raman study of the corrosion of zinc-coated steel in the presence of chloride. *J. Electrochem. Soc. 142*, pages 2162–2167, 1995.

[50] M. Matsuda and T. Ohtsuka. In situ raman spectroscopy for corrosion products of zinc in humified atmosphere in the presence of sodium chloride precipitate. *Corrosion (5th Ed.)*, pages 407–413, 2002.

[51] R.L. Frost, H.D. Ruan, and J.T. Kloprogge. Comparison of the raman spectra of bayerite, boehmite, diaspore and gibbsite. *J. Raman Spectrosc. 32*, pages 745–750, 2001.

[52] J. Cai, B. Cheng, G.R. Han, Y. Liu, G.P. Ling, and C.L. SOng. Study of Raman spectra for gamma-aluminium oxide models using first-principles method. *Solid State Commun. 178*, pages 16–22, 2014.

[53] E. Kostka, G.W. Luther, and K.H. Nealson. Chemical and biological reduction of Mn(iii)-pyrophosphate complexes; potential importance of dissolved Mn(iii) as an environmental oxidant. *Geochim. Cosmochim. Acta 59*, pages 885–894, 1995.

[54] M.H. Gharahcheshmeh and M.H. Sohi. Pulse electrodeposition of Zn-Co alloy coatings obtained form an alkaline bath. *Mater. Chem. Phys. 134*, pages 1146–1152, 2012.

[55] Y. Aoki, A.A. Farag, H. Habazaki, Y. Konno, and E. Tsuji. Formation of porous anodic films on carbon steels and their application to corrosion protection composite coatings formed with polypyrrole. *J. Electrochem. Soc. 163*, pages 386–393, 2016.

[56] Y.H. Chen, A. Erbe, O. Kasian, K.J.J. Mayrhofer, and M. Toparli, C. Rabe. Alkaline manganese electrochemistry studied by in situ and operando spectroscopic methods - metal dissolution, oxide formation and oxygen evolution. *Phys. Chem. Chem. Phys. 21*, pages 10457–10469, 2019.

[57] C.B. Azzoni, G. Flor, P. Galinetto, L. Malavasi, and M.C. Mozzati. Raman spectroscopy of AMn2O4 (A = Mn, Mg and Zn) spinels. *Phys. Chem. Chem. Phys. 4*, pages 3876–3880, 2002.

[58] F. Xiao and Y. Xu. Pulse electrodeposition of manganese oxide for high-rate capability supercapacitors. *Int. J. Electrochem. Sci. 7*, pages 7440–7450, 2012.

[59] E.B. Kashkarov, A.V. Kurochkin, T.L. Murashkina, A. Obrosov, Y. Shanenkova, and M.S. Syrtanova. Hydrogen sorption kinetics of SiC-coated Zr-1Nb alloy. *Coatings 9*, pages 1–10, 2019.

[60] S. Du, H. Guan, Y. Wang, and Y. Wang. A facile hydrothermal synthesis of Mn(iv) oxide nanorod– reduced graphene oxide nanocomposites possessing excellent microwave absorption properties. *RSC. Adv. 5*, pages 88979–88988, 2015.

[61] M. Ballester, C.M. Freire, and S.O. Pagotto Jr. Zn–Ni alloy deposits obtained by continuous and pulsed electrodeposition processes. *Surf. Coat. Technol. 122*, pages 10–13, 1999.

[62] D.R. Gabe and S.E. Hadian. Residual stresses in electrodeposits of nickel and nickel-iron alloys. *Surf. Coat. Technol. 122*, pages 118–135, 1999.

[63] T.C. Damen, P.S. Porto, and B. Tell. Raman effect in zinc oxide. *Phys. Rev. 142*, pages 570–574, 1966.

[64] K.C. Chan, W.N. Lei, N.S. Qu, and D. Zhu. Pulse electrodeposition of nanocrystalline nickel using ultra narrow pulse width and high peak current density. *Surf. Coat. Technol 168*, pages 123–128, 2003.

[65] B.H. Bairamov, A. Heinrich, G. Irmer, V.V. Toporov, and E. Ziegler. Raman study of the phonon halfwidths and the phonon - plasmon coupling in ZnO. *Phys. Status Solidi 119*, pages 227–234, 1983.

[66] A.E. Martel and L.G. Sillen. *Stability constants of metal-ion complexes*. Chemical Society:UK, 1965.

[67] L.S. Sanches, S.H. Domingues, A. Carubelli, and L.H. Mascaro. Electrodeposition of Ni-Mo and Fe-Mo alloys from sulfate-citrate acid solutions. *J. Braz. Chem. Soc. 14*, pages 556–563, 2003.

[68] H. Marchebois, S. Joiret, C. Savall, J. Bernard, and S. Touzain. Characterization of zinc-rich powder coatings by EIS and Raman spectroscopy. *Surf. Coat. Technol. 157*, pages 151–161, 2002.

Appendix

Pourbaix diagrams

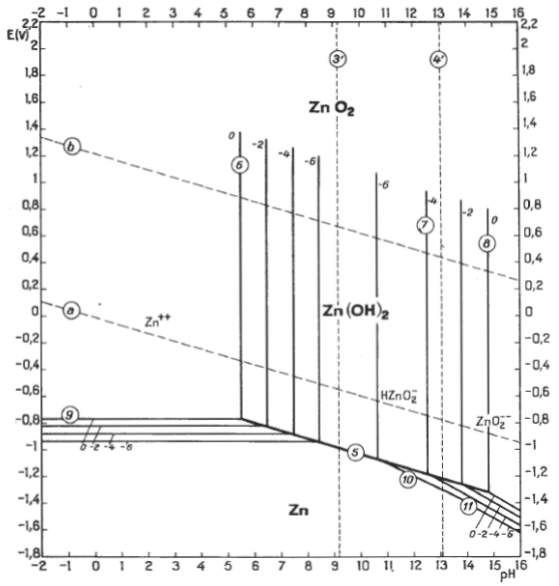

Figure A1: Pourbaix diagram for zinc vs. SHE in aqueous solutions at 25°C [18]

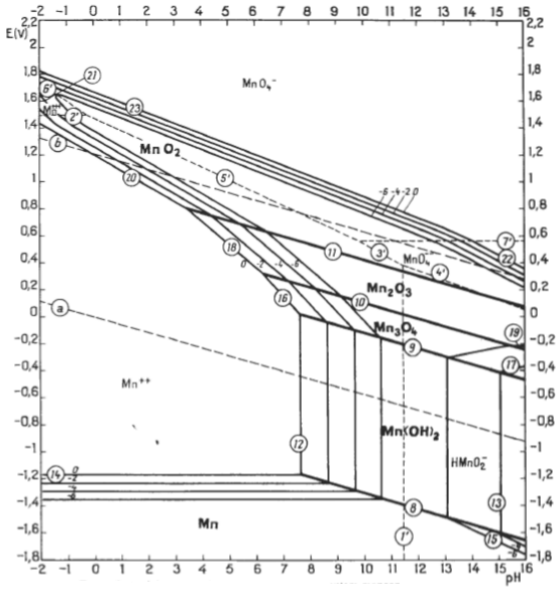

Figure A2: Pourbaix diagram for manganese vs. SHE in aqueous solutions at 25°C [18]

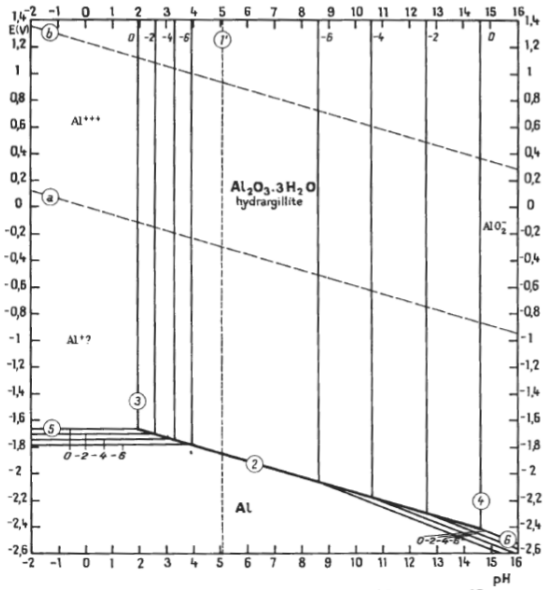

Figure A3: Pourbaix diagram for aluminium vs. SHE in aqueous solutions at 25°C [18]

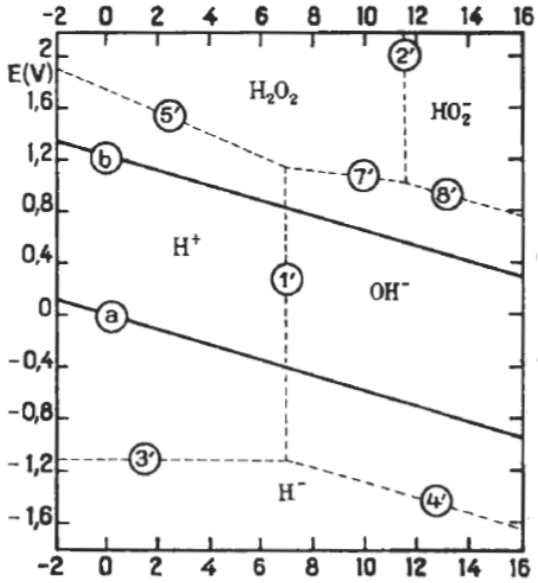

Figure A4: Pourbaix diagram for water vs. SHE in aqueous solutions at 25°C [18]

EDS Spectra

Alkaline pyrophosphate electrolyte EDS

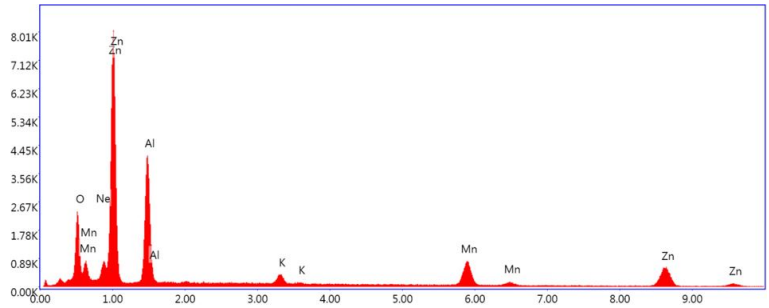

Figure A5: EDS spectrum for deposited coating at -1.80 V vs. Ag/AgCl (sat.) (DC) in alkaline pyrophosphate electrolyte

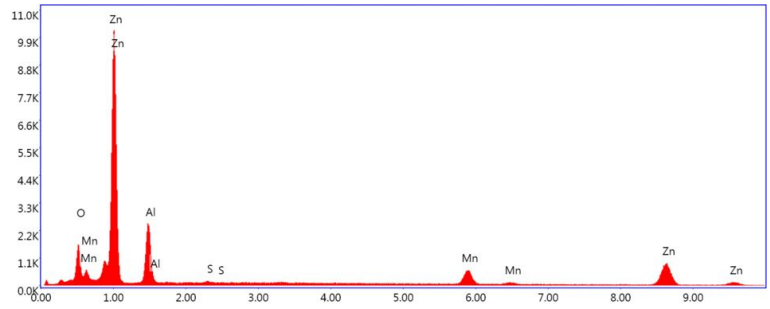

Figure A6: EDS spectrum for deposited coating at -1.90 V vs. Ag/AgCl (sat.) (DC) in alkaline pyrophosphate electrolyte

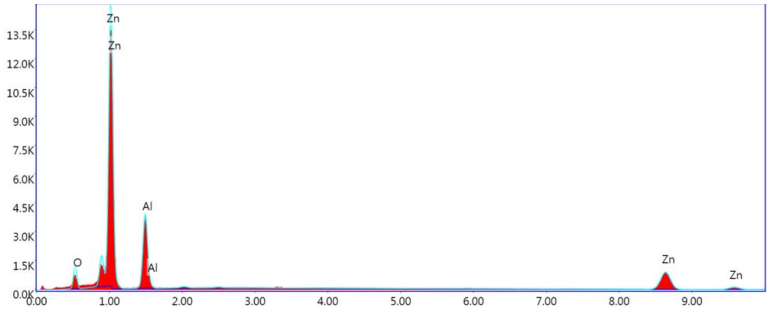

Figure A7: EDS spectrum for deposited coating at 48 $\mathrm{mA/cm^2}$ (PC, 10 Hz) in alkaline pyrophosphate electrolyte (centre)

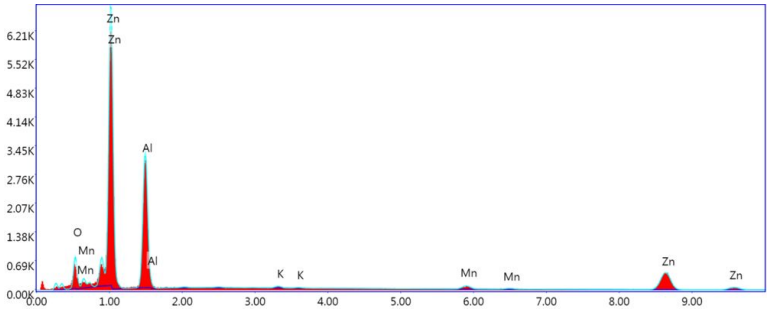

Figure A8: EDS spectrum for deposited coating at 48 $\mathrm{mA/cm^2}$ (PC, 20 Hz) in alkaline pyrophosphate electrolyte (centre)

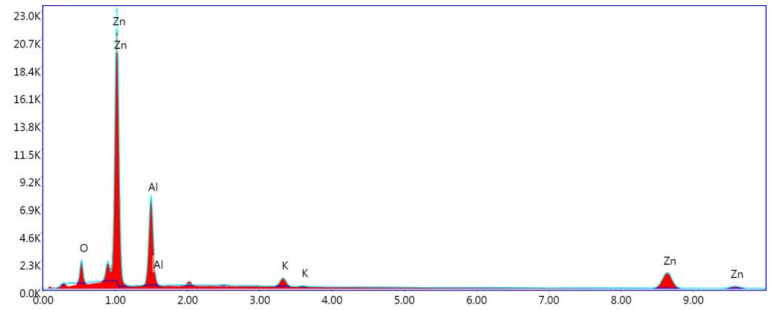

Figure A9: EDS spectrum for deposited coating at 48 $\mathrm{mA/cm^2}$ (PC, 4 Hz) in alkaline pyrophosphate electrolyte (centre)

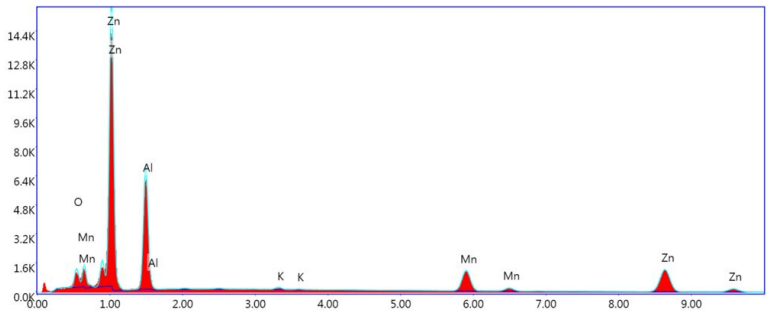

Figure A10: EDS spectrum for deposited coating at 48 $\mathrm{mA/cm^2}$ (PC, 4 Hz) in alkaline pyrophosphate electrolyte (edge)

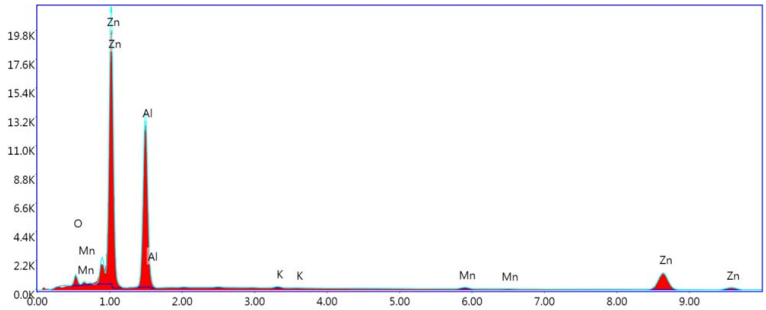

Figure A11: EDS spectrum for deposited coating at 60 $\mathrm{mA/cm^2}$ (PC, 4 Hz) in alkaline pyrophosphate electrolyte (centre)

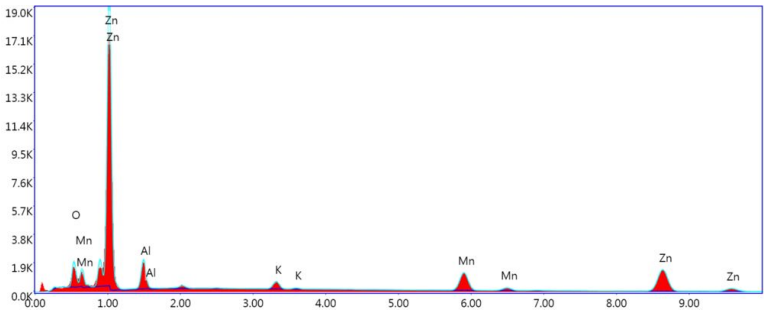

Figure A12: EDS spectrum for deposited coating at 60 $\mathrm{mA/cm^2}$ (PC, 4 Hz) in alkaline pyrophosphate electrolyte (edge)

Acidic sulphate electrolyte EDS

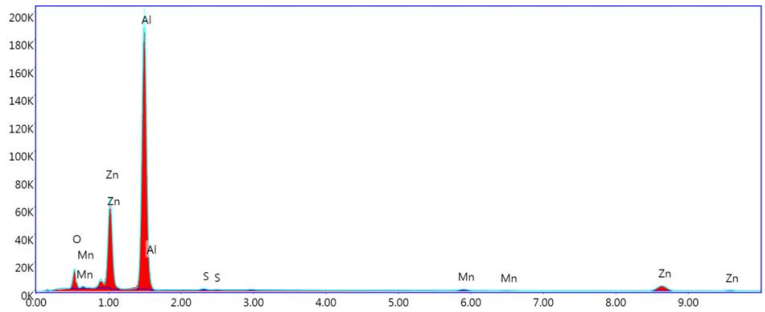

Figure A13: EDS spectrum for deposited coating at -1.50 V vs. Ag/AgCl (sat.) (DC) in acidic sulphate electrolyte

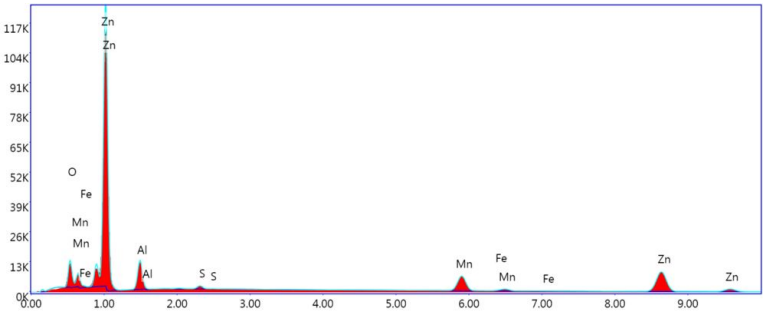

Figure A14: EDS spectrum for deposited coating at 32 $\mathrm{mA/cm^2}$ (PC, 4 Hz) in acidic sulphate electrolyte (centre)

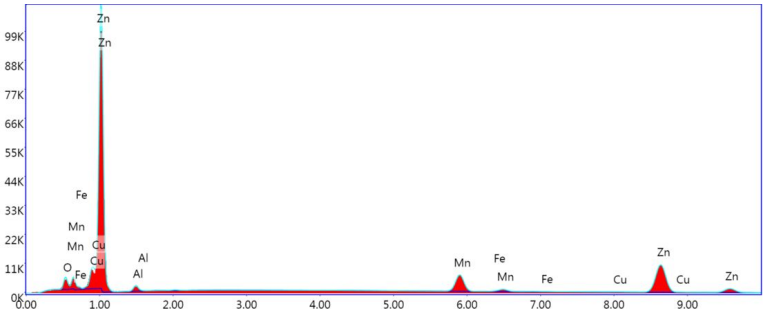

Figure A15: EDS spectrum for deposited coating at 32 $\mathrm{mA/cm^2}$ (PC, 4 Hz) in acidic sulphate electrolyte (edge)

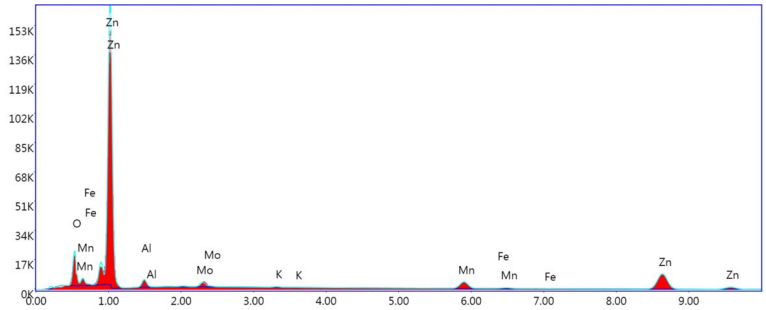

Figure A16: EDS spectrum for deposited coating at 36 $\mathrm{mA/cm^2}$ (PC, 4 Hz) in acidic sulphate electrolyte (centre)

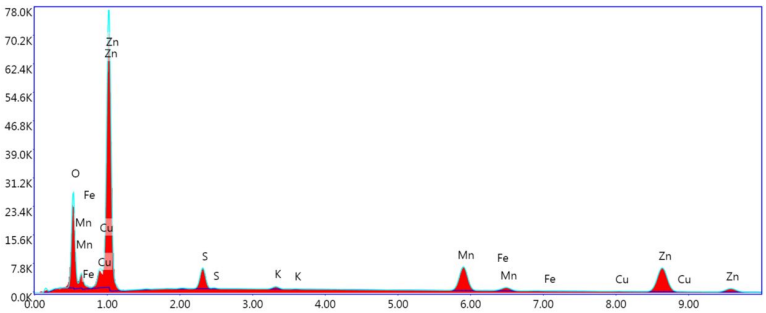

Figure A17: EDS spectrum for deposited coating at 36 $\mathrm{mA/cm^2}$ (PC, 4 Hz) in acidic sulphate electrolyte (edge)

Calculation of current efficiency and coating thickness

The current efficiency of the samples were calculated with Equation 2.2. The thickness displayed, d, is the addition of both the zincate layer (0.3 μm) and the theoretical thickness expected by applying Equation 2.4. The effective area for deposition was 5 cm^2 for all samples. Deposition time was 20 s for every sample except for the two DC alkaline pyrophosphate, which had a deposition time of 60 s.

Current efficiency calculation - alkaline pyrophosphate samples

Table A1: Current efficiency calculation for samples in alkaline pyrophosphate electrolyte

Sample	$\mathbf{m_{theo}}$ **[mg]**	$\mathbf{m_{deposition}}$ **[mg]**	**CE [%]**	d **[μm]**
(1, DC)	6.10	3.12	51	1.15
(2, DC)	14.23	4.55	32	1.82
(3, PC)	2.03	1.42	70	0.69
(4, PC)	2.71	1.76	65	0.79
(5, PC)	1.69	1.35	80	0.67
(6, PC)	2.03	1.22	60	0.64

Current efficiency calculation - acidic sulphate samples

Table A2: Current efficiency calculation for samples in acidic sulphate electrolyte

Sample	$\mathbf{m_{theo}}$ **[mg]**	$\mathbf{m_{deposition}}$ **[mg]**	**CE [%]**	d **[μm]**
(7, DC)	2.44	0.86	35	0.50
(8, PC)	1.10	0.54	49	0.64
(9, PC)	1.22	0.54	44	0.44

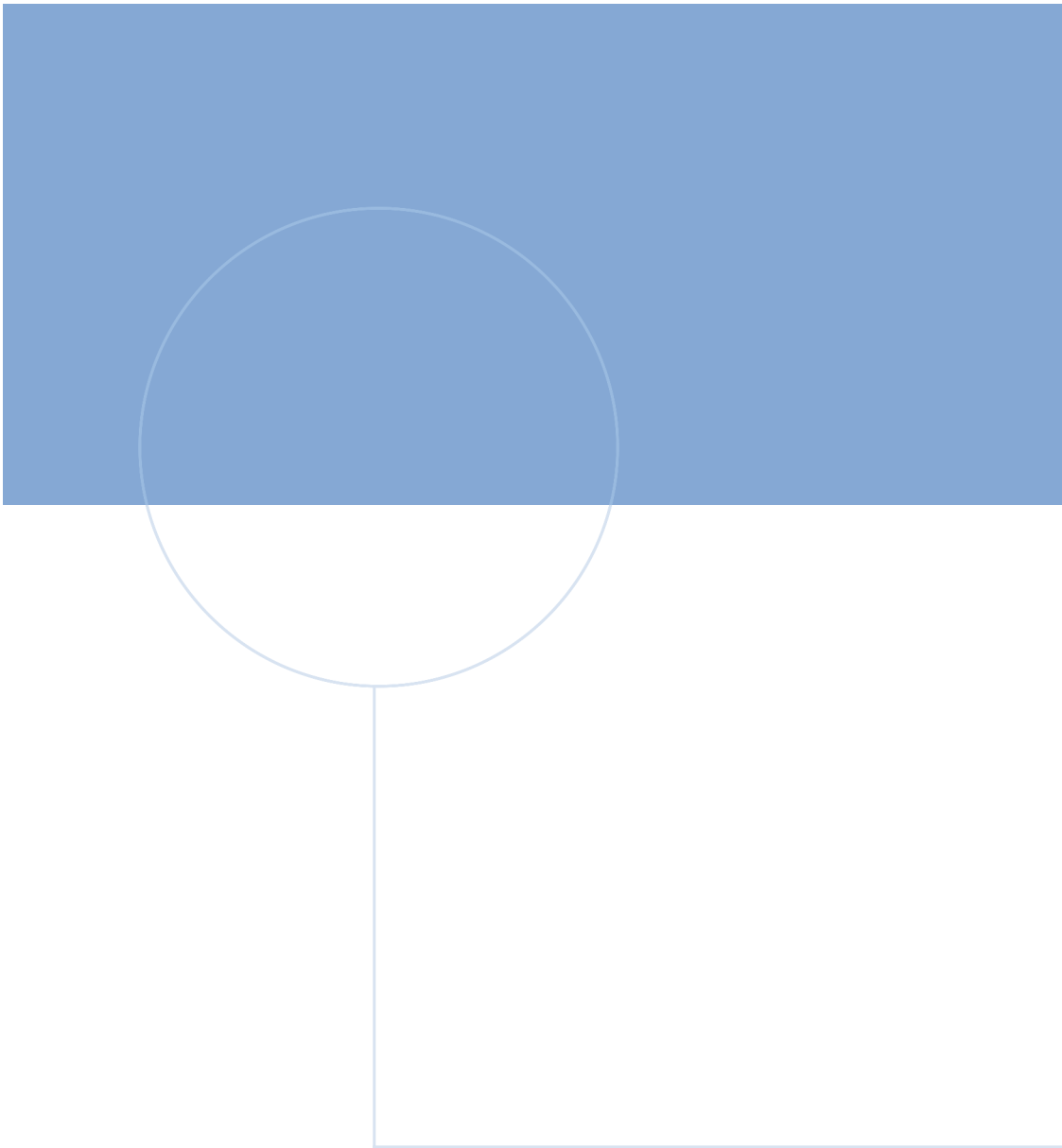

NTNU

Kunnskap for en bedre verden